IChF
Institute of Physical Chemistry PAS

Warsaw-4-PhD
Warsaw Doctoral School
in Natural and BioMedical Sciences

PhD Thesis

Inactivation of bacteriophages

Sada Raza

Supervisor:
dr. hab. Jan Paczesny, prof. ICHF

Doctoral dissertation prepared within the
Warsaw PhD School in Natural and BioMedical Sciences,
at the Institute of Physical Chemistry,
Polish Academy of Sciences
Marcina Kasprzaka 44/52,
01-244 Warszawa

June 2025

Acknowledgements

This dissertation is the result of my grandfather's dream, my *Pappa*, who saw doctoral potential in me when I read my first science books with him. His belief was the seed from which this journey began.

First and foremost, I extend my deepest gratitude to my supervisor, Jan Paczesny. I owe this entire endeavor to him. He stood by me during my lows, offered humility during my highs, and never once left my side. More than a mentor, he has been a constant, guiding me with patience, wisdom, and genuine care. In many ways, he has been a parent, a friend, and above all, a true mentor whose impact I will carry with me for life.

I am also immensely grateful to my friends in science: Bartek, Enkhlin, Bończak, Gunjan, Rafał, Natalia, Konrad, Hossein, Ziba, and Mateusz. Your companionship made this journey joyful, meaningful, and far less lonely. You reminded me every day why it is a gift to do science surrounded by kind, brilliant, and inspiring minds.

A heartfelt thanks to Ola for guiding me in becoming a better parent and a better person every day. Special thanks to Bartek and Enkhlin for giving me the dreamy trio, for being my constant cheerleaders and my emotional anchors. To Bończak, thank you for our long, meaningful discussions and for your warm friendship and wonderful company throughout this journey.

To my lovely parents, whose unwavering love and countless sacrifices have been the foundation of all my achievements. Your faith gave me the courage to dream and the strength to persevere. And to my dearest siblings, Zejo and Asad - thank you for grounding me, uplifting me, and shaping who I am today. Most importantly, I thank my unwavering support system, my husband, who entered my life during my PhD like a burst of light, constantly encouraging me to embrace the positive, to keep going, and to believe in myself. You gave me the greatest joy of my life - our two wonderful daughters. You three are my world.

List of Publications

Publications related to the thesis:

1. **Raza, S.**, Matuła, K., Karoń, S., & Paczesny, J. (2021). Resistance and adaptation of bacteria to non-antibiotic antibacterial agents: Physical stressors, nanoparticles, and bacteriophages. *Antibiotics*, 10(4), 435. https://doi.org/10.3390/antibiotics10040435
2. **Raza, S.**, Folga, M., Łos, M., Foltynowicz, Z., & Paczesny, J. (2022). The effect of zero-valent iron nanoparticles (nZVI) on bacteriophages. *Viruses*, 14(5), 867. https://doi.org/10.3390/v14050867
3. **Raza, S.**, Wdowiak, M., & Paczesny, J. (2023). An overview of diverse strategies to inactivate Enterobacteriaceae-targeting bacteriophages. *EcoSal Plus*, 11(1), eesp-0019-2022. https://doi.org/10.1128/ecosalplus.esp-0019-2022
4. **Raza, S.**, Wdowiak, M., Grotek, M., Adamkiewicz, W., Nikiforow, K., Mente, P., & Paczesny, J. (2023). Enhancing the antimicrobial activity of silver nanoparticles against ESKAPE bacteria and emerging fungal pathogens by using tea extracts. *Nanoscale Advances*, 5, 5786-5798, https://doi.org/10.1039/D3NA00220A
5. **Raza, S.**, & Paczesny, J. (2023). Nanotechnology for bacteriophages, bacteriophages for nanotechnology. In *Nanoscience* (pp. 243–271). Royal Society of Chemistry. https://doi.org/10.1039/9781839169427-00243
6. Kusior, A., Mazurkow, J., Jelen, P., Bik, M., **Raza, S.**, Wdowiak, M., Nikiforov, K., & Paczesny, J. (2024). Copper oxide electrochemical deposition to create antiviral and antibacterial nanocoatings. *Langmuir*, 40(27), 7890–7900. https://doi.org/10.1021/acs.langmuir.4c00642
7. **Raza, S.**, Bończak, B., Atamas, N., Karpińska, A., Ratajczyk, T., Łoś, M., Hołyst, R., & Paczesny, J. (2025). The activity of indigo carmine against bacteriophages: an edible antiphage agent. *Applied Microbiology and Biotechnology*, 109(24). https://doi.org/10.1007/s00253-025-13414-4

8. **Raza, S.**, Mente, P., Kamiński, B., Bończak, B., Maleki-Ghaleh, H., Vignesh, V., & Paczesny, J. (2025). Engineering hydrophobic and electrostatic interactions for selective inactivation of bacteriophages by mixed-ligand nanoparticles. *Nanoscale*, pages 1–9. https://doi.org/10.1039/D5NR00612K
9. Wdowiak, M., **Raza, S.**, Grotek, M., Zbonikowski, R., Nowakowska, J., Doligalska, M., Cai, N., Luo, Z., & Paczesny, J. (2025). Phage-Nanoparticle Cocktails as a Novel Antibacterial Approach: Synergistic Effects of Bacteriophages and Green-Synthesized Silver Nanoparticles. *bioRxiv*. https://doi.org/10.1101/2025.03.13.643104

Patent:

1. Patent: **Raza, S.**, Paczesny, J., Bonczak, B., & Los, M. (2023). The Use of Sodium Salt of 5,5'-Indigosulfonic Acid to Inhibit Bacteriophage Infections in Biotechnological Processes. *Patent No. P.441746*

Other publications:

1. Wdowiak, M., Paczesny, J., **Raza, S.**, (2022) Enhancing the stability of bacteriophages using physical, chemical, and nano-based approaches: A review, *Pharmaceutics*, 14(9), 1936. https://doi.org/10.3390/pharmaceutics14091936
2. Atamas, N., **Raza, S.**, Paczesny, J., Karpińska, A., Yablochkova, K. S., & Lazarenko, M. M. (2024). Competition between indigo carmine and water in the formation of dynamics behavior at different temperatures. *Dyes and Pigments, 226*, 112146. https://doi.org/10.1016/j.dyepig.2024.112146
3. Maleki-Ghaleh, H., Kamiński, B., Moradpur-Tari, E., **Raza, S.**, Khanmohammadi, M., Zbonikowski, R., Shakeri, M. S., Siadati, M. H., Akbari-Fakhrabadi, A., Paczesny, J. (2024). Visible Light-Sensitive Sustainable Quantum Dot Crystals of Co/Mg Doped Natural Hydroxyapatite Possessing Antimicrobial Activity and Biocompatibility. *Small*, 20(52), https://doi.org/10.1002/smll.202405708

Funding

1. The National Science Centre, Poland, within the SONATA BIS grant “*Modification of virion stability - stabilization and inactivation of viruses*” according to decision number 2017/26/E/ST4/00041.

Abstract

Bacteriophages, viruses that specifically infect bacteria, play a crucial role in natural ecosystems but pose major threats to industrial biotechnology, pharmaceutical production, and food safety. Phage infections can devastate bacterial cultures, leading to process failures and significant economic losses. Effective management of bacteriophages, therefore, requires strategies that selectively eliminate phages without harming beneficial bacteria.

This thesis addresses the challenge of phage control by progressively developing materials capable of selective bacteriophage inactivation. The first approach explored novel antimicrobial nanomaterials, such as green-synthesized silver nanoparticles (TeaNPs). TeaNPs exhibited potent antibacterial and antifungal activities but lacked selectivity, affecting a broad range of microorganisms and failing to inactivate bacteriophages effectively. Although they enhanced antibacterial action when combined with phages, they highlighted the limitation of general antimicrobial strategies. Additionally, other nanomaterials such as zero-valent iron (ZVI) nanoparticles and copper-based nanocoatings were evaluated for their antiviral potential. While these materials demonstrated measurable inactivation of some phages, their broad-spectrum activity and limited selectivity reinforced the need for more targeted antiphage solutions.

Seeking selective approaches, the study next identified compounds capable of targeting phages. Indigo carmine (IC), an FDA-approved food dye, was discovered to inactivate phages without compromising bacterial viability. Mechanistic studies revealed IC's selective binding to DNA, disrupting phage integrity while sparing the host bacteria. This milestone demonstrated that molecular specificity in phage control is achievable using naturally available, food-safe substances.

Building on this foundation, engineered nanomaterials were designed to optimize selectivity further. Mixed-ligand gold nanoparticles (MLNPs), combining positive, negative, and hydrophobic ligands, achieved efficient phage inactivation (99% reduction) while maintaining over 90% bacterial survival. Similarly, polypyrrole nanoparticles

(PPyNPs) functionalized with carboxyl groups selectively targeted bacteriophages while exhibiting minimal cytotoxicity to mammalian cells. These rationally designed nanoparticles offer scalable, biocompatible solutions for targeted phage management. Overall, this work advances the field of phage control by moving from broad-spectrum antimicrobials to naturally selective agents and finally to engineered nanomaterials with high specificity. The developed strategies offer innovative, environmentally sustainable, and effective approaches for safeguarding microbial processes in biotechnology and industrial microbiology.

Streszczenie

Bakteriofagi, wirusy infekujące bakterie, odgrywają istotną rolę w środowisku, lecz stanowią poważne zagrożenie dla biotechnologii przemysłowej, przemysłu farmaceutycznego i bezpieczeństwa żywności. Infekcje fagowe mogą prowadzić do całkowitego załamania hodowli bakteryjnych i znacznych strat ekonomicznych. Skuteczna ochrona przed bakteriofagami wymaga strategii umożliwiających ich selektywną eliminację bez szkody dla korzystnych bakterii.

W niniejszej pracy zmierzono się z wyzwaniem zapobieganiu infekcjom fagowym poprzez opracowanie materiałów zdolnych do ich selektywnej inaktywacji. Pierwszym etapem badań było zastosowanie nowych nanomateriałów przeciwdrobnoustrojowych, takich jak nanocząstki srebra syntetyzowane z wykorzystaniem ekstraktów z herbaty (TeaNPs). Choć TeaNPs wykazywały silne działanie przeciwbakteryjne i przeciwgrzybicze, brakowało im selektywności - oddziaływały na szeroki zakres mikroorganizmów, jednak nie inaktywując skutecznie fagów. Połączenie TeaNP z fagami poprawiało efekt przeciwbakteryjny, ale ukazało ograniczenia nieselektywnych metod. Dodatkowo zbadano właściwości przeciwwirusowe innych nanomateriałów, takich jak nanocząstki żelaza zerowartościowego (ZVI) oraz nanopkrycia bazujące na miedzi. Choć materiały te wykazały inaktywację niektórych fagów, ich zbyt szerokie spektrum działania i ograniczona selektywność podkreślają potrzebę opracowania bardziej specyficznych materiałów przeciwwirusowych.

Poszukując bardziej selektywnych podejść, odkryto związki zdolne do ukierunkowanego działania. Indygotyna (indigokarmin; IC), zatwierdzony przez FDA barwnik spożywczy, wykazał zdolność selektywnej inaktywacji fagów bez negatywnego wpływu na bakterie. Badania mechanistyczne potwierdziły selektywne wiązanie IC z DNA. Było to kluczowe osiągnięcie wskazujące, że specyficzne zwalczanie fagów jest możliwe.

Bazując na tych odkryciach, opracowano specjalnie zaprojektowane nanomateriały, by jeszcze bardziej zwiększyć selektywność ich działania. Nanocząstki złota pokryte wartswą

mieszanych ligandów (MLNPs), łączące dodatnie, ujemne i hydrofobowe ligandy, osiągnęły 99% redukcji fagów przy zachowaniu ponad 90% przeżywalności bakterii. Również nanocząstki polipirolowe (PPyNPs) funkcjonalizowane grupami karboksylowymi wykazały wysoką selektywność wobec fagów przy minimalnej toksyczności wobec komórek ssaczych.

Rozprawa przedstawia ewolucję podejścia do kontroli fagów - od środków przeciwdrobnoustrojowych o szerokim spektrum działania, przez selektywne związki, również pocodzenia naturalnego, po projektowane nanomateriały o wysokiej specyficzności - otwierając nowe możliwości dla zrównoważonej i skutecznej ochrony procesów mikrobiologicznych przed infekcjami fagowymi.

List of abbreviations

- **TSC** – Trisodium citrate
- **PVP** – Polyvinylpyrrolidone
- **PyCOOH** – 3-(1H-pyrrol-1-yl)propanoic acid
- **PVA** – Polyvinyl alcohol
- **MUA** – Mercaptoundecanoic acid
- **DDT** – Dodecanethiol
- **DDAB** – Didodecyldimethylammonium bromide
- **TMA** – (11-mercaptoundecyl)-N,N,N-trimethylammonium bromide
- **IC** – Indigo Carmine
- **IPTG** – Isopropyl β-D-1-thiogalactopyranoside
- **TM buffer** – Tris-Magnesium buffer
- **TeaNPs** – Tea Extract Silver Nanoparticles
- **C-AgNPs** – Citrate-Capped Silver Nanoparticles
- **G-TeaNPs** – Green Tea Extract Silver Nanoparticles
- **MLNPs** – Mixed-Ligand Nanoparticles
- **PPyNPs** – Polypyrrole Nanoparticles
- **PPy-COOH NPs** – Carboxyl-functionalized Polypyrrole Nanoparticles
- **LB** – Luria–Bertani (medium/agar)
- **YPD** – Yeast Extract Peptone Dextrose (medium)
- **PFU** – Plaque-Forming Units
- **SEM** – Scanning Electron Microscopy
- **TEM** – Transmission Electron Microscopy
- **XRD** – X-ray Diffraction
- **XPS** – X-ray Photoelectron Spectroscopy
- **FTIR** – Fourier Transform Infrared Spectroscopy
- **NMR** – Nuclear Magnetic Resonance
- **DSC** – Differential Scanning Calorimetry
- **MTT** – [3-(4,5-dimethylthiazol-2-yl)-2,5-diphenyltetrazolium bromide] assay
- **FCS** – Fluorescence Correlation Spectroscopy

Table of contents

CHAPTER 1
Introduction to Phage Inactivation

Parts of this chapter were previously presented as:

Raza, S., Wdowiak, M., & Paczesny, J. (2023). An overview of diverse strategies to inactivate Enterobacteriaceae-targeting bacteriophages. *EcoSal Plus, 11(1),* eesp-0019-2022. https://doi.org/10.1128/ecosalplus.esp-0019-2022

Raza, S., & Paczesny, J. (2023). Nanotechnology for bacteriophages, bacteriophages for nanotechnology. *Nanoscience (pp. 243-271).* Royal Society of Chemistry. https://doi.org/10.1039/9781839169427-00243

Raza, S., Matuła, K., Karoń, S., & Paczesny, J. (2021). Resistance and adaptation of bacteria to non-antibiotic antibacterial agents: Physical stressors, nanoparticles, and bacteriophages. *Antibiotics, 10*(4), 435. https://doi.org/10.3390/antibiotics10040435

1.1 The critical role of bacteria in food and industrial biotechnology

Bacteria have been of use to humankind since the beginning of time. Bacterial habitat spans from the human microbiome to hot springs and even space [1–3]. Louis Pasteur has described the significance of microbial life in human and animal existence [4]. Research on the gut microbiome also highlighted the importance of a symbiotic relationship between bacteria and humans [5]. While bacteria can cause a wide range of infections [6,7], they can also benefit the regular functioning of the human body.

The natural roles of microorganisms include nutrient cycling, the cause and control of diseases, and food spoilage [8]. With a better understanding of bacteria and yeast, microbes now have great biotechnological applications such as the production of yogurt and cheese [9], fermentation of vegetables like cabbage [10], manufacture of biofertilizers [11], drugs, e.g., insulin [12], and the treatment of diseases (like cystic fibrosis, hemophilia, hepatitis B [13]) to name a few. A variety of products can be extracted from different growth phases of bacterial cells. The exponential growth phase provides primary metabolites, such as amino acids [14], vitamins, solvents, and organic acids [15]. Smaller molecules produced during the stationary phase are called secondary metabolites [16]. Such products are widely used in medical applications, like antibiotics and antitumor agents [17]. Furthermore, challenging procedures for producing polymer precursors and various enzymes and hormones can be simplified by using bacterial cultures [18,19].

Beyond their role in the human body, bacteria have also been used for various industrial applications, demonstrating their versatility and significance in biotechnology. The biotechnology industry is one of the fastest-developing industries globally [20], and the advancements in biotechnology and molecular biology have enabled industries to use microorganisms in reducing pollution, manufacturing cleaner fuels, and producing and processing food and beverages [21].

Food preservation is one of our most important tasks, and this is made possible *via* bacterial fermentation products. Gram-positive

bacteria, in particular, are beneficial in food production, especially in the fermentation of dairy products [22]. The most common bacterial group used in fermentation is Lactic acid bacteria (LAB), and it is used to produce dairy, meat, and vegetable products [23]. In most cases of fermentation, additional useful substances like bacteriocins, aroma compounds, ethanol, exopolysaccharides, enzymes, etc., are also produced [24].

Bacteria have also come to dominate the pharmaceutical industry with their use in the production of pharmaceutical ingredients like solvents, vitamins, and amino acids [25]. The sales of drugs of microbial origin now cross 13 billion US dollars annually [13]. Some products of bacteria, like bacterial cellulose (BC), play a vital role as an additive in nutritionally rich diets, vegetarian meat, beverages, and food packaging because BC cannot be absorbed by the human body and is eliminated as it is [26]. Secondary metabolites with biological, immunosuppressive, anticancer, anti-inflammatory, and antimicrobial properties are also widely used [27]. Other uses of bacteria comprise recombinant proteins capable of treating broad-spectrum illnesses [28].

All the processes that involve bacterial use are prone to contamination, the most common contaminant being bacteriophages [25]. Bacteriophages are viruses that infect bacteria yet do not qualify as living organisms due to their inability to independently carry out most biological processes required for reproduction [29]. Phages rely on hosts to reproduce, and completing the phage reproduction cycle usually results in the host's death.

Contamination due to bacteriophages is a growing economic concern. 1-10% of batches are lost to phage contamination in dairy industries [30]; several companies have entirely shut down their function due to their inability to overcome phage contamination [25]. The most common source of new phages is raw milk [31]. Bacteriophages also interfere with fermentation processes as they are carried out in non-sterile conditions [32]. Such infections are especially intimidating because a single phage can attack a bacterial cell and convert it into a factory for new phages (up to hundreds of virions per bacterial cell) [25].

The source of contamination may either be external, introducing small amounts of phages, or secondary, arising from a previously contaminated process [25]. Therefore, executing periodic preventive procedures such as good laboratory practices, factory hygiene, sterilization, decontamination, and disinfection is essential. Still, new methods for dealing with page infections need to be developed. In numerous cases, it is impossible to fully block phage entrance to the process as virions might be introduced with the substrates (e.g., in the dairy industry).

1.2 Bacteriophages

Bacteriophages are considered the most abundant biological entities on Earth, with an estimated 10^{31} particles in existence [33]. Despite their ubiquity, the majority remain undiscovered, with only about 0.0002% of the global phage metagenome identified so far [34]. A schematic overview of the most common phage morphologies is presented in **Figure 1**. Phage virions typically measure between 50 and 200 nm, categorizing them as nanomaterials under the widely accepted definition, which includes structures with at least one physical dimension within the range of 1 to 100 nm. However, some filamentous phages, such as M13, can reach lengths of up to 900 nm [35]. Recently, even larger phages have been discovered in marine environments. For instance, researchers identified a family of marine 'megaphages' with genomes exceeding 650 kilobases, significantly larger than typical phage genomes [36]. These megaphages are thought to play a role in regulating carbon and nitrogen cycles in the ocean. Additionally, a novel bacteriophage, vB_HmeY_H4907, was isolated from the Mariana Trench at a depth of 8,900 meters, highlighting the presence of diverse and large phages in deep-sea ecosystems [37].

Structurally, a phage virion consists of genetic material (dsDNA, ssDNA, (+)ssRNA, or dsRNA) enclosed within a protein capsid, with Cystoviridae being the only family of enveloped phages identified to date [38–41]. Phages are classified based on three features: (i) cubic, filamentous, or pleomorphic forms, (ii) the presence or absence of a tail, and (iii) industrial relevance [42].

As bacterial viruses, phages specifically infect bacteria but cannot reproduce within Eukaryotic cells due to their inability to perform essential biological processes [29]. Found in all bacterial habitats, phages identify and infect host bacteria to facilitate their own reproduction [43]. Phages are classified as either lytic or lysogenic based on their life cycle [44]. Lytic phages hijack the host's machinery to replicate and ultimately lyse the bacterial cell. In contrast, lysogenic phages integrate into the bacterial genome as prophages, remaining dormant until specific triggers induce their transition to the lytic cycle [44,45]. Notably, lysogenic phages play a role in chronic bacterial infections by contributing to bacterial virulence and antibiotic resistance, making them significant in microbial ecology and human health [46].

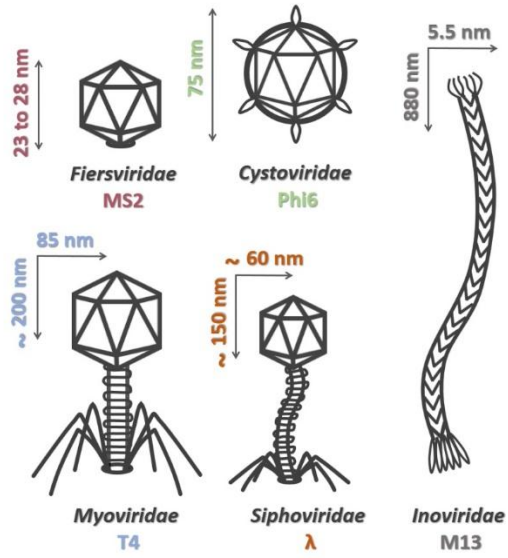

Figure 1. Schematic representation of selected families of bacteriophages. The exemplary representative phages are shown with their physical dimensions**.** Adapted from Raza, S., & Paczesny, J. (2023). *Nanotechnology for bacteriophages, bacteriophages for nanotechnology*. In *Nanoscience* (pp. 243-271). Royal Society of Chemistry. © 2023 Royal Society of Chemistry. Reproduced with permission.

Bacteriophages share structural and functional similarities with certain human viruses, making them valuable tools for understanding viral replication, stability, and inactivation methods. For example, MS2, a small RNA phage, is often used to model human RNA viruses, while Phi6, an enveloped bacteriophage, serves as a surrogate for lipid-enveloped viruses like influenza [47–49].

1.2.1 The role of bacteriophages

Bacteriophages, first described by Frederick Twort and Felix d'Herelle in the late 19th century, are viruses that infect bacteria and undergo either a lytic or lysogenic cycle [50]. While early phage therapy efforts were hindered by inconsistent results and the success of antibiotics, the rise of multidrug-resistant (MDR) bacteria has renewed interest in their therapeutic potential [51]. Clinical trials, including the first FDA-approved intravenous phage therapy in 2019, highlight their growing relevance in treating infections such as urinary tract infections, typhoid, and systemic MDR infections [52–56]. Phages also play a crucial role in veterinary medicine, effectively treating bacterial infections in animals with high success rates [57]. Beyond therapy, bacteriophages are employed in food safety applications, such as ListShield™, which targets *L. monocytogenes* in meat and poultry products [58]. Phages are favored for their bactericidal effects, specificity, low toxicity, and lack of cross-resistance with antibiotics, allowing them to selectively eliminate pathogens without harming commensal bacteria or human cells [50,59]. However, their interaction with the immune system remains complex; while some phages trigger immune responses, others evade detection, and factors like administration route and protein composition can influence immunogenicity [60–62]. Phages also exhibit antibiofilm activity by producing depolymerases that disrupt bacterial biofilms, such as those in *P. aeruginosa* infections [63,64]. The combination of phages with antibiotics, known as phage-antibiotic synergy (PAS), enhances bacterial clearance while reducing antibiotic resistance, making it a promising strategy against MDR pathogens [65]. However, challenges such as optimal phage-antibiotic ratios, host immune interactions, and pathogen specificity require further study [66–68]. Some antibiotics, like aminoglycosides, may even interfere with phage replication, limiting their

combined efficacy in certain cases [69]. Another innovative approach is the integration of phages with nanoparticles, where metallic nanoparticles enhance antibacterial effects while phages provide targeted delivery, a strategy that extends to photothermal ablation using phage-conjugated gold nanorods [70,71]. Furthermore, phages serve as templates for bio/nanomaterials, enabling the development of engineered peptides with bactericidal properties for various applications [72,73]. This resurgence of phage-based strategies highlights their potential in combating the global antibiotic resistance crisis while also expanding their role in biotechnology and medicine.

1.2.2 Phage-Bacteria Dynamics: Evolution, Resistance, and Industrial Challenges

Bacteria and phage diversity are individually affected by each other. They play an essential role in shaping microbial evolution since 20% of the bacterial genome comprises phage genetic material [74]. The coevolution of bacteria-phage populations is essential in microbiological systems for evolutionary [75] and ecological processes [76]. Phages are also responsible for bringing about changes in the ecosystem due to their predation on bacterial populations (approximately killing up to 40% of bacteria every day 33), thereby giving rise to horizontal gene transfer and, at the same time, altering host metabolism and redistributing compounds through cell lysis [29].

Bacteriophages directly affect the evolution of bacteria by stimulating resistance mechanisms. New adaptations counter these escape routes in phages, continuing the cycle [77]. Additionally, bacteriophages can enhance certain characteristics in bacteria, such as adaptability and virulence, like in the case of phage-resistant *Campylobacter jejuni* and *Pseudomonas aeruginosa* displaying loss of fitness and increased extracellular production, respectively [74]. They are also capable of spreading antibiotic resistance and pathogenicity factors [29]. Bacteria can also be manipulated to introduce novel genes, disrupt host genes, and modify cellular metabolism with the help of prophages [78]. This results in slower growth and decreased efficiency of byproduct synthesis [79,80]. Alternatively, temperate phages can be

used to boost host immunity by preventing the attachment of other phages or by preventing their propagation, thereby driving bacterial evolution [81].

Bacteriophages have a make-up to carry out precise functions of host identification, subsequent metabolism requisition, and reproduction [43]. The release of progeny virions (viral particles) results in the death of the host cell in most cases. Bacteriophage infection often results in the spread of resilient contamination followed by a heavy loss of product [82]. Such an effect is amplified while operating in biofoundries on large scales [80]. Contaminations like these that spread quickly are often endured by laboratories and bacteria-based industries [83]. Phage contamination was first reported by Whitehead and COX in 1935 in a dairy culture [84].

1.3 Current Strategies for Phage Inactivation and Their Limitations

Phages are hard to remove, and regular cleaning and disinfectants usually don't work against them. [85]. Fundamental approaches to managing contamination include selecting suitable equipment, optimizing process designs, and ensuring thorough cleaning and sterilization practices [25]. Decontamination of laboratories and biofoundries often relies on a combination of physical and chemical treatments [32]. Physical methods such as photocatalysis, high-pressure processing (up to 100 MPa) [86], and ultra-pasteurization are frequently employed [87]. Chemical strategies involve using a range of disinfectants, including benzalkonium chloride, chlorhexidine, hydrogen peroxide, triclosan, polyvinylpyrrolidone-iodine, alkaline detergents, potassium peroxymonosulfate (e.g., Virkon S, commonly used in laboratories), and sanitizers based on quaternary ammonium compounds [88–90].

Phage inactivation can be achieved through various methods, with new approaches continually being developed. These methods are generally classified into physical and chemical strategies (**Figure 2**). While temperature, high pressure, and UV exposure are critical physical factors, chemical approaches often rely on reactive oxygen species (ROS), natural extracts, salts, and polymers for phage inactivation. Recently, a new dimension has been added to this field: nanotechnology. The application of nanotechnology for phage inactivation is gaining

increasing attention, offering novel mechanisms and enhanced efficacy for controlling bacteriophage activity in various settings.

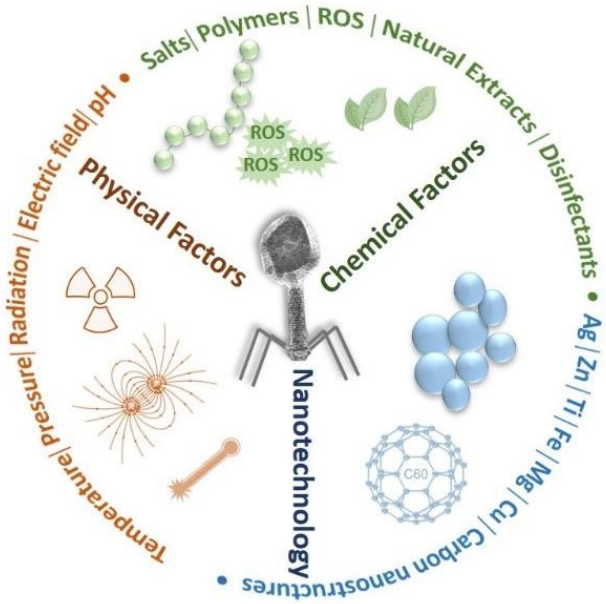

Figure 2. Three strategies of phage inactivation: physical, chemical, and nanotechnology*.*

A key distinction between current antiviral drugs and novel antiphage agents is their mode of action. Traditional antiviral treatments typically target the host cell after infection has occurred, aiming to disrupt viral replication. In contrast, some antiphage strategies work directly on the virion itself, preventing infection before the virus enters a host cell. This difference highlights the potential for developing new antiviral therapies inspired by bacteriophage-targeting approaches.

1.3.1 Physical Factors

Thermal inactivation is a widely applied method, particularly in industrial processes. Temperatures between 50 °C and 95 °C can induce morphological changes in bacteriophages, such as capsid deformation, DNA release, and the separation of head and tail structures [91]. Elevated temperatures above the DNA transition point promote DNA ejection, rendering phages inactive [92,93]. For example, MS2 phages lose

infectivity at around 72 °C, while lower temperatures fail to disrupt their integrity [94]. However, thermal methods are less effective against highly resistant phages (e.g., *Lactococcus* phage), such as those surviving pasteurization or boiling [87,95].

High-pressure processing (HPP) is another emerging non-thermal technique, ensuring product integrity while inactivating phages [87]. Pressures of 300–800 MPa can significantly reduce phage titers (up to 8 log reduction), depending on the phage structure [96,97]. While effective in many cases, certain bacteriophages, like those infecting *Salmonella*, resist pressures up to 250 MPa, making HPP a non-universal strategy [96].

Radiation inactivates phages primarily by inducing free radical formation and damaging the viral [98,99]. Modern techniques use UV, X-rays, or lasers for targeted applications, often enhanced by photocatalysts like titanium dioxide [100,101]. Electric fields also play a role in destabilizing phage capsids or filtering out virions using multi-walled carbon nanotube filters, achieving titer reductions up to 7 log [102]. However, radiation and electric field methods often require specialized equipment and pose safety challenges for personnel.

Osmotic shock may also be created by significant salt concentration changes to destabilize phages, causing virion bursting [103]. Studies report up to 90% inactivation of bacteriophage T2Rb with rapid effects within a minute [104,105]. This method, though effective, has been overlooked in recent years.

Another approach includes the application of extreme pH conditions for rapid phage inactivation. Acidic pH values (e.g., pH 1) achieve complete inactivation of phage T3 within 15 seconds [106]. Basic conditions (e.g., pH 9–10) can reduce coliphage titers by 5 log, but other phages like PhiX174 demonstrate higher resistance [107,108]. pH stability is critical for phage therapy applications, where genetic modifications may enhance survival through acidic environments [109].

1.3.2 Chemical Factors

Chemical methods for bacteriophage inactivation are diverse, leveraging polymers, proteins, natural extracts, commercially available disinfectants,

reactive oxygen species (ROS), and salts. Each class offers unique mechanisms, benefits, and limitations, contributing to advancements in phage control strategies.

Polymers such as poly-amino acids are gaining attention for sustainable phage inactivation methods. Poly-L-lysine, particularly α-poly-L-lysine and ε-poly-L-lysine, effectively inactivates coliphages T4 and T5 by binding to DNA phosphate groups, causing precipitation and subsequent inactivation [110–114]. Polymeric amphiphiles, such as PEG-polylactide copolymers, prevent phage adsorption by blocking lectin receptors [115,116]. Chitosan, a derivative of chitin, inactivates phages like coliphages and bacteriophage 1-97A, reducing titers by 5 log, though its mechanism remains unexplored [117–120].

Eukaryotic antibodies exhibit high specificity for bacteriophage antigens, making them effective antiviral agents. Plasma proteins also show broad-spectrum activity against phages [121–124]. While these approaches hold potential, they rely heavily on immune system responses, thus limiting scalability for industrial applications.

Natural plant and bacterial extracts are explored for phage inactivation due to their economic and ecological benefits. Tea extracts, rich in antibacterial and antiviral properties, show promise in inactivating microbes [125,126]. Extracts from thyme (*Thymus vulgaris*), rosemary (*Salvia rosmarinus*), and blueberry (genus *Vaccinium)* have demonstrated phage inactivation, with blueberry achieving complete MS2 inactivation after seven days [127–130]. However, pomegranate juice, effective against human enteric viruses, shows limited efficacy against phages [131]. Bacteria-derived molecules like daunorubicin and doxorubicin also exhibit antiphage activity but are non-specific in targeting [132–134].

Chemical disinfectants remain a cornerstone of phage control, encompassing agents like benzalkonium chloride, chlorhexidine, hydrogen peroxide, triclosan, and quaternary ammonium compounds [88–90,135–137]. Virkon S and ethanol are widely used in laboratory settings [137]. Chlorine and ozone are effective but have significant drawbacks, such as carcinogenicity, corrosiveness, and environmental

harm [138,139]. Emerging techniques like ozone nanobubbles offer novel approaches, achieving up to an 8 log reduction in bacteriophage titers [140].

ROS, including hydroxyl radicals, superoxide anions, and singlet oxygen, play a pivotal role in phage inactivation by damaging DNA and viral capsids. ROS can be generated by compounds like resveratrol-Cu(II) complexes, titanium oxide surfaces, or plasma-activated water, achieving over 99.99% inactivation of MS2 in seconds [141]. However, some phages inhibit ROS formation, limiting this method's universality [142].

Metal salts also inactivate phages by binding to capsid proteins and disrupting viral structure and function. Heavy metal salts (e.g., lead, mercury, copper, and cadmium) effectively inactivate phages but pose environmental and toxicity concerns [143]. Light metal salts, such as calcium and sodium, also contribute to phage inactivation by interfering with DNA release mechanisms [144–147]. Reversible inactivation using compounds like potassium cyanide highlights the versatility of metal salts [148,149]. Despite their efficacy, chemical approaches often face challenges like environmental toxicity, lack of specificity, and potential resistance development. Proper waste management and careful application are critical for integrating these methods into industrial and ecological settings [150,151].

Chemical inactivation methods provide a diverse platform for combating bacteriophages, with polymers, proteins, and natural extracts offering sustainable solutions, while ROS and salts bring precision and efficacy. However, balancing effectiveness with environmental and safety considerations remains a pressing challenge with chemical inactivation.

1.3.3 Nanoparticles

Nanotechnology has emerged as a promising tool in microbiology to address contamination challenges, with its effectiveness mediated by nanoparticle size, charge, and composition [152]. Nanoparticles inactivate bacteriophages through mechanisms such as toxic ion release [153–155], reactive oxygen species (ROS) generation [141,156], or interference with viral proteins [157].

Silver nanoparticles (AgNPs) are among the most extensively studied for their antiviral properties. AgNPs deactivate bacteriophages via adsorption, ion release, and ROS generation, achieving up to 96% PFU/mL reduction [155]. Studies exploring the application of colloidal and immobilized AgNPs have achieved complete inactivation of MS2 and T4 phages [158]. Additional applications include bacteriophage detection *via* silver-based inks and water disinfection using AgNP-coated filters or hybrid composites [159–164].

Other studies have explored the use of gold nanoparticles against bacteriophages. Richter et al. worked on negatively charged gold nanoparticles coated with varying ratios of negative (11-mercapto 1-undecanesulfonic acid) and hydrophobic (1-octanethiol) ligands. The study aimed to establish ratios that could inactivate bacteriophages without damaging bacterial cells. Such nanoparticles have the potential to be directly used in applications that require the selective removal of bacteriophages [157].

Iron nanoparticles, including hematite and zero-valent iron (nZVI), play a significant role in bacteriophage inactivation. Smaller nanoparticles offer greater efficacy due to increased surface area, achieving up to a 7 log reduction in bacteriophage titer for phages like M13 [165]. However, their effects vary depending on phage type, as T7 phages exhibit greater resistance.

Silica nanoparticles, while less studied, demonstrate potential for bacteriophage attenuation through adsorption. Modified silica particles can bind foodborne pathogen phages like those of *E. coli* and *Salmonella*, reducing titers by up to 8 log [166]. Functionalized silica particles also immobilize phages, making them promising for filtration and removal systems [167].

Carbon nanotubes (CNTs), including single-walled and multi-walled forms, are effective due to their high surface area, which enhances bacteriophage adsorption. These structures have been effective in water solutions and bioaerosols [168]. Other promising carbon-based nanomaterials include carbon dots, fullerene, fullerol, graphite, graphene, and graphene oxide [169–174].

Although nanotechnology offers significant advantages for bacteriophage inactivation, challenges remain unresolved. Nano-compounds may harm the environment [175,176], and overuse could lead to nanoparticle resistance akin to antibiotic resistance [177,178]. Proper waste management and regulatory approval are also crucial for industrial-scale applications of nanomaterials.

1.4 The Need for Innovative, Food-Safe, and Scalable Solutions

The increasing prevalence of bacteriophage contamination in industrial biotechnology and food production highlights the urgent need for innovative and scalable solutions. While the biotechnology and food industries rely heavily on bacteria for fermentation, drug production, and nutrient cycling, these processes are frequently compromised by phage infections. Bacteriophages, with their high specificity and ability to rapidly replicate, present a significant economic burden, leading to production inefficiencies and loss of entire batches. Despite decades of research, current phage inactivation methods face substantial limitations, necessitating the development of new, food-safe, and scalable strategies.

Although several physical, chemical, and nanotechnology-based strategies exist for bacteriophage inactivation, these approaches often fail to address industry needs. Physical methods, such as high-pressure processing, thermal treatments, and UV exposure, are effective in many cases but can be energy-intensive, impractical for real-time applications, or detrimental to the quality of sensitive products. Chemical approaches, including disinfectants and reactive oxygen species (ROS), pose risks of environmental toxicity and may leave harmful residues in food products. Furthermore, while nanotechnology-based methods hold immense promise, challenges such as potential nanoparticle resistance, environmental concerns, and high costs limit their widespread adoption.

A critical gap in current methods is the lack of antiviral agents that are non-toxic to bacterial cells and can be safely applied during active bioprocessing in bioreactors. Most strategies require process interruptions, which disrupt production cycles and increase operational costs. Moreover, traditional approaches often fail to provide the

specificity and scalability required for large-scale industrial applications. Thus, the development of targeted, safe, and real-time solutions is essential for overcoming these limitations.

To address these challenges, this thesis will explore three innovative strategies for bacteriophage inactivation:

1. **Novel antimicrobials:** Current antimicrobial methods are often ineffective against phages and viruses in general. New strategies, such as specially designed nanoparticles, are being developed to achieve more efficient phage inactivation and address this gap. However, while these approaches show promise, they may lack selectivity and pose risks to other organisms and the environment.
2. **Naturally selective antiviral strategies:** Certain molecules with inherent antiviral properties may offer promising avenues for phage inactivation. Investigating these molecules, particularly those that exhibit selectivity in disrupting phage activity without harming bacterial cells, presents a strategy for enabling their use in biotechnological applications, such as bioreactors, during active processes.
3. **Engineered selectivity through charge-based interactions:** A strategy for phage inactivation involves designing materials with mixed-charge surfaces, exploiting the charge distributions on phage capsids. By fine-tuning these surface charges, it is possible to enhance the binding specificity to phages and facilitate effective inactivation, providing a novel method for targeting phages without interfering with bacterial functions.

These strategies aim to bridge the existing gaps in bacteriophage management, offering scalable and food-safe solutions that align with industrial and environmental requirements. By focusing on innovative materials and mechanisms, this thesis seeks to contribute to developing robust, real-time, and sustainable antiphage technologies.

CHAPTER 2
Aim & Scope

The increasing prevalence of bacteriophage contamination presents a significant challenge to bacterial processes in food and industrial biotechnology. These contaminants disrupt bacterial cultures, leading to substantial losses in substrates and commercial products, and complicate bioprocesses due to their rapid infectivity and persistence. Despite advancements in bacterial strain development and improved laboratory practices, the current strategies primarily focus on preventing phage contamination through design-level interventions and microbiological techniques. However, these approaches often fail to address phage infections effectively once contamination occurs, leading to recurring infections and batch failures.

The demand for effective phage deactivation methods has become more pronounced due to the increasing reliance on bacterial cultures for biotechnological applications. Although physical and chemical strategies for phage inactivation exist, they often lack specificity, can be harsh on bacterial cells, or pose environmental concerns. Biotechnology and material science innovations offer new possibilities, particularly by exploring nanotechnology and bio-safe chemical agents. The aim is to develop scalable, efficient, and environmentally sustainable solutions for managing phage-related disruptions in bacterial processes. This thesis seeks to contribute to this goal by exploring novel approaches to phage deactivation, enhancing our understanding of bacterial-phage interactions, and providing practical solutions for industrial implementation.

The thesis begins by examining the broad potential of nanotechnology in antimicrobial applications (**Chapter 4**). This chapter highlights how metallic nanoparticles, particularly silver and iron-based systems, are applied across food science, medicine, and environmental fields. Special emphasis is placed on the antibacterial and antifungal properties of green tea-synthesized silver nanoparticles (G-TeaNPs) and the synergistic potential of combining nanoparticles with bacteriophages to enhance antimicrobial effects. Additionally, copper-based nanocoatings and iron nanoparticles are evaluated for their antiviral activities, underscoring the promise and challenges of using nanomaterials to manage pathogens.

Building on the need for more selective approaches, **Chapter 5** introduces the discovery of naturally occurring compounds capable of selectively inactivating phages without harming host cells. Indigo carmine (IC), an FDA-approved food dye, demonstrated significant antiphage activity against DNA bacteriophages while maintaining bacterial viability and productivity. This finding represents a crucial proof-of-concept that selective antiviral agents can exist naturally, paving the way for the rational design of even more targeted strategies.

Finally, **Chapter 6** explores the engineering of selective nanomaterials through charge-based interactions. Mixed-ligand nanoparticles (MLNPs) and polypyrrole nanoparticles (PPyNPs) are developed and optimized to achieve high phage inactivation rates while preserving bacterial and mammalian cell viability. These materials offer precise, targeted antimicrobial action with minimal toxicity by fine-tuning the surface chemistry, e.g., balancing positive, negative, and hydrophobic functionalities. This chapter highlights the potential of engineered selectivity for safe, efficient pathogen control in industrial and medical contexts.

Together, these chapters chart a progression from broad-spectrum nanomaterials toward naturally inspired and ultimately engineered solutions for selective antimicrobial strategies, providing a foundation for safer and more sustainable pathogen management technologies.

By addressing the limitations of current decontamination strategies, this research contributes to developing cost-effective, environmentally friendly solutions to phage-related challenges. The findings aim to support industrial stakeholders in maintaining phage-free bacterial cultures, improving process reliability, and enhancing product quality in diverse microbial applications.

CHAPTER 3
Materials & Methods

3.1. Materials

Silver nitrate ($AgNO_3$, >98%, Sigma-Aldrich), sodium borohydride ($NaBH_4$, >98%, Sigma-Aldrich), trisodium citrate (TSC, >98%, Sigma-Aldrich), sodium hydroxide (NaOH, analytical grade, Sigma-Aldrich), lactic acid (88%, Chempur, Poland), d-(+)-glucose (POCH, Poland), polyvinylpyrrolidone (PVP, Mw 40,000, Alfa Aesar), copper(II) sulfate pentahydrate ($CuSO_4 \cdot 5H_2O$, EuroChem, Poland), hydrochloric acid (HCl, 35%, standard chemical supply), iron(III) chloride hexahydrate ($FeCl_3 \cdot 6H_2O$, Merck, Germany), iron(II) chloride tetrahydrate ($FeCl_2 \cdot 4H_2O$, Merck, Germany), pyrrole (Merck, Germany), 3-(1H-pyrrol-1-yl)propanoic acid (PyCOOH, ChemBridge, USA), polyvinyl alcohol (PVA, Merck, Germany), hydrazine hydrate (Sigma-Aldrich, freshly distilled over KOH), mercaptoundecanoic acid (MUA, Sigma-Aldrich), dodecanethiol (DDT, Sigma-Aldrich), didodecyldimethylammonium bromide (DDAB, TCI, Japan), (11-mercaptoundecyl)-N,N,N-trimethylammonium bromide (TMA, synthesized according to literature method), tetrabutylammonium borohydride (Sigma-Aldrich), tetramethylammonium hydroxide (25% in water, Sigma-Aldrich), indigo carmine (E132, Food Colors, Poland), chloramphenicol and kanamycin (standard suppliers), isopropyl β-D-1-thiogalactopyranoside (IPTG, standard supplier), and uranyl acetate (2% aqueous solution, EM Resolutions). Organic solvents, including toluene, chloroform, and methanol, were purchased from Linegal Chemicals (Poland) and used without further purification. Ethanol was used as analytical grade (POCH, Poland). Deionized water (Milli-Q system, resistivity 18.2 MΩ·cm) was used for all aqueous solutions.

LB medium, LB-agar, and Top LB-agar were prepared using NaCl, tryptone, yeast extract, and agar (Carl Roth, Germany). YPD medium was used for yeast strains (Carl Roth, Germany). TM buffer was prepared with 10 mM Tris base, 10 mM $MgSO_4$, 5 μM $CaCl_2$, and deionized water (pH 7.4), with all components sourced from Sigma-Aldrich. All media and buffers were sterilized by autoclaving before use.

3.2. Nanoparticle Synthesis

3.2.1. Synthesis of Tea Extract Silver Nanoparticles (TeaNPs)

Silver nanoparticles using tea extracts (TeaNPs) were synthesized following a modified method by Nakhjavani et al [179]. Black, green, and Pu-erh teas were frozen in liquid nitrogen, ground into a powder, and extracted in hot water (60 °C) for 15 minutes. The extract was centrifuged, filtered (0.22 µm), and mixed with a silver nitrate solution (10 mM) while maintaining the temperature below 50 °C. After 2 hours of stirring, the resulting yellow-brown nanoparticle suspension was centrifuged and washed six times with deionized water, yielding purified TeaNPs stored at 4 °C at a concentration of 1 mg/mL.

3.2.2. Synthesis of Citrate-Capped and Green Tea Silver Nanoparticles (C-AgNPs)

Citrate-capped silver nanoparticles (C-AgNPs) were synthesized by reducing silver nitrate with sodium borohydride in the presence of trisodium citrate. An aqueous solution containing 2 mM $NaBH_4$ and 2 mM TSC was heated to 60 °C and stirred for 30 minutes, after which silver nitrate solution was added dropwise. The mixture was heated to 90 °C, pH adjusted to 10.5 with NaOH, and stirred for 20 minutes to yield citrate-capped silver nanoparticles.

Green Tea silver nanoparticles (G-TeaNPs) were prepared similarly to TeaNPs but using only green tea extract. The purified extract was reacted with silver nitrate at 50 °C, stirred for 2 hours, and the resulting nanoparticles were isolated by centrifugation, washed, and suspended in deionized water to 1 mg/mL.

3.2.3. Synthesis of Zero-Valent Iron Nanoparticles (ZVI)

Zero-valent iron (ZVI) nanoparticles were synthesized by reducing iron(III) chloride with sodium borohydride under an argon atmosphere. A 0.05 M $FeCl_3$ solution was purged with argon and reacted dropwise with a 0.15 M $NaBH_4$ solution. After precipitation, the product was washed thoroughly with water, filtered through a nylon mesh, lyophilized, and stored under argon. Partially oxidized ZVI (PO ZVI) and oxidized ZVI

(O ZVI) were prepared by exposing ZVI to air for 2 minutes and 2 days, respectively.

3.2.4. Synthesis of Copper Oxide Nanocoatings

Copper oxide nanocoatings were electrodeposited on titanium foil substrates using a three-electrode setup. The electrolyte consisted of 0.4 M $CuSO_4$ and 3 M lactic acid, with optional addition of glucose or PVP to control crystal growth. The solution pH was adjusted to 10 with NaOH. Deposition was carried out at 750 mV for 30 minutes at 60 °C after pretreatment scans between -1 V and 1.3 V. Coated foils were rinsed and dried at room temperature.

3.2.5. Synthesis of Mixed-Ligand Gold Nanoparticles (MLNPs)

Mixed-ligand gold nanoparticles (MLNPs) were synthesized by first producing DDA-capped gold nanoparticles in toluene using the method by Jana and Peng [180]. The DDA-AuNPs were purified by methanol washing and redispersed in toluene. Ligand exchange reactions were performed using premixed solutions of TMA, MUA, and DDT in various ratios. The functionalized MLNPs were purified by chloroform/acetone washing and redispersed in water at a concentration of 1 mg/mL.

3.2.6. Synthesis of Polypyrrole Nanoparticles (PPyNPs)

Polypyrrole nanoparticles were synthesized by chemical oxidative polymerization. Pyrrole monomer, optionally mixed with various molar ratios of PyCOOH, was polymerized in the presence of polyvinyl alcohol and iron(III) chloride at 5 °C. The reaction was conducted overnight under constant stirring. Resulting nanoparticles were purified by differential centrifugation and redispersed in deionized water. Five types of PPyNPs with varying carboxyl content (0–10 %) were prepared and stored at 4 °C.

3.3. Material Characterization

3.3.1. UV-Visible Spectroscopy (UV-Vis)

UV-visible absorption spectra of nanoparticle suspensions and dye-containing samples were recorded using an Evolution 220 UV-Vis spectrophotometer (Thermo Scientific, Waltham, USA). Measurements were performed in 10 mm quartz cuvettes (Hellma, Germany) over the wavelength range of 200–800 nm with 1 nm increments. Samples

containing indigo carmine and food dyes were diluted 100-fold prior to measurement.

3.3.2. Fourier-Transform Infrared Spectroscopy (FTIR)

FTIR spectra were recorded using a Vertex 80v spectrometer (Bruker, USA) equipped with a deuterated triglycine sulfate (DTGS) detector and OPUS 6.5 software. Measurements were performed in reflection mode under reduced pressure (6 hPa) using 1,024 scans per spectrum at a resolution of 2 cm^{-1}. Dried extracts and nanoparticle samples were placed directly on the ATR crystal or gold-coated glass slides.

3.3.3. Raman Spectroscopy

Raman spectra of polypyrrole nanoparticles were collected using a BRAVO Raman spectrometer (Bruker, Germany) equipped with a Duo Laser system operating at 700–1,100 nm. Spectral resolution ranged from 2–4 cm^{-1}, with an acquisition time of 6 seconds per spectrum. Measurements were performed under ambient conditions and averaged over three spectra per sample.

3.3.4. Dynamic Light Scattering (DLS) and Zeta Potential

Hydrodynamic size and surface charge (zeta potential) of nanoparticles were measured using a Zetasizer Nano ZS instrument (Malvern Instruments, UK), equipped with a He-Ne laser (633 nm, max 4 mW). DLS measurements were performed at 20 °C with a backscattering angle of 173°. Before measurements, samples were dispersed by ultrasonication and diluted in deionized water or TM buffer. Zeta potential was determined using folded capillary cells, with tetramethylammonium hydroxide added when required for MUA deprotonation.

3.3.5. Scanning Electron Microscopy (SEM) and Energy-Dispersive X-ray Spectroscopy (EDS)

SEM imaging was performed using the FEI Nova NanoSEM 450 microscope (USA) and Thermo Fisher Phenom XL Desktop SEM for structural and elemental analysis. Accelerating voltages ranged from 5 to 15 kV. Backscattered electron mode was used for topography, and elemental composition was assessed with EDS (Octane Elect Plus). Samples were mounted on carbon tape or gold-coated glass slides.

Cross sections were polished and nickel-plated using a Watts bath in the Langmuir copper oxide experiments.

3.3.6. Transmission Electron Microscopy (TEM)

High-resolution TEM images were acquired using the FEI Tecnai Spirit BioTWIN electron microscope with a digital camera. Nanoparticle suspensions were drop-casted onto C400Cu100 copper grids (400 mesh, carbon layer; EM Resolutions), and negatively stained with 2 % uranyl acetate for 15 seconds at room temperature. Samples were air-dried before imaging.

3.3.7. X-ray Diffraction (XRD)

Powder X-ray diffraction was analyzed using a PANalytical Empyrean diffractometer (Malvern, UK) in Bragg–Brentano and grazing incidence (GID) modes. Cu Kα radiation (λ = 0.154 nm) was used as the X-ray source, and diffraction patterns were obtained at room temperature.

3.3.8. X-ray Photoelectron Spectroscopy (XPS)

XPS was conducted using a CLAM2 spectrometer (VG Microtech Ltd., UK). Dried powder samples were mounted directly on the holder and measured in high vacuum. The spectral range spanned from 0 to 1300 eV.

3.3.9. Nuclear Magnetic Resonance (NMR)

Proton NMR spectroscopy was performed using a Bruker 400 MHz spectrometer. Dried MLNP samples were dissolved in a methanol-iodine solution to etch ligands, re-dried, and re-dissolved in dry deuterated DMSO. Measurements were taken under an argon atmosphere. Excess iodide was added where necessary to shift residual water peaks.

3.3.10. Surface Area and Porosity (BET Analysis)

Surface area measurements were conducted using the ASAP 2020 instrument (Micromeritics, USA). Krypton was used as the adsorbate at 77 K, and samples were degassed at 373 K for 15 hours prior to analysis. The BET method was applied to calculate specific surface areas.

3.3.11. Differential Scanning Calorimetry (DSC)

Thermal behavior of PVME formulations was studied using a MICROCAL VP-Capillary DSC system (Malvern, UK). Samples were scanned between 25°C and 80°C, including pre-heated samples to assess structural transitions. Reproducibility was ensured by running replicate samples from the same batch.

3.4. Microbiological Assays

3.4.1. Bacterial Culturing

Bacterial strains used in this work included *Escherichia coli* BL21, *E. coli* C3000, *Pseudomonas aeruginosa* PAO1, *Salmonella enterica* DSM 18522, *Staphylococcus aureus* ATCC 43300 and DSM 105272, *Acinetobacter baumannii* ATCC 19606, *Enterococcus faecium* DSM 13590, *Klebsiella pneumoniae* ATCC 700603, *Enterobacter cloacae* PCM 2569, *Listeria monocytogenes* EGDe, *Bacillus subtilis* DSM 5547, and *E. durans* PCM 1857. Bacteria were grown in LB medium unless otherwise noted. For *L. monocytogenes*, BHI medium and BHI agar were used. Cultures were prepared by inoculating a single colony into 10 mL of medium and incubating overnight at 37 °C in an orbital shaker at 200 rpm. Cultures were refreshed by mixing 2.5 mL of overnight culture with 7.5 mL of fresh medium and incubating for 1 hour to reach OD_{600} of ~1.0. For *P. syringae*, incubation was carried out at 28 °C.

3.4.2. Bacteriophage Propagation and Storage

Bacteriophages used in this study included T1, T4, T7, MS2, M13, λ, P001, P22, Φ6, Φ29, LR1_PA01, vB_SauS_CS1, and QBeta. Phages were propagated by infecting early logarithmic-phase host cultures. After visible lysis, phages were p

recipitated using polyethylene glycol (for DNA phages), centrifuged, and purified by CsCl density gradient ultracentrifugation. MS2 was directly filtered through a 0.22 µm syringe filter. Final suspensions were dialyzed in TM buffer and treated with viscolase (0.2 µg/mL). All stocks were stored at 4 °C.

3.4.3. Double Overlay and Droplet Titration

Phage titers were quantified using the double overlay method or droplet plaque assay. For the double overlay, 4 mL of 0.5% top LB agar mixed with 200 µL of fresh bacterial culture was poured over solidified 1.5% LB agar plates. Diluted phage suspensions were either mixed with this layer or applied as 5 µL droplets (7–8 per plate). Plates were incubated overnight at 37 °C (or 45 °C for λ). Plaques were counted, and phage titers were expressed as PFU/mL using the equation PFU/mL = n × d × 200.

3.5. Cytotoxicity Studies

3.5.1. Alamar Blue Assay

3T3 NIH fibroblast cells were used to assess the cytotoxicity of AgNPs, G-TeaNPs, MLNPs, and PPyNPs. Cells were cultured in DMEM supplemented with 10% FBS and 1 % penicillin-streptomycin under standard conditions (37 °C, 5 % CO_2). After seeding 1.5 × 10^4 cells/well in 96-well plates and overnight incubation, cells were treated with nanoparticles (0.1 mg/mL for MLNPs, 0.3 mg/mL for PPyNPs) for 24 or 48 hours. After exposure, media were replaced with 10 % (v/v) Alamar Blue in fresh medium and incubated for 4 hours. Fluorescence (Ex 530–570 nm, Em 580–620 nm) was measured with a SpectraMax i3x plate reader.

3.5.2. MTT Assay

HeLa and A549 cancer cell lines were used to assess BB-PVME formulation toxicity. Cells (10,000/well) were seeded in 96-well plates, incubated for 6 hours, and then treated with dye–polymer formulations at five concentrations (two-fold dilutions). After 6 hours, the medium was replaced with 1 mM MTT reagent and incubated for 3 hours. Afterward, DMSO was added, and absorbance at 540 nm was recorded. Cell viability was calculated relative to untreated controls.

3.6. Special Experiments

3.6.1. Dose–Response Tests with Indigo Carmine

Phages (T4, T1, T7, λ, MS2, and P001) were incubated with varying concentrations of indigo carmine (0.1–0.5 mg/mL) in TM buffer at 37 °C

for 24 hours. Controls without dye were included. Phage titers were determined using droplet plaque assays after incubation.

3.6.2. Fluorescence Correlation Spectroscopy (FCS) Binding Studies

Fluorescence correlation spectroscopy (FCS) was used to assess binding interactions between indigo carmine and nucleic acids (dsDNA, ssDNA, ssRNA). Measurements were conducted using a Nikon Eclipse TE2000U confocal microscope with a PicoHarp 300 FCS unit. The diffusion coefficients were analyzed to determine dye binding affinity differences between DNA and RNA.

3.7. Instrumentation

- UV-Vis spectrophotometer: Evolution 220 (Thermo Scientific, USA)
- DLS & zeta potential: Zetasizer Nano ZS (Malvern, UK)
- SEM and STEM: Nova NanoSEM 450 (FEI, USA); Phenom XL (Thermo Fisher)
- TEM: Tecnai Spirit BioTWIN (FEI)
- XRD: PANalytical Empyrean (Malvern, UK)
- XPS: CLAM2 (VG Microtech Ltd., UK)
- Raman spectrometer: BRAVO (Bruker, Germany)
- FTIR spectrometer: Vertex 80v (Bruker, USA)
- NMR: Bruker 400 MHz
- DSC: MicroCal VP-Capillary DSC (Malvern, UK)
- Microplate reader: SpectraMax i3x (Molecular Devices, USA)
- Shaker-incubator: ES-20 (Biosan, Latvia)
- Ultrasonic bath: Polsonic, Poland
- Autoclave: Prestige UK (Venus Michał Matuszczak, Poland)

3.8. Statistical Analysis

All experiments were conducted in triplicate unless stated otherwise. Statistical significance of differences between control and experimental

groups was determined using the unpaired two-tailed Student's t-test. Results were considered significant at $p < 0.05$, $p < 0.01$, *and* $p < 0.001$. Error bars in all graphs represent standard deviations (SD).

CHAPTER 4
Novel antimicrobials

Parts of this chapter were previously presented as:

Raza, S., Wdowiak, M., Grotek, M., Adamkiewicz, W., Nikiforow, K., Mente, P., & Paczesny, J. (2022). Enhancing the antimicrobial activity of silver nanoparticles against ESKAPE bacteria and emerging fungal pathogens by using tea extracts. *Nanoscale Advances, 14(9), 1936.* DOI https://doi.org/10.1039/D3NA00220A

Raza, S., Folga, M., Łos, M., Foltynowicz, Z., & Paczesny, J. (2022). The effect of zero-valent iron nanoparticles (nZVI) on bacteriophages. *Viruses, 14(5), 867.* https://doi.org/10.3390/v14050867

Kusior, A., Mazurkow, J., Jelen, P., Bik, M., Raza, S., Wdowiak, M., Nikiforov, K., & Paczesny, J. (2024). Copper oxide electrochemical deposition to create antiviral and antibacterial nanocoatings*. Langmuir, 40(27), 7890–7900*. https://doi.org/10.1021/acs.langmuir.4c00642

and as a preprint:

Wdowiak, M., Raza, S., Grotek, M., Zbonikowski, R., Nowakowska, J., Doligalska, M., Cai, N., Luo, Z., Paczesny, J., Phage-Nanoparticle Cocktails as a Novel Antibacterial Approach: Synergistic Effects of Bacteriophages and Green-Synthesized Silver Nanoparticles. *bioRxiv.* https://doi.org/10.1101/2025.03.13.643104

Chapter acknowledgement: Tea nanoparticles were synthesized by Mateusz Grotek, an undergraduate student I supervised during his lab work. XRD measurements were performed by Andrzej Żywociński, BET by Magdalena Bonarowska, FTIR by Pumza Mente. SEM images of ZVI were provided by Rafał Zbonikowski, and TEM images were obtained by Marcin Łoś. Copper nanocoatings and related characterization were provided by Anna Kusior and her team.

4.1 Nanotechnology and bacteriophages

Phages are notoriously difficult to eliminate, especially with standard cleaning routines and disinfectants, which are often ineffective against them [85]. Current strategies for phage inactivation, along with their limitations, are described in this thesis in section 1.3. New approaches are needed, and nanotechnology might answer this problem.

Nanoscience is a field that influences multiple areas of research. It deals with objects having at least one geometrical dimension in the range from 1 to 100 nm. The inclusion of nanotechnology in biology has especially gained popularity in recent decades, encompassing multiple economic sectors [181]. Nanotechnology has contributed immensely to the developments in the food industry by providing effective avenues for energy conservation, sustainability, and cues to improve capital funds well [182]. Nanomaterial engineering is also a leading technology in developing crops for sustainable farming systems. A significant contribution was also witnessed in active and intelligent food packaging and food safety, resulting in the increased shelf life of food products, infrequent contamination, and enhanced quality. Most of these applications arise from the potential of nanomaterials to lead to qualitative and quantitative production of healthier, safer, and high-quality functional foods [183].

As nanomedicine, nanotechnology can be applied in diagnosing, monitoring, controlling, and treating biological systems [184]. Furthermore, nanomedicine includes fields like nanomachines, nanofibers, sensors, polymeric nano-bio materials, etc [185]. Nanomaterials are physically and chemically adjustable as nanocarriers, nano vaccines, cytokine storm suppressors, antiviral agents at the site of

infection, and viral antigens in body fluids [186]. Nanoparticles can also be essential for better understanding complex systems, such as the interaction between gut microbiota and SARS-CoV-2 [187]. The usage of organic or biological (e.g., proteins or nucleic acids [188]) components also makes nanoparticles perfect candidates for application in controlled drug delivery systems [189,190], bioimaging [191,192], biosensing [193], tissue regeneration [194], and antibacterial applications [195]. Such systems also exhibit biodegradability, non-toxicity, stability in circulation in the bloodstream, and the ability to permeate cell membranes effectively [194]. Despite advances in nanotechnology, man-made self-assembling systems are relatively simple with limited functionalities [72].

The majority of virions fulfill the formal definition of a nanoparticle. Phages are biological nanomaterial that can be assembled into ordered nanostructured materials, laying the foundation for advancing nanobiotechnology [196]. Phages, alone or in combination with non-biological nanomaterials, have been employed to develop new nanobiotechnologies for applications such as biosensing, drug and gene delivery, cancer therapy, vaccinations, tissue regeneration, antibacterial treatment, energy storage and generation, and higher-order materials assembly [197].

Nanotechnology is often applied to microbiology to tackle the growing concerns of contamination. The baggage of toxicity borne by nanomaterials can be mediated by their size, charge, and composition [152]. New biomedical applications have emerged with the growing advancements of nanotechnology linked with microbiology, especially with silver nanoparticles (AgNPs). Due to the broad spectrum of antibacterial, antifungal, and antiviral properties, AgNPs are popularly adopted as disinfectants and antimicrobial agents [198]. More than 500 tons of nanoparticles per year are now supplied to meet different industries' demands, drawing attention to their biological activity, safety, and mechanism of action [199]. Experiments combining silver nanoparticles with bacteriophages have resulted in lower minimum inhibitory concentration (from 1.1% to 0.13%) and minimum bactericidal concentration (from 2.15% to 0.25%) as compared to silver nanoparticles alone [200]. Conversely, nanoparticles also aid the internalization of

bacteriophages in mammalian cells to target intracellular bacterial infections [201].

Additionally, silver nanoparticles were also employed to inactivate bacteriophages. Zero-valent silver nanoparticles, often referred to as biogenic silver, inactivated UZ1 bacteriophages (infecting *Klebsiella aerogenes*) from drinking water [202]. Some experiments with colloidal silver nanoparticles presented a complete inactivation of MS2 and T4 bacteriophages, with a starting concentration of 10^3 PFU/mL [158]. Moreover, bacteriophage contaminations can also be detected by using silver nanoparticle-based inks [159]. Silver nanoparticles also had inhibitory effects on hepatitis B virus (HBV) and human immunodeficiency virus (HIV), with an unknown antiviral mechanism [203]. Other antiviral applications of silver include silver-nanoparticle-decorated silica hybrid composites for water disinfection [160], to coat air filters [161,162], amine-functionalized glass substrate immobilized with silver nanoparticles [158], and silver-doped titanium dioxide nanoparticles [163] for drinking water treatment. Antiviral inactivation by silver nanoparticles is enhanced by impregnation with granular activated carbon (GAC) [154]. A coating of GAC modified with AgNPs on household filters resulted in 3 log reductions in PFU/mL of T4 [164].

4.2 Silver Nanoparticles from Green Sources: The Role of Tea Extracts

Another method of making nanoparticles more suitable for biomedical and environmental applications involves green synthesis, which utilizes eco-friendly and sustainable processes to minimize hazardous chemical use and reduce environmental impact. By incorporating natural extracts, such as plant-based compounds, this approach enhances the biocompatibility of nanoparticles while leveraging their natural reducing and stabilizing properties.

My research hypothesis was that I would achieve an efficient anti-bacteriophage agent by combining silver and tea extracts, both known for their antiviral properties. The antiviral activity of tea extracts has been demonstrated in various studies. For instance, a study highlighted that

Pu-erh ripe tea extract effectively inhibited HIV by preventing the fusion of normal cells with HIV-infected cells [204]. Another study confirmed the antiphage properties of tea extract combined with ferrous sulfate (TeaF) for four different phage strains, determining that while tea extract and $FeSO_4$ individually can inactivate phages, their combination produces a highly potent antiphage solution [205]. Similarly, silver nanoparticles have exhibited antiviral efficacy against multiple viruses. A recent study demonstrated that silver nanoparticles possess antiviral activity against the H1N1 influenza virus, suggesting their potential as broad-spectrum antiviral agents [206]. These findings support the rationale for exploring the synergistic effects of silver nanoparticles synthesized with tea extracts as a novel antibacteriophage agent.

4.2.1 TeaNPs characterization

In this study, three popular tea varieties—black, green, and Pu-erh (red)—were used to synthesize silver nanoparticles (TeaNPs), where tea extracts acted as both reducing and capping agents. Characterization of TeaNPs revealed core sizes of 64 ± 17 nm for black tea (B-TeaNPs), 61 ± 19 nm for green tea (G-TeaNPs), and 34 ± 7 nm for red tea (R-TeaNPs). B-TeaNPs and G-TeaNPs displayed irregular shapes and polydisperse distributions, whereas R-TeaNPs were smaller, more uniform, and had a narrower size distribution (**Figure 3a-f**).

The UV-Vis analysis revealed plasmonic peaks for G-TeaNPs at 467 nm, B-TeaNPs at 485 nm, and R-TeaNPs at 490 nm, suggesting size-dependent optical properties (**Figure 3g-i**). Notably, R-TeaNPs had a larger plasmon resonance peak, inconsistent with SEM measurements, highlighting how particle shapes influence optical properties. BET analysis indicated that G-TeaNPs had the largest surface area (2.2495 ± 0.1411 m^2/g) despite not being the smallest, likely due to their irregular shapes.

XRD revealed a face-centered cubic crystalline structure of metallic silver in all TeaNPs, with additional peaks at 28° in B-TeaNPs and R-TeaNPs, indicating silver oxide presence (**Figure 3j-l**). This was absent in G-TeaNPs, likely due to the antioxidative properties of catechins, which are particularly abundant in green tea. These findings

underline the influence of tea polyphenol content on the stability and properties of TeaNPs.

FTIR confirmed the presence of functional groups, such as polysaccharides, polyphenols, and caffeine, in the tea extracts and TeaNPs. Notably, green tea extracts exhibited higher concentrations of polyphenols like epigallocatechin gallate (EGCG), which correlated with their superior antimicrobial potential. The UV-Vis spectra of TeaNPs showed peaks corresponding to catechins (270 nm) and their oxidized forms (350 nm) [207], with a shift toward oxidized moieties (**Figure 3g- h**).

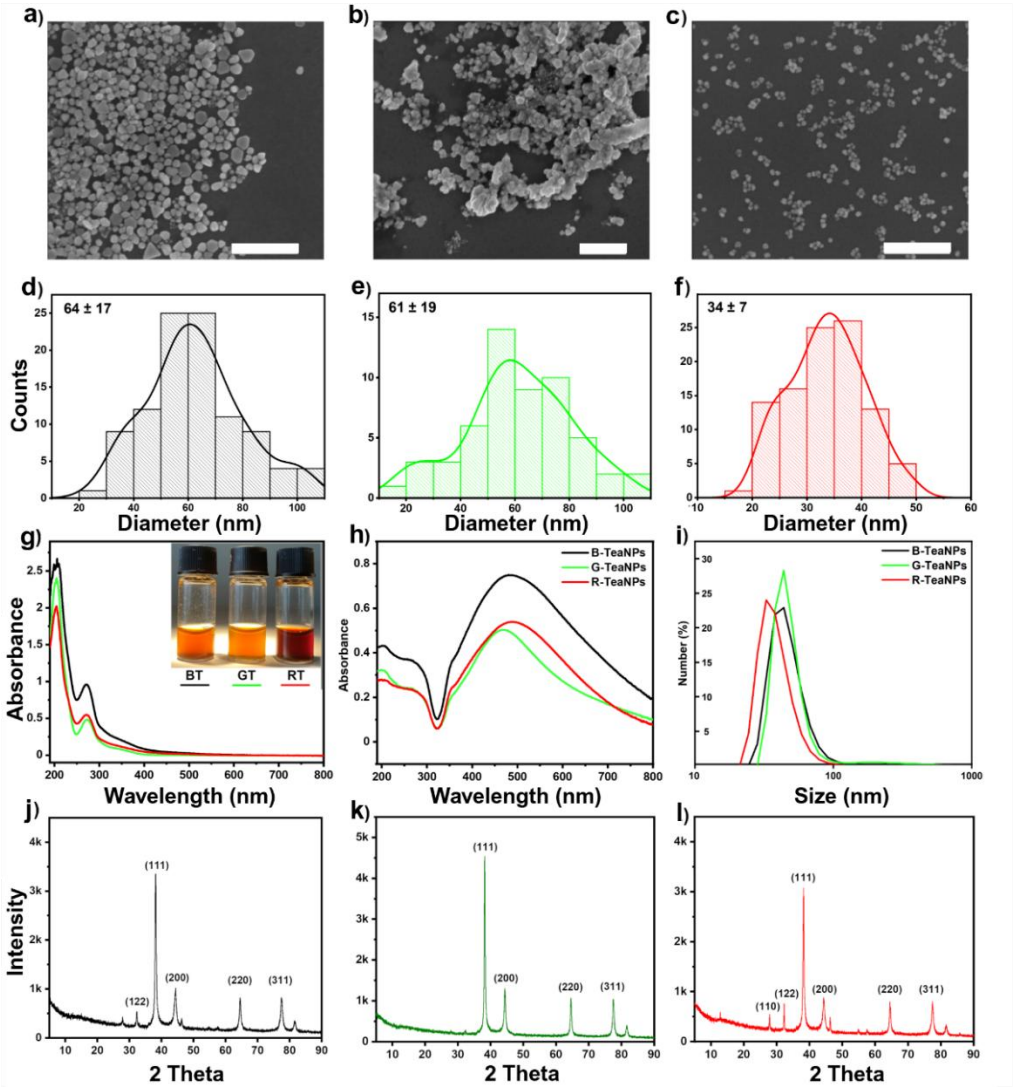

Figure 3. The characterization of synthesized TeaNPs: SEM pictures of **a)** B-TeaNPs, **b)** G-TeaNPs, and **c)** R-TeaNPs. Scale bars correspond to 500 nm. Size distributions of **d)** B-TeaNPs, **e)** G-TeaNPs, and **f)** R-TeaNPs; **g)** UV-Vis spectra of tea extracts, **h)** UV-Vis spectra of TeaNPS (the spectra were normalized) **i)** DLS size estimation of TeaNPs. The XRD diffractograms of **j)** B-TeaNPs, **k)** G-TeaNPs, and **l)** R-TeaNPs. Figure reproduced from Raza et al., 'Enhancing the antimicrobial activity of silver nanoparticles against ESKAPE bacteria and emerging fungal pathogens by using tea extracts,' *Nanoscale Advances, 21(5), 2023,* DOI: 10.1039/D3NA00220A , licensed under CC BY 4.0.

4.2.2 TeaNPs as antiphage agents

After the green synthesis of silver nanoparticles to obtain black tea nanoparticles (B-TeaNPs), green tea nanoparticles (G-TeaNPs), and red tea nanoparticles (R-TeaNPs), their efficacy against bacteriophages was tested. Three model phages were selected for this study: T4, PAO1, and Phi6. T4 was chosen because it is one of the most abundant and well-studied phages, with a morphology (tailed structure) representative of most known bacteriophages. PAO1, a phage infecting *Pseudomonas aeruginosa*, was selected due to its known resistance, making it an excellent model for evaluating treatments against difficult-to-inactivate phages. Phi6, a lipid-enveloped phage infecting *Pseudomonas syringae*, was included for its unique morphology. Unlike tailed phages, Phi 6 possesses a lipid membrane surrounding its nucleocapsid, resembling the structure of some eukaryotic viruses. This diversity in phage models allowed us to evaluate the broad-spectrum antiphage potential of TeaNPs.

The antiphage experiment was performed by incubating each selected phage (T4, PAO1, and Phi 6) with TeaNPs at a concentration of 1 mg/mL for 24 hours. Phage titers were measured to determine the extent of inactivation compared to untreated controls and a silver nanoparticle control (C-AgNPs, citrate-capped silver nanoparticles, synthesized without tea extracts). The results revealed no significant reduction in phage titers when treated with TeaNPs. The reductions in phage titers were not significant, with a reduction of only around 1 log, particularly in the case of the PAO1 phage. In contrast, the control silver nanoparticles (C-AgNPs), synthesized without tea extracts, showed minimal inactivation. As expected, the lower concentrations of the above nanoparticles also proved ineffective against bacteriophages (not shown).

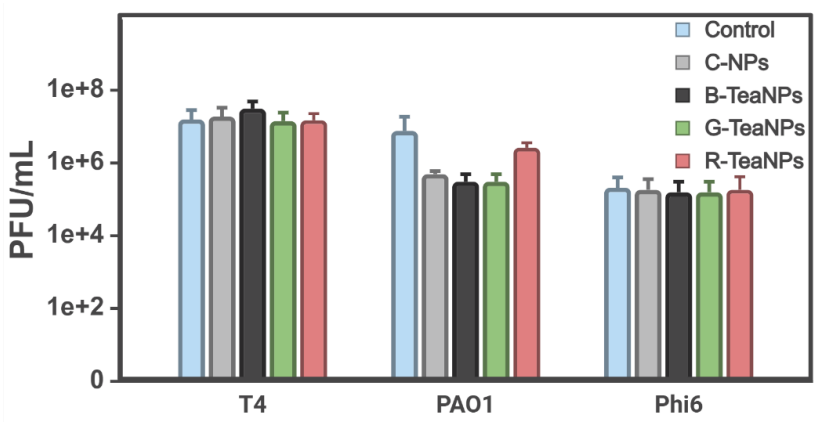

Figure 4. Antiphage activity of black tea nanoparticles (B-TeaNPs), green tea nanoparticles (G-TeaNPs), and red tea nanoparticles (R-TeaNPs) against three model bacteriophages: T4 (infecting *E. coli* BL21), PAO1 (infecting *P. aeruginosa*), and Phi 6 (infecting *P. syringae*). Phage titers are presented as PFU/mL of surviving phages after incubation with TeaNPs at a concentration of 1 mg/mL for 24 hours, compared to the control (untreated phages) and C-AgNPs (citrate-capped Ag NPs).

4.2.3 TeaNPs as antibacterial and antifungal agents

Even though the nanoparticles did not exhibit significant activity against bacteriophages, it was hypothesized that they would still possess notable antimicrobial effects against bacterial strains. To this end, silver nanoparticles synthesized using tea extracts were evaluated against representative strains of Gram-negative bacteria (*Escherichia coli*) and Gram-positive bacteria (*Enterococcus faecium*). This evaluation was based on the known structural differences in the cell envelopes of Gram-positive and Gram-negative bacteria, particularly the significant variation in the thickness of the peptidoglycan layer, which influences susceptibility to nanoparticles. Control experiments were conducted using citrate-capped silver nanoparticles (C-AgNPs) synthesized without tea extracts to compare the effects.

Antibacterial tests were performed using three concentrations of nanoparticles (1 mg/mL, 0.5 mg/mL, and 0.1 mg/mL), with bacteria exposed to the nanoparticles for three hours at room temperature under

stirring. The reduction in bacterial counts was assessed using the plating method.

All TeaNPs displayed superior antibacterial activity compared to C-AgNPs, with 0.1 mg/mL selected for further experiments, allowing a comparative analysis of the antibacterial effects without causing total bacterial elimination. G-TeaNPs showed the most significant efficacy, reducing *E. coli* counts by approximately 80% compared to 20% by C-AgNPs at the same concentration.

The antibacterial potential of TeaNPs was further evaluated against ESKAPE pathogens: *E. faecium, Staphylococcus aureus, Klebsiella pneumoniae, Acinetobacter baumannii, Pseudomonas aeruginosa*, and *Enterobacter cloacae*. At 0.1 mg/mL, G-TeaNPs reduced bacterial counts by 60-90% for all strains except *E. faecium*, which showed a lower reduction of about 25%. Comparatively, C-AgNPs were less effective, with reductions ranging from 12% to 30%. Notably, incorporating tea extracts enhanced the efficacy of nanoparticles against both Gram-positive and Gram-negative bacteria.

The observed differences in TeaNPs' efficacy against Gram-positive and Gram-negative bacteria align with the structural characteristics of their cell walls. Gram-negative bacteria, with thinner peptidoglycan layers but protective lipopolysaccharides, were more susceptible to TeaNPs than Gram-positive bacteria, which have thicker peptidoglycan layers [208]. This discrepancy underscores the multifaceted antimicrobial mechanisms of TeaNPs, which may include direct nanoparticle penetration, silver ion release, and the delivery of polyphenolic compounds from the tea extracts. These results suggest a "poisoned arrow" mechanism, where the nanoparticles deliver both silver ions and bioactive compounds to target bacterial cells effectively.

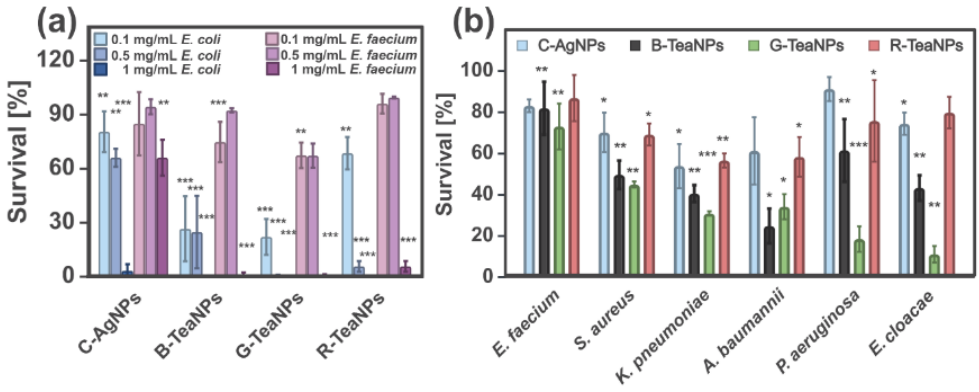

Figure 5. a) Dose compensation of TeaNPs against Gram-positive (*E. faecium*) and Gram-negative (*E. coli*) bacteria with three concentrations: 0.1 mg/mL, 0.5 mg/mL, and 1 mg/mL. **b)** Antibacterial effect of AgNPs (0.1 mg/ml) against the ESKAPE bacterial strains. The results were presented as a percentage of survival, * $p < 0.05$; ** $p < 0.01$; *** $p < 0.001$, p values were calculated with respect to the control sample (not exposed to any AgNPs). Figure reproduced from Raza et al., 'Enhancing the antimicrobial activity of silver nanoparticles against ESKAPE bacteria and emerging fungal pathogens by using tea extracts,' *Nanoscale Advances, 21(5), 2023,* DOI: 10.1039/D3NA00220A , licensed under CC BY 4.0.

To further evaluate the effectiveness of TeaNPs compared to standard antibiotics, *S. aureus* and *E. cloacae* were exposed to ampicillin at two concentrations: the minimum inhibitory concentration (MIC, 0.01 mg/mL) and 10× MIC (0.1 mg/mL), which matched the concentration of TeaNPs used in this study. These bacterial strains were selected for their susceptibility to ampicillin, while additional strains, including *E. faecium*, *K. pneumoniae*, *A. baumannii*, and *P. aeruginosa*, were included for their multidrug-resistant properties.

The antibacterial activity of tea extracts alone was also assessed to determine the synergistic role of the metallic core and the natural capping layer in TeaNPs. Black, green, and red tea extracts were dried using a rotary evaporator and dissolved in 0.9% NaCl to a concentration of 0.1 mg/mL. *S. aureus* and *E. cloacae* were then incubated with these solutions for three hours. Results demonstrated negligible antibacterial

effects of tea extracts alone, as indicated by the lack of statistically significant changes in bacterial survival (**Figure 6**).

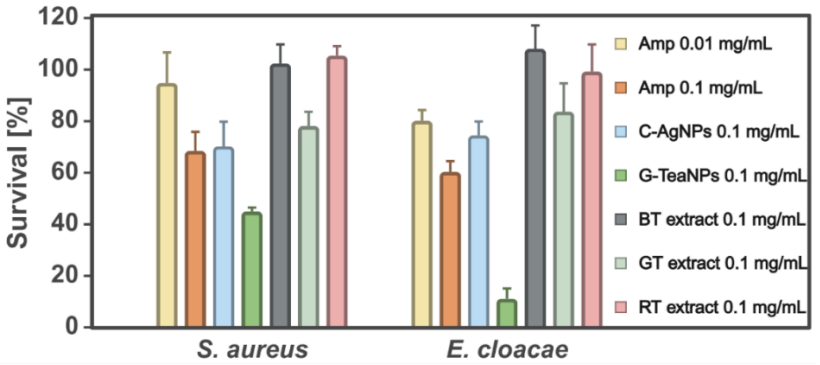

Figure 6. The comparison of antibacterial activity of ampicillin (MIC and 10× MIC), C-AgNPs, G-TeaNPs, and tea extracts in the concentration of 0.1 mg/mL against A) *S. aureus* and B) *E. cloacae*. The results were presented as a percentage of survival, * $p < 0.05$; ** $p < 0.01$; *** $p < 0.001$, p values were calculated with respect to the control sample (not exposed to any AgNPs). Figure reproduced from Raza et al., 'Enhancing the antimicrobial activity of silver nanoparticles against ESKAPE bacteria and emerging fungal pathogens by using tea extracts,' *Nanoscale Advances, 21(5), 2023,* DOI: 10.1039/D3NA00220A , licensed under CC BY 4.0.

To assess whether the addition of tea extracts during the synthesis of silver nanoparticles (AgNPs) is crucial for enhancing their antimicrobial activity, an experiment was conducted by mixing citrate-capped silver nanoparticles (C-AgNPs) with tea extracts (black tea, BT; green tea, GT; red tea, RT) post-synthesis (**Figure 7**). C-AgNPs (1 mg/mL) were combined with tea extracts (1 mg/mL in PBS buffer), diluted to a final concentration of 0.1 mg/mL, and tested against *E. coli* BL21 (~10^5 CFU/mL). Controls included C-AgNPs alone, as well as pre-synthesized B-TeaNPs, G-TeaNPs, and R-TeaNPs at the same concentration.

Adding tea extracts to C-AgNPs moderately enhanced their antibacterial activity, reducing *E. coli* survival from 80% to 60-65%. Among the mixtures, C-AgNPs with green tea extract (GT) showed slightly better performance (60% survival) compared to those with black tea (BT) or red tea (RT) extracts. However, TeaNPs synthesized directly

with tea extracts exhibited significantly greater antibacterial activity compared to C-AgNP mixtures. For instance, B-TeaNPs reduced survival to 45% compared to 65% in the C-AgNP+BT mixture, while G-TeaNPs reduced survival to 35% compared to 60% in the C-AgNP+GT mixture. This indicates that using tea extracts during AgNP synthesis yields superior antibacterial effects, likely due to synergistic or structural modifications during the synthesis process. Further studies are required to understand these phenomena.

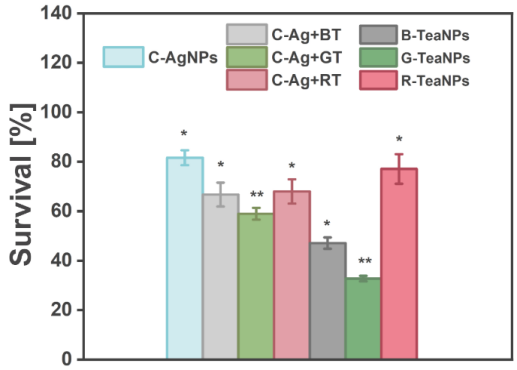

Figure 7. The comparison of antibacterial activity of citrate-capped silver nanoparticles (C-AgNPs), C-AgNPs mixed with tea extracts (BT, GT, RT) and adequate TeaNPs (B-TeaNPs, G-TeaNPs, R-TeaNPs) on *E. coli*. The results were presented as a percentage of survival, * $p < 0.05$; ** $p < 0.01$; *** $p < 0.001$, p values were calculated with respect to the control sample (not exposed to any AgNPs).

Next, the green-synthesized tea nanoparticles were tested against fungal pathogens, given the growing concern over multidrug-resistant fungal infections and the limited availability of effective antifungal treatments. The antifungal potential of TeaNPs was tested against multiresistant strains of *C. auris* and *C. neoformans*.

C. auris and *C. neoformans* were ideal model organisms for these experiments because they represent significant global health threats due to their multidrug resistance and high mortality rates in immunocompromised individuals [209–211]. Their differing pathogenic mechanisms and environmental adaptability provided a robust platform

to evaluate the antifungal efficacy and broad-spectrum potential of green-synthesized tea nanoparticles.

These experiments included citrate-capped AgNPs as a control and were performed at three concentrations: 1 mg/mL, 0.5 mg/mL, and 0.1 mg/mL. Yeast suspensions were incubated with nanoparticles at room temperature for three hours, and changes in cell counts were recorded.

TeaNPs, particularly G-TeaNPs, displayed significant antifungal activity. At a concentration of 0.5 mg/mL, G-TeaNPs reduced *C. auris* cell numbers by approximately 80%, while at 0.1 mg/mL, *C. neoformans* exhibited a reduction of around 90%. At the same concentration, C-AgNPs showed small effectiveness, with a reduction of about 25% (**Figure 8a**).

Control experiments confirmed that tea extracts alone did not exhibit antifungal properties. Interestingly, *C. auris* sometimes exhibited growth slightly above 100% in the presence of red tea extract, potentially due to the metabolism of extract components, which has been noted to facilitate biofilm formation in other *Candida* species (**Figure 8b**) [212].

The enhanced antifungal activity of TeaNPs highlights their potential as a therapeutic agent at lower concentrations. However, higher concentrations were necessary for *C. auris* than for *C. neoformans*, possibly due to the resistance mechanisms triggered by TeaNP exposure, akin to those induced by fungicidal drugs. A concentration of 0.5 mg/mL was selected for reliable fungal inhibition across species.

TeaNPs' antifungal mechanism likely involves disrupting cell envelope integrity, consistent with known AgNP activities, such as reactive oxygen species (ROS) generation, DNA replication interference, and increased membrane permeability [198]. The specific effectiveness of TeaNPs appears to correlate with the polyphenol content from the tea extracts [213], further supporting their "poisoned arrow" mechanism.

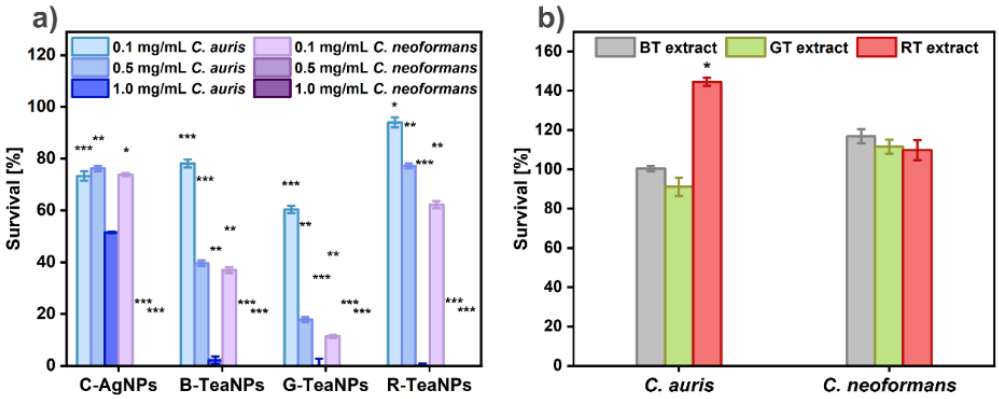

Figure 8. **a)** Dose compensation of TeaNPs against *C. auris* and *C. neoformans* with three concentrations: 0.1 mg/mL, 0.5 mg/mL, and 1 mg/mL. **b)** Antimicrobial activity of tea extracts (0.5 mg/mL) against *C. auris* and *C. neoformans*. The results were presented as a percentage of survival, * $p < 0.05$; ** $p < 0.01$; *** $p < 0.001$, p values were calculated with respect to the control sample (not exposed to any AgNPs). Figure reproduced from Raza et al., 'Enhancing the antimicrobial activity of silver nanoparticles against ESKAPE bacteria and emerging fungal pathogens by using tea extracts,' *Nanoscale Advances, 21(5), 2023,* DOI: 10.1039/D3NA00220A , licensed under CC BY 4.0.

4.2.4 TeaNPs – bacteriophage cocktails

TeaNPs were found to be safe for phages while exhibiting strong antibacterial activity - an outcome contrary to initial expectations. However, this unexpected result opened the possibility of utilizing TeaNP-phage combinations as innovative antibacterial agents. While antibiotic-phage cocktails are well-documented and extensively studied, research on phage-nanoparticle mixtures remains limited. This is primarily due to the challenge of designing nanostructures that selectively target bacteria while preserving phage viability.

Combining bacteriophages with nanoparticles (phage–NP cocktails) has emerged as a promising strategy to enhance antimicrobial efficacy. Nanoparticles can facilitate the attachment of phages to bacterial surfaces, improve phage stability, and even help overcome bacterial resistance mechanisms. Recent studies, such as the work by

Golec et al., demonstrated that silver nanoparticles can boost phage infectivity and bacterial killing efficiency, highlighting the synergistic potential of these hybrid systems [214]. Other research also shows that nanoparticles can protect phages from environmental stressors, prolonging their activity in challenging conditions [215]. Together, these findings provide a strong foundation for developing advanced phage–nanoparticle systems for antibacterial applications.

After confirming that the nanoparticles did not have any direct inactivating effect on phages, testing of phage-nanoparticle (phage-NP) cocktails was carried out using green tea silver nanoparticles. G-TeaNPs had previously been identified as the most effective against bacteria and fungi among a series of silver particles prepared with extracts from various teas. [216].

For the novel phage-NPs cocktails, *S. enterica*, one of the most frequently occurring foodborne pathogens (a Gram-negative bacterium), and a methicillin-resistant strain of *S. aureus* (MRSA, a Gram-positive bacterium) were selected. The efficacy of these combinations was assessed across a range of rates of infection (ROI, representing the ratio of phages to bacterial cells) and concentrations of nanoparticles. In **Figure 9a**, ROI = 1 was kept constant, but the concentration of G-TeaNPs varied from 0.1 mg/mL to 0.0001 mg/mL. **Figure 9b** shows the results of experiments where the concentration of G-TeaNPs was constant (0.001 mg/mL), but ROIs varied from 1 to 100.

Adding phages at an ROI = 10 or higher significantly enhanced antibacterial effects, allowing for a substantial reduction in the required working concentrations of G-TeaNPs. Specifically, with phages at ROI = 10, the bacterial survival rate decreased to 10–20%, depending on the species, even when the concentration of G-TeaNPs was as low as 0.001 mg/mL (1 µg/mL). In contrast, a similar efficacy with G-TeaNPs alone required a 100 times higher concentration (0.1 mg/mL).

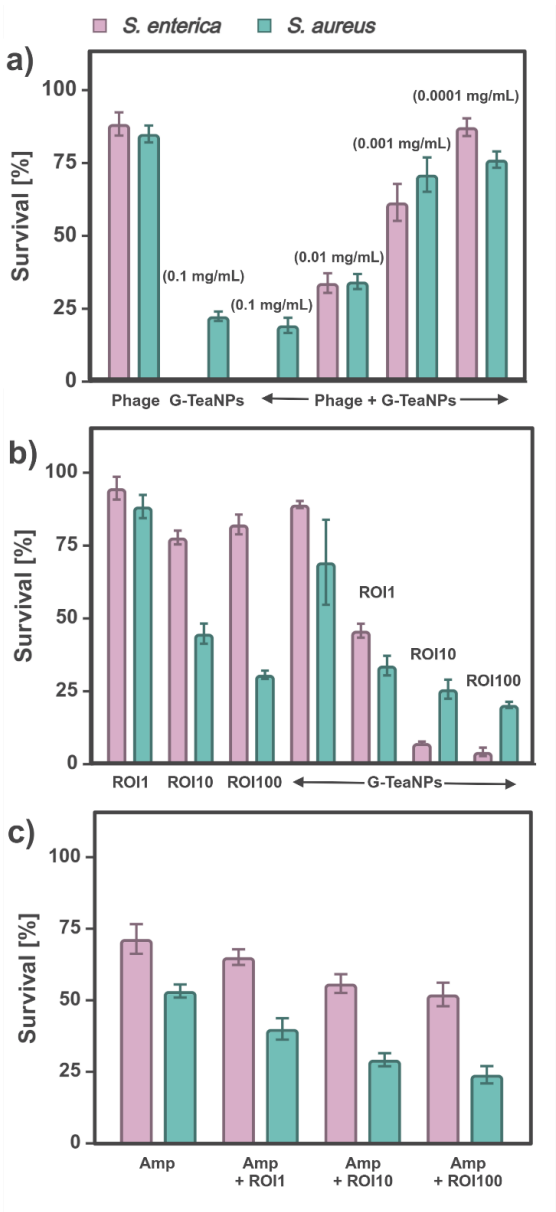

Figure 9. a) Antibacterial activity of G-TeaNPs (0.1 mg/mL to 0.0001 mg/mL) in combination with bacteriophages (ROI = 1). **b)** Antibacterial efficacy of phage-NPs cocktails ([G-TeaNPs] = 0.001 mg/mL) at ROIs ranging from 1 to 100. **c)** Survival of *S. aureus* (Gram-positive) and *S. enterica* (Gram-negative) after treatment with ampicillin (AMP) alone or in combination with bacteriophages at varying ROIs.

For comparison with commonly used phage-antibiotic cocktails, we tested the combined effects of bacteriophages and ampicillin (AMP) against *S. aureus* and *S. enterica* across various rates of infection (ROIs). The results showed that the AMP-phage combination was more effective against *S. aureus* (**Figure 9d**). Specifically, AMP alone reduced bacterial survival to approximately 60%, while adding phages further reduced survival to around 30% at ROI 10 and 25% at ROI 100.

In the case of *S. enterica*, the impact of the AMP-phage combination was less pronounced but still significant. AMP alone decreased bacterial survival to approximately 75%. Adding phages reduced survival to around 70% (AMP + ROI 1) and 58% (AMP + ROI 100). Notably, the phage-NPs cocktails at ROIs 10 and 100 achieved far greater reductions in survival, with bacterial survival rates dropping to approximately 10%.

The overall efficacy of the AMP-phage combination was similar to or less than that of the phage-NPs cocktails. This might be crucial when fighting multidrug-resistant bacteria, where antibiotics are not efficient and novel agents are needed. We also underline that these results were obtained after only 3 h incubation. This study demonstrated the potential of green tea extract-capped silver nanoparticles (G-TeaNPs) as multifunctional agents, combining antimicrobial efficacy with broad biological applicability.

4.3 Iron-based strategies for combatting bacteriophages

In addition to silver, iron chemistry also provides a promising approach to combat bacteriophages, as their life cycle often exploits bacterial iron uptake mechanisms. The presence of Fe ions in phage tails, as suggested by the Ferrojan horse hypothesis, facilitates adsorption to bacterial cell receptors and subsequent lysis [217,218]. Fe ions present in the tails of bacteriophages assist in adsorption to the receptors of the host cells [218]. Iron-based compounds reduce phage titers through three primary mechanisms: (i) adsorption of virions onto nanoparticle surfaces [217], (ii) redox reactions [219], and (iii) the action of free iron ions [220].

Iron hydroxides such as hematite (α-Fe_2O_3), goethite (α-FeOOH), magnetite (Fe_3O_4), and amorphous iron (III) hydroxide ($Fe(OH)_3$) exhibit similar virus adsorption capabilities. However, adsorption rates vary in the order FeOOH > Fe_2O_3 > Fe_3O_4 ≈ $Fe(OH)_3$ [221]. Adsorption to hematite nanoparticles can reduce bacteriophage titers, such as MS2 and rotavirus (RV), by up to 1.5 log within 45 minutes [222]. Iron oxide-modified biosand filters enhance disinfection by adsorbing negatively charged virion particles onto positively charged iron oxides [223]. Additionally, nanoporous iron oxide ceramics eliminate viral contamination from water using ferroxane nanoparticles [224]. Batch reactors with iron granules have also demonstrated inactivation or irreversible adsorption of phages such as MS2 and φX174 [225].

The photocatalytic inactivation of bacteriophages is enhanced by ferrous sulfate via hydroxyl radical production in Fenton's reaction) [226]. Metal-catalyzed Fenton systems cause virus inactivation in natural systems and water treatment by complex oxidation processes [227–229]Free iron ions released from iron-based disinfectants play a role in phage inactivation. At low concentrations, ferrous ions (Fe^{2+}) demonstrate a linear relationship with bacteriophage inactivation, although higher doses may lead to limited decontamination due to flocculation[220]. For instance, Fe^{2+} ions alone (0.1 mM) inactivate up to 1.5 log of MS2 phages, compared to 4 log inactivation achieved via the Fenton process [228]. Ferrous ions are particularly effective against f2 phages due to their higher solubility compared to Fe^{3+} [219,230].

Recently, zero-valent iron (ZVI) has gained attention for its versatile mechanisms of bacteriophage inactivation, including adsorption, redox reactions (e.g., Fe(0) to Fe(II) and Fe(II) to Fe(III)), and release of free iron ions. The oxygen dependency of nZVI (nano-ZVI) is notable; for instance, f2 phages show a 5.1 log reduction when treated with nZVI [230,231]. nZVI's higher surface area, smaller size, and greater reactivity compared to larger particles enhance its effectiveness [231]. nZVI-containing columns also inactivate eukaryotic viruses like Aichi virus, Tulane virus, and murine norovirus [165,232].

Surface passivation of nZVI can be mitigated by oxidants such as $KMnO_4$, H_2O_2, or CrO_4^{2-}, which enhance reactivity in water remediation [233]. Methods of improving the reactivity of nZVI include metal doping to produce bimetallic nanoparticles with Cu, Ni, or Ag that increase the dissolution of iron [234].

In this study, nZVI nanoparticles were synthesized using an unconventional method that excluded $FeSO_4$ to simplify the post-reaction separation of anions [235]. The reduction of iron(III) chloride with sodium borohydride in an aqueous solution produced nZVI under patented conditions [236]. Scanning electron microscopy previously confirmed the sub-100 nm size of the synthesized nZVI particles [235]. The synthesis and purification of ZVI was executed by the team of Prof. Foltynowicz in Poznań.

A comparison between reduced (pristine; ZVI) and oxidized ZVI (O ZVI) is shown in **Figure 10a-b**. Large aggregates were visible because powdered samples were used for sample preparation and not ZVI dispersed in the solvent. This was done to speed up the analysis and avoid unwanted oxidation of pristine ZVI. Both pristine and oxidized ZVI nanoparticles were similar in size and shape, but oxidation changed the surface features of the studied material. The surface of oxidized ZVI resembled macroscopic rust, as expected.

Given the current knowledge of the antiviral properties of ZVI nanoparticles, and to evaluate their broad-spectrum potential against bacteriophages, anti-phage tests were conducted. An hourly analysis was performed to assess the effects of ZVI nanoparticles in three different oxidation states: native (reduced) ZVI, partially oxidized ZVI (PO ZVI), and fully oxidized ZVI (O ZVI), as shown in **Figure 10c**. Three forms of ZVI were selected to determine which mechanism of action, i.e., adsorption, redox reactions, or the effect of released iron ions, dominates in the inactivation of phages. Pristine ZVI can undergo redox reactions with viral components even in a degassed medium and inert atmosphere. For partially oxidized ZVI, exposure to air triggers redox reactions within the nanoparticles while also allowing the release of iron ions that create local environments conducive to phage inactivation. In contrast, fully

oxidized ZVI can release iron ions, but no redox reactions occur due to the complete oxidation of the nanoparticles. In all cases, adsorption of virions onto the ZVI particle surfaces is possible, which is also essential for redox reactions in pristine ZVI.

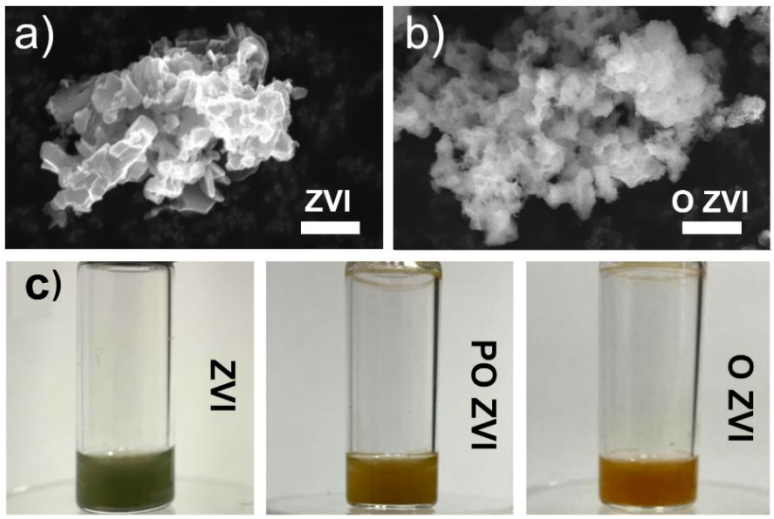

Figure 10. SEM pictures of **a)** pristine (reduced) ZVI and **b)** oxidized ZVI (O ZVI). Scale bars correspond to 1 µm. **C)** Visual discrimination between ZVI, partially oxidized ZVI (PO ZVI), and oxidized ZVI (O ZVI). Figure reproduced from Raza et al., 'The Effect of Zero-Valent Iron Nanoparticles (nZVI) on Bacteriophages,' *Viruses, 14(867), 2022,* DOI: 10.3390/v14050867, licensed under CC BY 4.0.

To prepare the partially oxidized samples (PO ZVI), the ZVI suspension was exposed to air for exactly 2 minutes prior to the experiment. Fully oxidized samples (O ZVI) were obtained by allowing the ZVI suspension to oxidize completely through exposure to air for two days. The visual differences between ZVI, PO ZVI, and O ZVI are depicted in Figure 17c, highlighting the progressive changes in their appearance.

These three forms were selected to identify the dominant mechanism of action against phages, whether it be adsorption, redox reactions, or the effect of released ions. The samples were handled under controlled conditions throughout the experiment to maintain their respective oxidation states. Native ZVI samples were kept in an inert

atmosphere, retaining their green color. In contrast, PO ZVI, exposed to air, transitioned from green to orange during the experiment, while O ZVI, which had already been fully oxidized, remained orange throughout. This setup ensured a clear distinction between the oxidation states and their corresponding antiviral mechanisms.

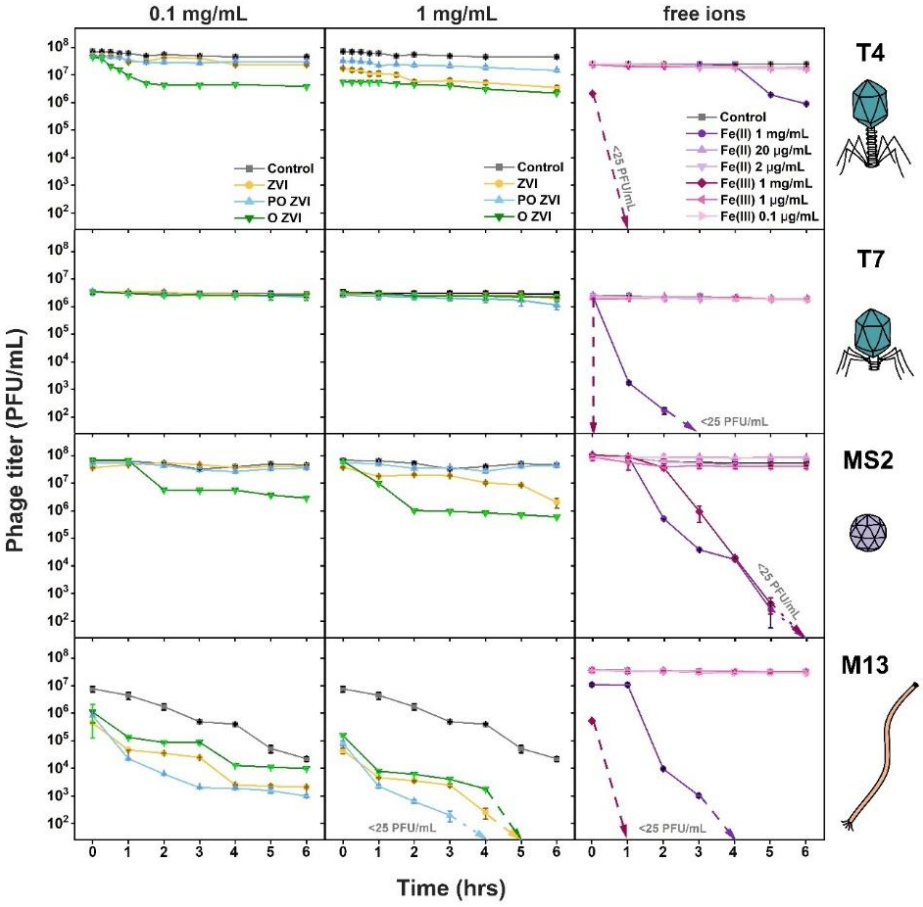

Figure 11. PFU/mL calculation of bacteriophages in TM buffer, ZVI (0.1 and 1 mg/mL), partially oxidized and M13 in the presence of Fe (II) (1 mg/mL 20 µg/mL and 2 µg/mL) and Fe (III) ions (1 mg/mL, 1 µg/mL and 0.1 µg/mL). Figure reproduced from Raza et al., 'The Effect of Zero-Valent Iron Nanoparticles (nZVI) on Bacteriophages,' *Viruses, 14(867), 2022,* DOI: 10.3390/v14050867, licensed under CC BY 4.0.

During the experiments, no significant increase in phage inactivation was observed when the ZVI concentration was increased from 1 mg/mL to 10 mg/mL, likely due to nanoparticle aggregation at higher concentrations. Additionally, no measurable antiviral effect was observed at lower ZVI concentrations, such as 0.01 mg/mL. This highlights the importance of optimizing ZVI concentrations to balance efficacy and stability during antiviral applications.

The inactivation efficiency of ZVI nanoparticles against the selected bacteriophages followed the order: M13 > MS2 ≈ T4 > T7, with reductions of 7 log, 2 log, 1.5 log, and 0.5 log PFU/mL within the first 6 hours, respectively (**Figure 11**). Notably, partially oxidized ZVI (PO ZVI) was the most effective against M13, while oxidized ZVI (O ZVI) demonstrated higher efficacy against T4 and MS2. In contrast, T7 exhibited the highest resistance to all forms of ZVI. The slight decrease observed in the control samples for M13 was attributed to the mechanical agitation required to prevent nanoparticle sedimentation.

To investigate the impact of free Fe^{2+} and Fe^{3+} ions on bacteriophages, phages were exposed to iron(II) chloride ($FeCl_2$) and iron(III) chloride ($FeCl_3$) solutions. Initially, a scenario was tested where all ZVI nanoparticles (1 mg/mL) were assumed to dissolve, resulting in an equivalent 1 mg/mL concentration of iron ions. To better reflect realistic environmental conditions, lower concentrations of released ions were approximated and tested: 20 µg/mL and 2 µg/mL for Fe^{2+} and 1 µg/mL and 0.1 µg/mL for Fe^{3+}.

These concentrations were derived from literature data on the solubility of iron compounds. For example, at pH 7, approximately 250 µM Fe^{2+} ions (139 µg/mL) are released from 0.7 mg/mL magnetite (Fe_3O_4) suspensions [237]. Additionally, the European Chemicals Agency (ECHA) reports that the concentration of dissolved iron ions in a 10 mg/mL Fe_2O_3 solution is typically below 1 µg/mL. These values, alongside other published solubility data [238], informed the chosen experimental concentrations.

At realistic Fe^{2+} and Fe^{3+} ion concentrations, no significant effect on bacteriophage viability was observed after 6 hours of

incubation (**Figure 11**). However, at higher concentrations (1 mg/mL Fe^{2+} and Fe^{3+}), significant phage inactivation occurred. Fe^{3+} ions demonstrated more pronounced antiviral activity, causing complete inactivation of T7, MS2, and M13 phages within minutes. In contrast, Fe^{2+} ions had minimal effects on T4 phages, though Fe^{3+} ions caused their complete inactivation.

Interestingly, Fe^{3+} ions acted much faster against T4, M13, and T7 compared to MS2, with T7 showing inactivation within approximately 30 seconds of exposure. These findings suggest that while free iron ions can inactivate bacteriophages at high concentrations, their role in realistic environmental conditions appears negligible. Instead, localized interactions of ions released near ZVI particle surfaces may play a more prominent role in the observed antiviral mechanisms.

To further investigate the long-term effects, phages were incubated with all three forms of ZVI for 48 hours under controlled conditions. Throughout the experiment, native ZVI retained its green color in an inert atmosphere, while PO ZVI gradually turned orange upon air exposure, and O ZVI remained consistently orange. After 48 hours, M13 was completely inactivated across all ZVI forms, reaching the detection limit (~25 PFU/mL), corresponding to a 7 log reduction **Figure 12**.

In contrast, T7 displayed remarkable resistance, with reductions of only 80.4%, 66.6%, and 52.3% observed after exposure to ZVI, PO ZVI, and O ZVI, respectively. For MS2 and T4, O ZVI showed the highest inactivation, achieving between 99.99% and 99.92% reduction in titers. Prolonged incubation improved the efficacy of pristine ZVI against T4, increasing the reduction from 1 log to 5 log after 48 hours. However, no such improvement was observed for MS2, which remained at a consistent 1–2 log reduction. Interestingly, PO ZVI, despite limited activity against MS2 and T4 within the first 6 hours, achieved only a modest 2 log reduction after 48 hours.

The observed antiviral activity of ZVI nanoparticles likely arises from three primary mechanisms: (a) redox processes, (b) the effect of released Fe^{2+} and Fe^{3+} ions, and (c) the adsorption of phages onto ZVI

surfaces. Experimental results indicated that the contribution of free iron ions in bulk solution was minimal, as realistic concentrations of Fe^{2+} and Fe^{3+} ions did not result in significant phage inactivation. However, localized environments at the ZVI surface, where higher ion concentrations and redox activity occur, could contribute to phage inactivation upon adsorption. This suggests that effective inactivation is restricted to virions adsorbed directly onto the ZVI surface.

Additionally, experimental observations revealed that T7 phage likely does not efficiently adsorb onto ZVI surfaces, explaining its resistance across all ZVI forms. Previous studies by Armanious et al. have shown that phage adsorption properties vary significantly, even among morphologically similar phages, due to differences in capsid surface chemistry [239].

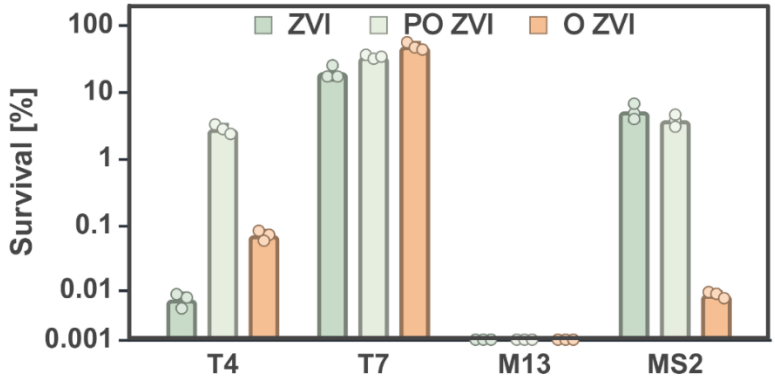

Figure 12. 48 h experiment of bacteriophages in the presence of ZVI, PO ZVI, and O ZVI, all at a concentration of 1 mg/mL. The squares on each bar represent the three biological repetitions, and the bar itself is the average. The initial concentration of the phages was around 10^7 PFU/mL in all cases. Figure modified from Raza et al., 'The Effect of Zero-Valent Iron Nanoparticles (nZVI) on Bacteriophages,' *Viruses, 14(867), 2022,* DOI: 10.3390/v14050867, licensed under CC BY 4.0.

In contrast, M13 phages exhibited high susceptibility across all ZVI forms, with PO ZVI showing slightly greater effectiveness. The precise mechanism remains unclear, as there is limited data on interactions between filamentous phages and ZVI nanoparticles. However, it is

hypothesized that the inactivation of M13 may result from direct contact with ZVI surfaces, as evidenced by the similarity in titer reduction dynamics across all forms of ZVI (**Figure 12**).

Overall, these findings highlight the complex interplay of adsorption, redox reactions, and ion-mediated effects in determining the antiviral efficacy of ZVI nanoparticles against different bacteriophages.

To gain insight into the morphological changes induced by ZVI nanoparticles, Transmission Electron Microscopy (TEM) was performed on partially oxidized ZVI (PO ZVI) and fully oxidized ZVI (O ZVI) samples (**Figure 13**). Pristine ZVI was excluded from TEM analysis due to its susceptibility to oxidation during sample preparation. Two phages - T4 and M13 - were selected for visualization because they exhibited the most pronounced effects.

In the case of T4 phages, exposure to O ZVI resulted in significant structural damage, with numerous tails detached from the virions (**Figure 13b**) and capsids showing signs of structural disintegration (**Figure 13c**). These observations suggest that physical and possibly chemical interactions with O ZVI disrupted the phage structure.

For M13 phages, STEM revealed an interesting phenomenon. Despite the phage titer being the same in control and experimental samples, fewer virions were observed in the supernatant of ZVI-treated samples (**Figure 13e**). This suggests that ZVI nanoparticles may have adsorbed to M13 virions, causing sedimentation of virus-nanoparticle aggregates. To confirm this, the samples were agitated, and subsequent imaging revealed a higher concentration of virions in freshly suspended samples, with clear associations between M13 filaments and ZVI particles (**Figure 13f**).

These results point to two possible mechanisms for M13 phage inactivation: structural damage caused by direct interactions with ZVI nanoparticles and inhibition of phage functionality due to the adsorption of nanoparticles along the filament, potentially obstructing attachment to bacterial pili or interfering with capsomere function.

To further validate these observations, phage recovery experiments were conducted using Tween 20, a surfactant with a strong

affinity for surfaces. No viable M13 virions were detected after recovery attempts, supporting the hypothesis that phage inactivation was not solely due to adsorption but also structural or functional damage. Additionally, the absence of a zone of inhibition around ZVI-treated samples suggests that immobilized phages remain inactive and cannot infect bacterial hosts.

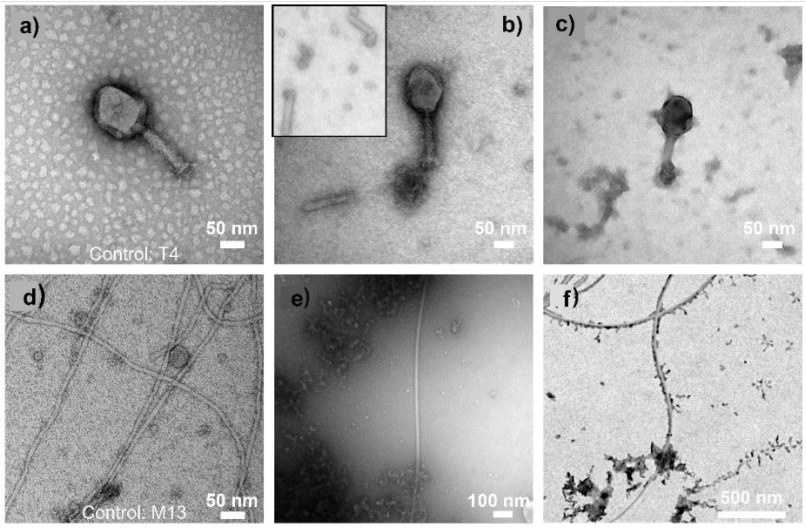

Figure 13. TEM visualization of bacteriophages. **a)** T4 bacteriophages in the absence of zero-valent iron. **b), and c)** T4 bacteriophages exposed to O ZVI. Inset in **b)** shows the detached tails, which were in abundance in the sample. **d)** M13 bacteriophages in the absence of zero-valent iron, **e)** Supernatant of the suspension containing only a small number of M13 virions, among which most were in contact with nZVI particles. **f)** STEM image of the freshly agitated suspension wherein nZVI and M13 appeared in close proximity. Figure reproduced from Raza et al., 'The Effect of Zero-Valent Iron Nanoparticles (nZVI) on Bacteriophages,' *Viruses, 14(867), 2022,* DOI: 10.3390/v14050867, licensed under CC BY 4.0.

4.5 Copper-based coating as antiviral and antimicrobial agents

While silver and iron exhibit antimicrobial properties, as discussed earlier, it was time to explore another well-known metal, copper (Cu), renowned for its antiviral capabilities. Copper, copper ions, and copper-based nanostructures have demonstrated antiviral activity against various

viruses, including poliovirus [240], Human Immunodeficiency Virus Type 1 (HIV-1) [241], and West Nile Virus (WNV) [242]. Moreover, copper has been found to act synergistically with free chlorine, effectively inactivating bacteriophages such as MS2 [243], PhiX174, Phi6, and T7 [244]. Salah et al. highlighted the role of reactive oxygen species (ROS) generation and ion release from copper surfaces in virus inactivation, particularly against SARS-CoV-2, influenza A, and murine norovirus [245].

Electrodeposition is one of the oldest and environmentally friendly methods for producing nanostructured layers, mainly in the form of nanowires, nanotubes, or particles with well-defined facets [246–248]. Cu_2O layers have been obtained using various electrolytes, surfactants, and pH adjustments [249], which significantly influence the grain morphology and packing structure. Polyhedral shapes and compact oxide layers have also been synthesized by complexing copper ions [250]. This methodology made it possible to modify the surface properties of Cu_2O using additional agents directly.

In this study, three different copper-based coatings were prepared by Dr Anna Kusior and her team in Kraków [251]: CuL, CuL-PVP, and CuL-D(+)G. All were synthesized under the same conditions, with CuL-PVP supplemented with poly(vinylpolypyrrolidone) (PVP) and CuL-D(+)G with glucose. Although PVP adsorbs onto highly active surfaces (high-index facets) [252], glucose serves to reduce or maintain low levels of elemental oxidation.

Figure 14 shows SEM images of the copper oxide layers grown via electrochemical deposition. All samples consist of aligned, polyhedral-shaped crystals. The packing of these crystal-like particles varied depending on the surfactant agent used during synthesis. It is assumed that the large elongated polyhedral crystals grow above the CuL-D(+)G surface due to internal stresses that arise during the growth of crystal-like grains.

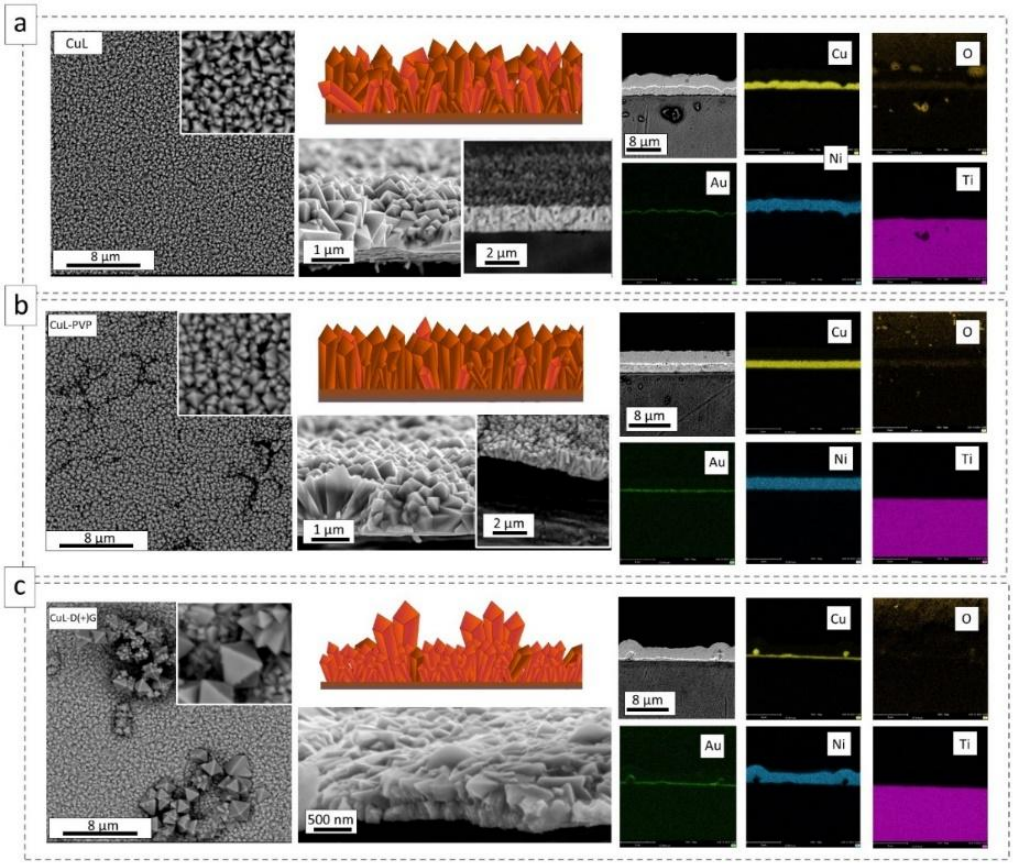

Figure 14. SEM images of the deposited (a) CuL, (b) CuL-PVP, and (c) CuL-D(+)G copper oxide layers (top view and side view) with the cross-sectional microstructure EDS analysis. Figure reproduced from Kusior et al., 'Copper Oxide Electrochemical Deposition to Create Antiviral and Antibacterial Nanocoatings,' *Langmiur, 40(29), 2024,* DOI: 10.1021/acs.langmuir.4c00642, licensed under CC BY 4.0.

The antiviral activity of CuL, CuL-PVP, and CuL-D(+)G coatings was tested against bacteriophages T4 and MS2. Results showed a 2.5–3 log reduction in T4 titer for all coatings, with CuL-D(+)G performing slightly better (**Figure 15a**). For MS2, CuL reduced the phage titer by 2.5 logs, while CuL-PVP and CuL-D(+)G caused a 5-log reduction, likely due to the additives used in their synthesis [90,155]. The antibacterial activity was evaluated against *E. coli* and *S. aureus* (**Figure 15b**). CuL caused

a 1-log reduction in *E. coli*, while CuL-PVP reduced the titer by 2 logs, and CuL-D(+)G decreased it by 5 logs. For *S. aureus*, all materials showed similar activity with a 2.5 log decrease in bacterial titer. Non-modified titanium did not show significant activity. CuL-D(+)G's enhanced activity may be due to its unique morphology, with Cu(I) being more toxic to *E. coli*, particularly under anaerobic conditions, and potentially through a Fenton-like reaction that produces reactive oxygen species [253–255].

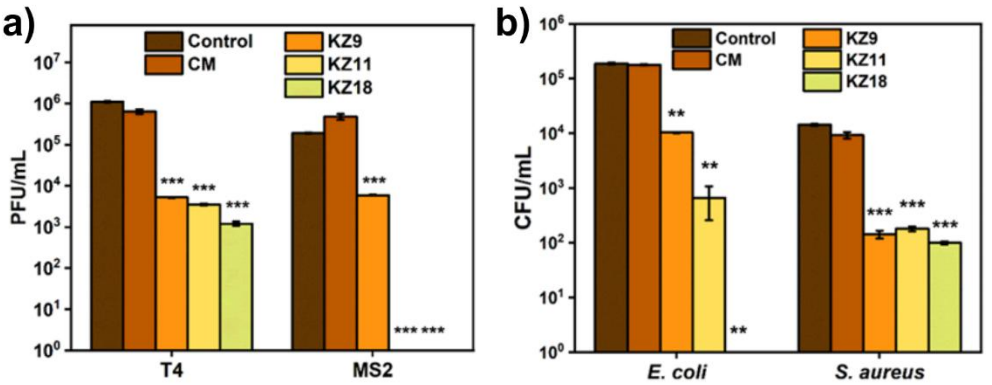

Figure 15. The evaluation of the biological activity of copper oxide nanocoatings. (a) The antiviral activity of CuL (KZ9), CuL-PVP (KZ11), and CuL-D(+)G (KZ18) against T4 and MS2 bacteriophages. The results were presented as plaque-forming units per milliliter (PFU/mL). (b) The antibacterial activity CuL, CuL-PVP, and CuL-D(+)G against *E. coli* and *S. aureus*. The results were presented as colony-forming units per milliliter (CFU/mL). CM stands for control material, i.e., unmodified substrate, and control is the suspension of phages or bacteria without anything added to it. Statistical analysis was performed using Student`s t-test with respect to CM, * $p < 0.05$; ** $p < 0.01$; *** $p < 0.001$. Figure reproduced from Kusior et al., 'Copper Oxide Electrochemical Deposition to Create Antiviral and Antibacterial Nanocoatings,' *Langmiur, 40(29), 2024,* DOI: 10.1021/acs.langmuir.4c00642, licensed under CC BY 4.0.

The findings of this study highlight the significant antiviral and antibacterial efficacy of copper oxide nanocoatings, particularly when modified with additives such as PVP and glucose. The coatings demonstrated potent activity against bacteriophages T4 and MS2, as well as representative strains of Gram-negative and Gram-positive bacteria (*E. coli* and *S. aureus*). CuL-D(+)G exhibited superior antiviral and

antibacterial activity, which is attributed to its composition and morphology, including glucose presence and the formation of large polyhedral crystals rich in Cu_2O. These findings suggest potential biomedical applications for the synthesized coatings due to their antimicrobial properties and tailored compositions.

4.6 Chapter summary

This chapter looks at how nanotechnology is used in different areas like food science, medicine, microbiology, and cleaning up the environment. Nanomaterials are useful in many ways—they help make food safer, improve packaging, and support eco-friendly farming. In medicine, they play a big role in better tests, targeted drug delivery, healing tissues, and fighting antibiotic-resistant bacteria.

The use of silver nanoparticles (AgNPs) as antimicrobial agents is highlighted, particularly their application in addressing bacterial and viral contamination. AgNPs synthesized *via* green methods using natural tea extracts are shown to be effective against bacteria and fungi, offering a sustainable and eco-friendly alternative to chemical synthesis. Green-synthesized tea nanoparticles (TeaNPs) displayed superior antibacterial and antifungal properties compared to citrate-capped AgNPs, with green tea nanoparticles (G-TeaNPs) emerging as the most effective variant. This is attributed to green tea's high polyphenol content, enhancing nanoparticle stability and bioactivity.

Further advancements include the combination of bacteriophages with nanomaterials, particularly in the form of phage-TeaNP cocktails. These combinations leverage the synergistic effects of both phages and nanoparticles to enhance antimicrobial efficacy. The phage-TeaNP cocktails have demonstrated significant antiviral and antibacterial activity, providing a promising strategy for the treatment of bacterial infections.

This chapter also examines iron-based strategies, including zero-valent iron (ZVI) nanoparticles, for bacteriophage inactivation. ZVI nanoparticles exhibit diverse antiviral mechanisms, including redox reactions, ion release, and adsorption onto virions. Experiments demonstrated ZVI’s potential to inactivate a variety of bacteriophages, such as T4, T7, M13, and MS2, revealing differences in susceptibility

based on phage morphology and surface properties. Prolonged exposure to ZVI or oxidized ZVI effectively reduced phage titers, with adsorption and redox processes identified as key contributors to inactivation.

Lastly, copper oxide nanocoatings, including CuL, CuL-PVP, and CuL-D(+)G, present another powerful approach for antiviral and antibacterial applications. These copper-based coatings demonstrate strong antimicrobial properties, particularly against bacteriophages like T4 and MS2, as well as bacteria such as *E. coli* and *S. aureus*. The addition of PVP and glucose during the synthesis of the coatings enhances their activity, with CuL-D(+)G exhibiting superior performance. The combination of copper nanocoatings with other antimicrobial agents opens new avenues for sustainable and effective pathogen control.

In conclusion, this chapter highlights the role of nanotechnology in microbiology. While nanoparticles bear a load of toxicity, which can be mitigated by fine-tuning their size, charge, and composition [152]. Silver nanoparticles (AgNPs) remain among the most widely used disinfectants due to their broad-spectrum activity against bacteria, fungi, and viruses; however, other metallic nanoparticles are increasingly gaining attention. Nanoparticles offer advantages over conventional antimicrobials by evading bacterial resistance mechanisms, although reports of emerging nanoparticle resistance are beginning to appear. Their antimicrobial actions involve cellular uptake, contact killing, ion release, and mechanical stress. In some circumstances, combining bacteriophages with nanostructures might, on the other hand, enhance antibacterial effects [200,256], as demonstrated in this chapter. In particular, green tea-synthesized silver nanoparticles (G-TeaNPs) showed strong antibacterial and antifungal activities but limited antiviral properties, suggesting their potential use in combination therapies with bacteriophages. However, achieving selective inactivation of virions without harming bacterial or mammalian cells remains a significant challenge. Most antiviral agents, including copper-based structures discussed here, also exhibit antibacterial activity, complicating efforts to design truly selective antiviral strategies. This underscores the need for continued innovation in developing highly specific and safe antimicrobial materials.

CHAPTER 5
Naturally selective antiviral compounds

Parts of this chapter were previously presented as:

Raza, S., Bończak, B., Atamas, N., Karpińska, A., Ratajczyk, T., Łoś, M., Hołyst, R., & Paczesny, J. (2025). The activity of indigo carmine against bacteriophages: an edible antiphage agent. *Applied Microbiology and Biotechnology, 109(24),* Springer. https://doi.org/10.1007/s00253-025-13414-4

Chapter acknowledgement: TEM images presented in this chapter were obtained by Marcin Łoś. FCS analysis was performed by Aneta Karpińska.

5.1 Use of natural compounds against phages

Phage infections necessitate proper disinfection of facilities. Even a low number of survivor phages can cause recurring infections [25]. It is important to note that some phages can resist extreme conditions, such as being heated at 90 °C for 15 minutes or, in some cases, even boiling [87]. Several physical factors, such as temperature, the acidity of the environment, UVC irradiation or salinity, and ions, were individually explored to determine the survivability of bacteriophages under harsh conditions [257–259]. It was also found that phages are highly resilient against most physical factors. Moreover, radiation-based methods face significant difficulties due to hindered penetration into cloudy media or tight spaces within the biofoundries [260]. Another means of fighting phage infections is the utilization of specific chemical agents. For instance, Virkon S, which contains potassium monopersulphate as its primary active ingredient, has strong antiphage and bactericidal properties [261]. However, these compounds are usually very toxic to humans and the environment and might cause corrosion on surfaces and damage to equipment. Another effective method for inactivating phages is the use of quaternary ammonium compounds (QACs), which are active ingredients in over 200 disinfectants recommended by the U.S. EPA for inactivating SARS-CoV-2 [262].

Research on antiphagents is still in its early stages, with limited advancements in technologies designed to deactivate phages within an active bioreactor, such as anti-phage nanoparticles [157,263]. Developing a method for bacteriophage inactivation remains challenging, as it must be safe for bacteria, humans, and the environment, cost-effective (unlike gold nanoparticles, as noted by Richter et al. [157]), and easy to implement. This challenge has driven researchers back to nature, seeking naturally occurring compounds with effective anti-bacteriophage properties. In the past, several food dyes have been tested against the activity of some viruses. Indigo is confirmed to have anti-inflammatory,

antioxidant, and antiviral properties [264,265]. Native Americans also exploited *Isatis indigotica* for its anti-microbial activity, especially in the oral cavity [266]. Experiments with extracts of *Isatis tinctora* against the Japanese Encephalitis Virus (JEV) demonstrated the potential virucidal properties of the herb and its ability to inhibit viral attachment [267]. Lignans extracted from the root of this herb have also shown some anti-influenza properties [268]. Inhibition of viral replication can also be achieved by a 3,2'-bisindole isomer of indigo-indirubin [269]. Due to the COVID-19 pandemic, the antiviral activity of numerous herbs and natural compounds has been revisited [270]. Experiments performed with *Indigo naturalis* tone down the detrimental effects of coronavirus on the lungs [264].

5.2 The effect of IC on T4

In the past, several food dyes have been tested against the activity of some viruses. In the following study, the influence of temperature on the efficacy of indigo carmine (IC) was examined. Similar to previous studies on antiphagents, the activity of IC increased with an increase in temperature. At 50 °C, IC (2 mg/mL) caused a 2 log reduction in the T4 phage titer after approximately 12 hours, leading to complete inactivation (titer below the detection limit, i.e., more than 6 log reduction) after overnight incubation. In comparison, at 37 °C, IC caused only a 1 log reduction in PFU/mL (**Figure 16a**). It is worth noting that elevated temperatures alone (control samples) also contributed to a decrease in the phage titer, with final titers after 24 hours being approximately 3.65×10^5 PFU/mL at 50 °C versus 2×10^6 PFU/mL at 37 °C.

Bacteriophages were further exposed to IC across a range of temperatures (4 °C to 55 °C) for 24 hours before titration (**Figure 16b**). Prolonged exposure confirmed that IC activity improved with increasing temperature, achieving complete inactivation at 50 °C, and above.

To further determine the optimal parameters, T4 phages were incubated with IC at concentrations ranging from 10^{-4} mg/mL to 10^0 mg/mL at 50 °C for 24 hours (**Figure 16c**). Additionally, the effect of mixing the sample during the incubation was also compared. Approximately a 1 log reduction was observed at 0.1 mg/mL, while

complete inactivation required a minimum concentration of 0.5 mg/mL. The optimal conditions for IC's antiphage activity were identified as a temperature of 50 °C, an IC concentration of at least 0.5 mg/mL, mixing at 220 rpm, and an initial phage titer not exceeding 10^7 PFU/mL, ensuring maximum deactivation within 24 hours.

To gain insights into the mechanism of IC's action, phage titers were compared under the following conditions: phages incubated alone for 12 hours at 50 °C, IC incubated for 12 hours at 50 °C with phages added 5 minutes before titration, phages incubated for 12 hours at 50 °C with pristine IC added 5 minutes before titration, IC and T4 phages incubated together for 12 hours at 50 °C, and IC and T4 phages incubated separately for 12 hours at 50 °C, then mixed and titrated. This approach aimed to determine whether IC decomposition (expected in the second sample) or capsid structural changes due to elevated temperature (expected in the third sample) played a critical role in phage inactivation. The results indicated that the decrease in phage titer occurred only when IC was incubated with T4 from the beginning of the experiment (fourth sample), as shown in **Figure 16d**.

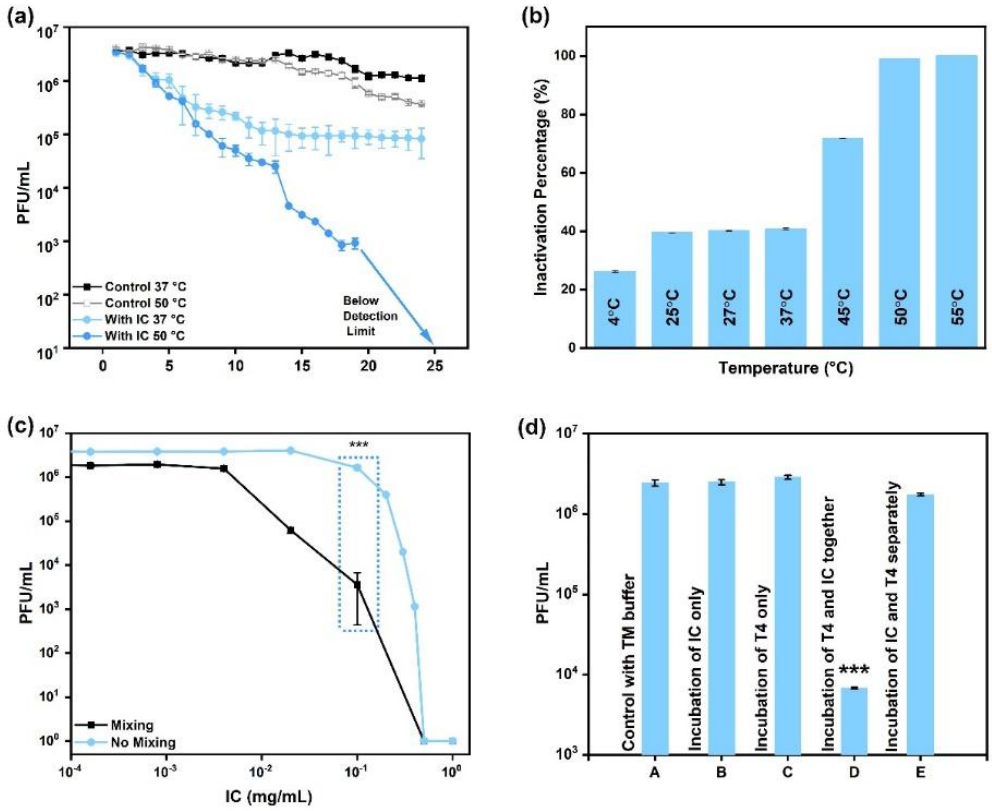

Figure 16. (a) Analysis of T4 titer at 37 °C and 50 °C in the presence and absence of indigo carmine. The concentration of IC was 2 mg/mL. **(b)** Experimental efficiency of IC against T4 bacteriophage at temperatures varying from 4 °C to 55 °C. The phage samples were incubated with IC for 24 hours before performing titration. **(c)** Effect of mixing (220 rpm) on antiphage activity of indigo carmine against T4 bacteriophages at 50 °C. The marked p-values (stars) correspond to the statistical difference between IC concentrations of 10^{-1} mg/mL. **(d)** The panel aims to establish the root cause of inactivation. Five different samples (left to right) were incubated at 50 °C (no mixing) and titrated as follows: control sample with only phages in TM buffer (no IC), IC only incubation followed by addition of phages just before titration, phage only incubation followed by addition of IC just before titration, incubation of IC and phages together followed by titration and separate incubation of IC and phages followed by combining them and immediate titration. Figure reproduced from Raza et al., 'The activity of indigo carmine against bacteriophages: an edible antiphage agent,' *Applied Microbiology and Biotechnology, 109(1), 2025,* DOI: 10.1007/s00253-025-13414-4, licensed under CC BY 4.0.

5.3 Evaluation of IC action against T4

Indigo carmine's mechanism of action was further investigated from the perspective of virions under specific conditions (0.5 mg/mL, 50 °C, 24 hours, mixing at 220 rpm). Transmission electron microscopy (TEM) was employed to visualize the structural differences in T4 virions before and after treatment with indigo carmine (**Figure 17**).

The results showed that indigo carmine caused contraction of the tail sheath in the majority of observed virions (**Figure 17b**). This contraction is typically associated with driving the tail tube through the bacterial outer membrane during host cell attachment [271]. Importantly, tail sheath contraction is irreversible. Additionally, changes in capsid morphology were noted, including a rounded shape and DNA ejection in some particles (**Figure 17d**, and **17c**, respectively).

In contrast, in the absence of indigo carmine, the bacteriophage structure remained intact, even at an elevated temperature. These findings highlight the structural impact of indigo carmine on T4 virions (**Figure 17a**).

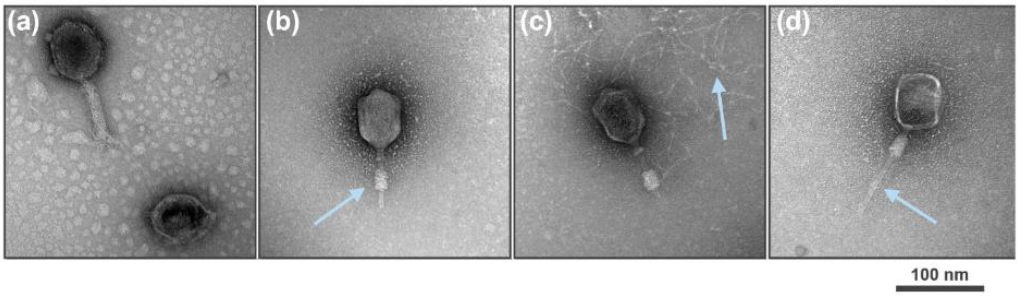

Figure 17. TEM of T4 bacteriophages in TM buffer **(a)** and in indigo carmine solution (0.5 mg/mL) after incubation at 50 °C for 24 h **(b-d)**. The blue arrows in the images highlight the contracted sheath, release of DNA, and the tube post-tail contraction, respectively. The bar corresponds to 100 nm. Figure reproduced from Raza et al., 'The activity of indigo carmine against bacteriophages: an edible antiphage agent,' *Applied Microbiology and Biotechnology, 109(1), 2025,* DOI: 10.1007/s00253-025-13414-4, licensed under CC BY 4.0.

5.4 Broad-spectrum effect of IC

The half-maximal effective concentration (EC50) of indigo carmine (IC) was determined at 50 °C after 24 hours of incubation for a range of bacteriophages, including T4, T1, T7, MS2, λ, and P001 (**Figure 18**). The EC_{50} values were calculated by fitting the data to the Hill equation [272] and were normalized to account for differences in the initial concentrations of each phage.

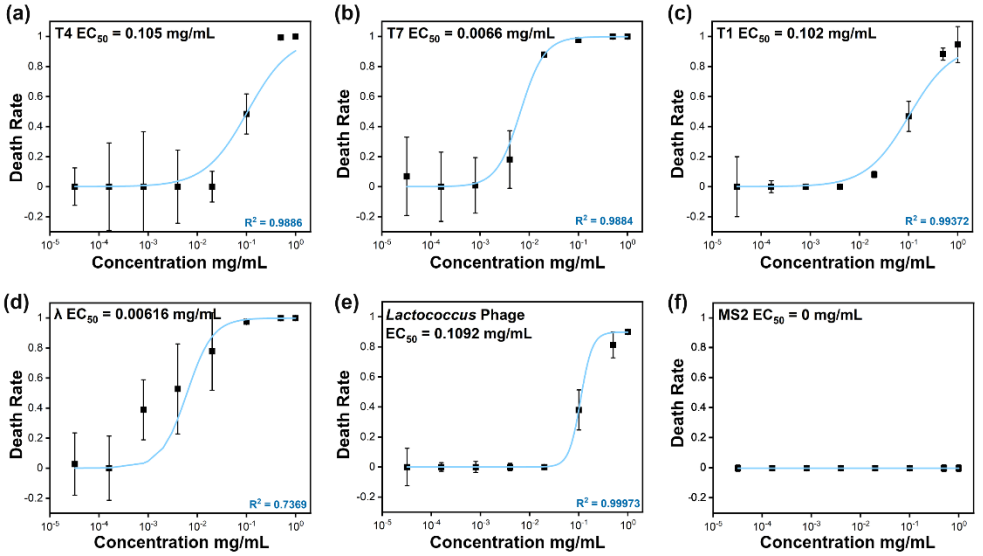

Figure 18. Hills curves showing the effect of indigo carmine (50 °C, 24 h, no mixing) on different phages – T4 **(a)**, T7 **(b)**, T1 **(c)**, λ **(d)**, P001 phage **(e)**, and **(f)** MS2. Figure reproduced from Raza et al., 'The activity of indigo carmine against bacteriophages: an edible antiphage agent,' *Applied Microbiology and Biotechnology, 109(1), 2025,* DOI: 10.1007/s00253-025-13414-4, licensed under CC BY 4.0.

The recalculated EC_{50} values revealed that 4.03×10^{14} molecules of IC were required per T4 phage (approximately 0.105 mg/mL, with an initial titer of ~4×10^5 PFU/mL), 8.91×10^{14} molecules per T7 phage (around 0.007 mg/mL, initial titer ~6×10^4 PFU/mL), 1.77×10^{17} molecules per T1 phage (around 0.102 mg/mL, initial titer ~4×10^3 PFU/mL), 4.3×10^{13} molecules per λ phage (around 0.006 mg/mL, initial titer ~9×10^6 PFU/mL), and 2.65×10^{15} molecules per P001 phage

(around 0.109 mg/mL, initial titer ~4 × 10^5 PFU/mL). Interestingly, indigo carmine was ineffective against MS2 phages (**Figure 18f**).

It was further observed that at higher phage titers (above ~10^9 PFU/mL), a concentration of 0.5 mg/mL IC was insufficient to achieve complete deactivation of phages. These findings highlight the broad-spectrum efficacy of IC against multiple phages, with its effectiveness influenced by both the initial phage titer and specific phage properties.

5.5 IC interactions with DNA and RNA

To explain the ineffectiveness of IC against MS2, the hypothesis that this was solely due to differences in morphology was rejected, as the tested bacteriophages represented a broad range of families and even orders. Instead, it was hypothesized that the observed difference stemmed from the fact that MS2 is an RNA phage, while all other tested phages were DNA phages. It is known that small molecules, such as dyes used for phage staining [273], can penetrate the capsid and bind to the stored genetic material.

Fluorescence correlation spectroscopy (FCS) measurements were conducted with the support of collaborators (Aneta Magiera, *de domo* Karpińska) to verify whether IC interacts differently with RNA and DNA. IC, which fluoresces at 528 nm upon irradiation at 488 nm [274], was tracked to assess binding behavior. First, the diffusion coefficient and hydrodynamic radius of free IC were determined (Figure 19a). These values were then compared to those obtained after incubating IC with dsDNA, ssDNA, and ssRNA (Figure 19b–d). The autocorrelation curves were fitted using a one-component normal diffusion model, and the results are summarized in Table 1.

A clear decrease in the diffusion coefficient and an increase in the hydrodynamic radius were observed exclusively in samples containing dsDNA, indicating selective binding of IC to double-stranded DNA rather than to RNA or single-stranded DNA.

Table 1. Diffusion coefficients and hydrodynamic radii were obtained for free indigo carmine dye, DNA-enriched IC solution, and RNA-enriched solution (the RNA radius ≈ 57 nm [275], the DNA radius ≈ 1 nm).

Probe	Diffusion coefficient [$\mu m^2/s$]	Hydrodynamic radius [nm]
IC	475.20 ± 42.87	0.51 ± 0.05
IC + dsDNA	304.08 ± 30.21	0.79 ± 0.08
IC + RNA	445.32 ± 47.78	0.54 ± 0.06
IC + ssDNA	476.39 ± 68.61	0.50 ± 0.07

5.6 Application of IC in industry

To evaluate the applicability of indigo carmine (IC) in biobased industries, an experiment was designed to simulate a bioreactor environment facing phage contamination. Bioreactors are essential for large-scale bacterial cultures used in biotechnology, where phage infections can disrupt production processes and lead to significant economic losses. Thus, assessing IC's ability to protect bacterial cultures under realistic growth conditions, such as temperature, agitation, and nutrient availability, becomes crucial. Additionally, ensuring that IC does not interfere with bacterial viability or protein production is key to its practical implementation in industrial settings.

The experiments were executed in optimal conditions for bacterial growth, i.e., in LB medium, at 37 °C, and 220 rpm. We analyzed the number of viable bacteria in the LB medium and the LB medium containing IC. Next, we spiked the samples with the same number of T4 virions (final concentration of 10^3 PFU/mL). The addition of IC resulted in a small decrease in the concentration of bacteria (from around 4×10^9 CFU/mL to 9.8×10^8 CFU/mL). The number of bacterial cells decreased upon spiking the culture with T4 phages by around 6 log (from around 4×10^9 CFU/mL to 7×10^3 CFU/mL). However, when IC was present in the medium before the addition of T4, *E. coli* was protected. There was no statistically significant difference in the number of viable *E. coli* cells between samples containing IC and IC along with T4 ($p > 0.05$). The results are presented in **Figure 19a**.

To ensure the industrial applicability of indigo carmine (IC), it is essential to confirm that its presence does not interfere with bacterial metabolic processes, such as protein production. A comparative study was conducted to analyze green fluorescent protein (GFP) induction in *E. coli* cultures with and without IC. **Figure 19b** shows a comparative study of green fluorescent protein (GFP) induction in *E. coli* in the absence (control) and presence of indigo carmine. It was observed that the addition of IC to an *E. coli* culture did not impact the overexpression of the example protein (GFP), as the overall production of GFP was comparable to that of the control (without IC).

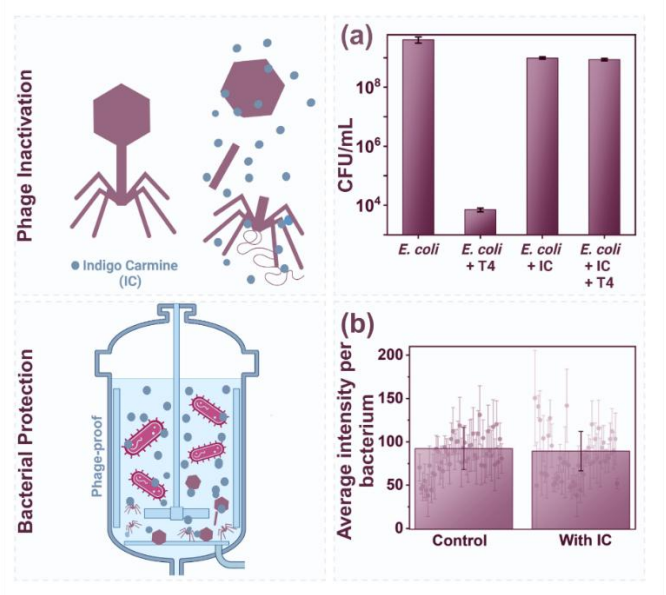

Figure 19. (a) Establishing the potential of IC as an antiphage agent by letting *E. coli* grow in the presence of both IC and T4 bacteriophages at 37 °C for 6 h. The panel shows the individual effects of IC and T4 on *E. coli*. IC protects *E. coli* from T4 infection. **(b)** A comparison of GFP expression in *E. coli* in the absence and presence of IC. to determine the possible effects of IC on protein expression by bacterial cells. There were no statistically significant differences between the samples. Figure reproduced from Raza et al., 'The activity of indigo carmine against bacteriophages: an edible antiphage agent,' *Applied Microbiology and Biotechnology, 109(1), 2025,* DOI: 10.1007/s00253-025-13414-4, licensed under CC BY 4.0.

5.7 Effect of IC over time

The efficiency of indigo carmine (IC) in inactivating T4 bacteriophages was observed to vary with the progressive color changes of the dye during its degradation. Indigo carmine naturally undergoes color transitions from blue to green, yellow, and eventually colorless, which corresponds to its chemical decomposition over time. From existing literature, key intermediates formed during indigo carmine (IC) degradation have been identified, including isatin and isatin-5-sulfonic acid (**Figure 21a**). These compounds were proposed as potential contributors to the antiphage activity observed during the decomposition of IC, especially during the green stage, when maximum inactivation was recorded. To determine whether these intermediates exhibit greater or lesser efficacy compared to IC, their effects on T4 bacteriophages were tested.

Phage inactivation tests were performed after a 12-hour incubation at 50 °C using indigo carmine solutions at different stages of this degradation process. A freshly prepared solution (blue) exhibited significant activity, causing a 2.5 log reduction in T4 phage titer. Interestingly, the green solution, sampled on Day 25, demonstrated enhanced efficacy, reducing the phage titer by 3.5 log, suggesting that intermediate degradation products might possess heightened antiphage activity (**Figure 20b**).

However, as the solution continued to degrade, turning yellow by Day 53, its ability to inactivate phages diminished substantially. By Day 82, no measurable phage inactivation was observed when the solution became colorless, indicating a complete loss of antimicrobial efficacy.

The photograph (**Figure 20a**) visually represents the stages of indigo carmine degradation, progressing from the vibrant blue of the fresh solution to the green, yellow, and ultimately clear colorless stages. The accompanying graph (**Figure 20b**) quantifies the corresponding phage inactivation levels, highlighting the peak efficacy during the green stage (Day 25) and the progressive decline as the dye further degrades. These findings suggest that the degradation state of indigo carmine significantly impacts its ability to inactivate bacteriophages and point to the potential

role of intermediate degradation products in enhancing its antiphage activity.

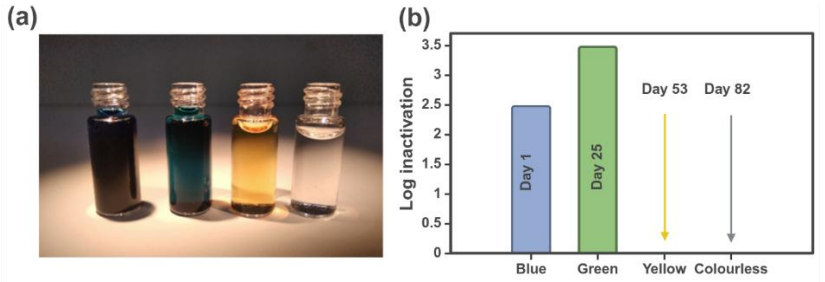

Figure 20. The activity of indigo carmine and its different stages against T4 bacteriophages. A blue solution of indigo carmine (freshly prepared, Day 1) causes a titer reduction of 2.5 log after an incubation of 12h at 50 °C. An intermediate green solution reduced phage titer at a higher efficiency by 3.5 logs when incubated at 50 °C for 12h. The yellow and colorless solutions, however, do not cause the inactivation of T4 bacteriophages.

The intermediates of the IC degradation, isatin and isatin-5-sulfonic acid [276], were incubated with T4 phages to assess their capacity to reduce phage titers. This analysis was crucial for pinpointing whether these compounds played a significant role in the heightened activity observed during the degradation process of IC or if other factors were responsible. The experiment was performed as above, with 24-hour incubation with the test compounds at 50 °C.

However, experimental results indicated that neither isatin nor isatin-5-sulfonic acid exhibited any inactivating effect on bacteriophages. The phage titer in these treatments remained comparable to the control, showing no statistically significant reduction (**Figure 21b**). These findings suggest that the heightened antiphage activity observed during the green stage of IC degradation is unlikely to be directly attributable to these intermediates alone.

The results underscore the complexity of IC's decomposition process and point to the involvement of other intermediate products or synergistic effects that may contribute to its activity. This highlights the need for further investigation into the detailed mechanisms and products responsible for IC's antiphage properties.

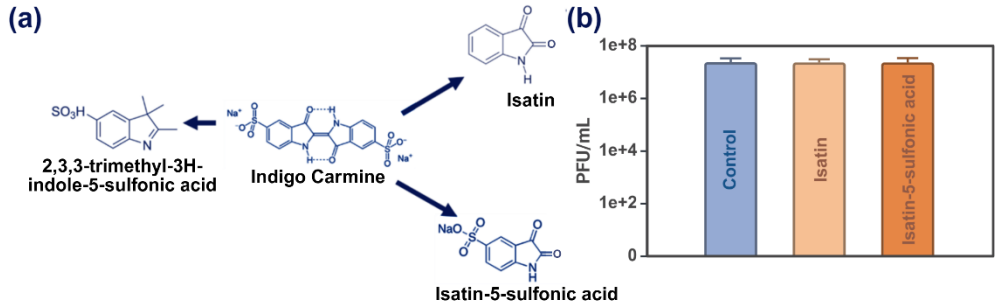

Figure 21. (a) Previously identified intermediates that form upon the degradation of indigo carmine [277,278]. **(b)** Effect of indigo carmine degradation intermediates (isatin and isatin-5-sulfonic acid) on T4 bacteriophages. The phages were incubated with the compounds at 50 °C for 24 hours. The starting phage titer was around 10^7 PFU/mL

Next, some of the most common FDA-approved food dyes, green (E140), yellow (E100), red (E120), and blue (E132), were selected for testing. The bacteriophages were incubated with food dyes at 50 °C for 24 hours. In **Figure 23**, it was observed that while green, yellow, and red dyes were ineffective against T4 bacteriophages, blue dye (indigo carmine, IC) caused complete inactivation. This result provided a starting point for further studying the effect of indigo carmine against phages.

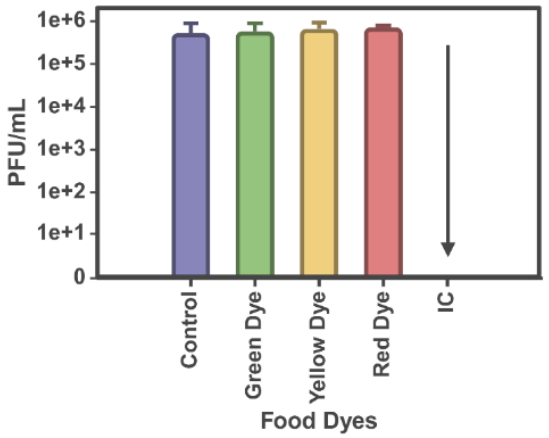

Figure 22. Effect of FDA-approved food dyes on T4 bacteriophages. The bacteriophages were incubated with green (E140), yellow (E100), red (E120), and IC (E132) dyes at 50 °C for 24 hours. PFU/mL values indicate the remaining phage infectivity after treatment.

5.8 Chapter summary

Recent advancements in molecular biology and biotechnology have unveiled the immense potential of microorganisms for industrial applications. Microbes, such as bacteria and yeast, are now essential for producing food, biofertilizers, pharmaceuticals, and treating diseases. The global market for microbial-origin pharmaceuticals exceeds $13 billion annually, emphasizing their critical role in various industries. Research into the gut microbiome further highlights the symbiotic relationship between humans and bacteria, underscoring the value of these microbial allies.

However, bacteriophages pose significant threats to industrial processes. Phage infections can devastate bacterial cultures, causing product losses in industries like dairy and biofoundries, where contamination rates are high. Despite preventive measures, including facility disinfection, protocol optimization, and bacterial strain engineering, phages remain highly resilient, with some surviving extreme conditions like boiling or irradiation. Existing countermeasures, such as

toxic disinfectants (e.g., quaternary ammonium compounds) or expensive nanoparticles, often fall short due to environmental concerns, high costs, or damage to equipment and bacterial cultures.

In this context, indigo carmine (IC), an FDA-approved food dye, has shown promising antiphage activity. In experiments, IC effectively inactivated the T4 bacteriophage, a model organism due to its structural similarity to most phages. Elevated temperatures (50 °C) enhanced IC's efficacy, with optimal conditions requiring a concentration of at least 0.5 mg/mL and an initial phage titer of $\leq 10^7$ PFU/mL. Mechanistic studies revealed that IC disrupts phage capsids and induces irreversible tail sheath contraction, rendering them inactive.

IC also demonstrated broad-spectrum activity against other DNA phages (e.g., T1, T7, λ, and P001) but was ineffective against RNA phages like MS2, likely due to its preferential binding to DNA over RNA. Interestingly, IC's antiphage activity peaked during its intermediate degradation stage, characterized by a green solution, while advanced degradation products (e.g., isatin) showed no efficacy. IC did not hinder bacterial growth or protein expression, making it a promising candidate for safeguarding industrial bacterial cultures without adverse effects. These findings underscore IC's potential as an inexpensive, safe, and environmentally friendly antiphage agent, paving the way for innovative solutions to combat phage-related challenges in biotechnology.

These findings highlight the potential of IC as an inexpensive, safe, and environmentally friendly antiphage agent. Importantly, IC demonstrated selective inactivation of bacteriophages without harming bacterial hosts, offering proof that naturally occurring compounds can achieve targeted antiviral effects. This observation represents a key milestone in the broader narrative of this thesis: establishing that selective antimicrobial strategies are possible and can be further optimized.

Building on this foundation, the next chapter explores how principles of molecular recognition, particularly through engineered surface charge interactions, can be harnessed to develop advanced nanomaterials with even greater selectivity. By moving from natural

selectivity, as exemplified by IC, toward rationally designed systems, the thesis aims to define a path toward safe, efficient, and highly targeted antimicrobial technologies.

Chapter 6

Engineered selectivity through charge-based interactions

Parts of this chapter were previously presented as:

Raza, S., Mente, P., Kamiński, B., Bończak, B., Maleki-Ghaleh, H., Vignesh, V., & Paczesny, J. (2025). Engineering hydrophobic and electrostatic interactions for selective inactivation of bacteriophages by mixed-ligand nanoparticles. *Nanoscale*, pages 1–9. https://doi.org/10.1039/D5NR00612K

Submitted manuscript:

Raza, S.[†], Korol, D.[†], Ochirbat, E., Kamiński, B., Cieplak, M., Sharma, Piyush Sindhu.[*], Paczesny, J.[*] (2025). Targeted inactivation of bacteriophages by polypyrrole nanoparticles, *Materials & Design*.

Chapter acknowledgement: The mixed-charge nanoparticles were synthesized and characterized by Pumza Mente. NMR analysis was carried out by Bartłomiej Bonczak and Pumza Mente, while the STEM image was provided by Witold Adamkiewicz. Polypyrrole (PPy) nanoparticles were synthesized by Dominik Korol under the supervision of Piyush Sharma. TEM images used in this chapter were obtained by Marcin Łoś.

6.1 Mixed charge surfaces and their application in biology

The application of nanotechnology in combating microbial infections has witnessed transformative advancements in recent years, driven by the unique physicochemical properties of nanoparticles (NPs). Among various approaches, mixed-charge nanoparticles (MLNPs) have emerged as a powerful platform for developing selective antimicrobial agents. These nanoparticles, characterized by their surface functionalization with both positive (cationic) and negative (anionic) ligands, offer precise control over surface charge distribution, enabling targeted interactions with bacterial cells and bacteriophages. Such selective targeting is particularly important in biotechnological and medical settings, where the elimination of phages is necessary without disrupting beneficial bacterial populations.

Grzybowski et al. have previously demonstrated the remarkable potential of mixed-ligand gold nanoparticles (AuNPs) in differentiating between bacterial surfaces based on their surface chemistry and charge profiles [279]. Their study highlighted the ability of MLNPs to exploit the structural and electrostatic differences between bacterial morphologies. This mosaic surface charge model paved the way for the development of MLNPs tailored for applications such as gram-selective inactivation and antimicrobial coatings.

Furthermore, adding hydrophobic ligands to MLNPs increased their stability in biological environments, reducing aggregation and ensuring prolonged activity against phages. Richter et al. demonstrated that MLNPs with the addition of hydrophobic (hydrophobic 1-octanethiol, OT) ligand exhibited phage inactivation efficiency, while maintaining bacterial survival rates above 90% [157]. This study recognized

hydrophobicity as a key factor in promoting effective phage inactivation through surface interaction.

6.2 Mixed ligand gold nanoparticles

6.2.1 Nanoparticle synthesis and characterization

This study presents a targeted approach to phage inactivation based on tailored interactions between nanoparticles and the mosaic of surface charges on bacteriophages while leaving bacterial cells unaffected. The strategy involves leveraging well-designed electrostatic and hydrophobic interactions for selective phage inactivation, offering potential advantages over existing methods. Gold nanoparticles were synthesized and functionalized with three types of ligands – (11- Mercaptoundecyl)-N,N,N- trimethylammonium (TMA, positive), 12-mercaptododecanate (MUA, negative), and dodecane-1-thiol (DDT, hydrophobic) – to generate nanoparticles with varied surface charges. The nanoparticles were synthesized by Dr Pumza Mente.

The STEM image of gold nanoparticles before the ligand exchange reaction showed spherical nanoparticles with an average diameter of 11.6 ± 2.9 nm and a monodisperse size distribution (**Figure 23a,b)**. This well-defined structure indicates successful synthesis, with the average size aligning with previous reports on gold nanoparticles used in antimicrobial studies [180]. The narrow size distribution suggests high reproducibility, essential for uniform behavior during ligand exchange and functionalization [280]. This size range is optimal for entering biological systems without triggering excessive immune responses [281], and the spherical shape facilitates consistent interaction with bacterial surfaces and phages, crucial for selective bacteriophage inactivation [157].

The hydrodynamic diameters of the MLNPs were determined using the DLS technique and are presented in **Figure 23c.** DLS analysis showed that mixed-ligand nanoparticles (MLNPs) with a near-equal ratio of positive (TMA) and negative (MUA) ligands (56:44:0) formed large aggregates (~450 nm), indicating reduced stability due to decreased electrostatic repulsion [282]. In contrast, nanoparticles with purely positive (100:0:0) or negative (0:100:0) ligands exhibited smaller, more

stable hydrodynamic diameters. This was further supported by zeta potential measurements (**Figure 23d**), where TMA-functionalized particles had a positive charge (+29 mV), MUA-functionalized particles had a negative charge (-35 mV), and mixed-ligand particles had reduced zeta potentials, approaching neutrality, leading to aggregation [157]. NPs covered by pure TMA or MUA ligands presented zeta potentials of +29 mV and -35 mV, respectively, and the sample 56:44:0 showed -4 mV, which is consistent with the literature [283]. Zeta potential from around -10 mV to +10 mV is usually associated with unstable colloidal suspension, where electrostatic repulsion is insufficient to prevent aggregation [284].

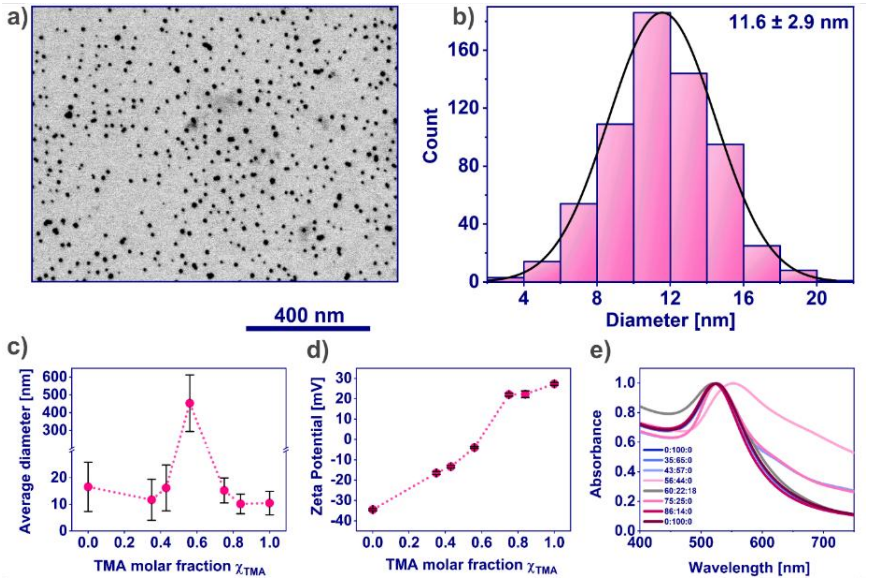

Figure 23. (a) Representative STEM image showing spherical gold nanoparticles with an average diameter of 11.6 ± 2.9 nm. **(b)** Size distribution curve based on STEM measurements. **(c)** DLS and **(d)** zeta potential of the mixed ligand nanoparticles (MLNPs) where the core is gold nanoparticles and the ligands are positively charged (11-mercaptoundecyl)-N,N,N-trimethylammonium, TMA), negatively charged (mercaptoundecanoic acid, MUA), and hydrophobic (dodecanethiol, DDT) in nature. **(e)** UV-Vis analysis. Figure reproduced from Raza et al., 'Engineering hydrophobic and electrostatic interactions for selective inactivation of bacteriophages by mixed-ligand nanoparticles,' *Nanoscale, 2025,* DOI: 10.1039/D5NR00612K, licensed under CC BY 4.0.

UV-Vis absorption spectra (**Figure 23e**) showed that purely positive MLNPs had a peak at 522 nm, while negative MLNPs exhibited a slight shift to 525 nm. Intermediate ligand ratios displayed red-shifted peaks around 610 nm, further indicating particle aggregation [280,285–287]. These results underscore the importance of controlling ligand ratios to maintain nanoparticle stability, which is critical for applications such as selective bacteriophage inactivation [288].

The proton NMR spectra of the modified nanoparticles (**Figure 24**) revealed distinct signals corresponding to the different ligands attached to the gold nanoparticle surface. The peaks for mercaptoundecanoic acid (MUA) and trimethylammonium bromide (TMA) confirmed the successful functionalization of the nanoparticles. The spectrum of pure MUA in DMSO reveals overlapping signals arising from CH2COOH and SH groups, complicating the integration (**Figure 24a**). However, when AuNPs were treated with iodine, the ligands detached from the gold surface, and sulfur atoms were oxidized to form a disulfide bond [288,289]. As a result, the SH signal disappeared, and the methylene group signal next to the sulfur atom (-CH_2S-) shifted to 2.68 ppm [290]. In some spectra, a triplet at 2.17 ppm, attributed to the methylene group next to the deprotonated carboxyl group, was also observed. The integrals of these signals were combined to quantify the MUA ligands [291]. Signals at 3.24 ppm, corresponding to the CH_2 protons adjacent to the $N(CH_3)^+$ group in TMA (**Figure 24b**), were often difficult to integrate due to the overlapping water peak at 3.33 ppm [290]. Therefore, the $N(CH_3)^+$ singlet at 3.02 ppm was used for quantifying the TMA ligand, with the integral ratio of 9:2 correlating with the 3.24 ppm signal whenever possible (**Figure 24b**) [292]. The chemical shifts of relevant groups are combined in **Table 2**. The ability to control ligand ratios is crucial for fine-tuning nanoparticle surface properties, which in turn affect their interaction with biological targets, enabling selective bacteriophage inactivation while preserving bacterial viability [279].

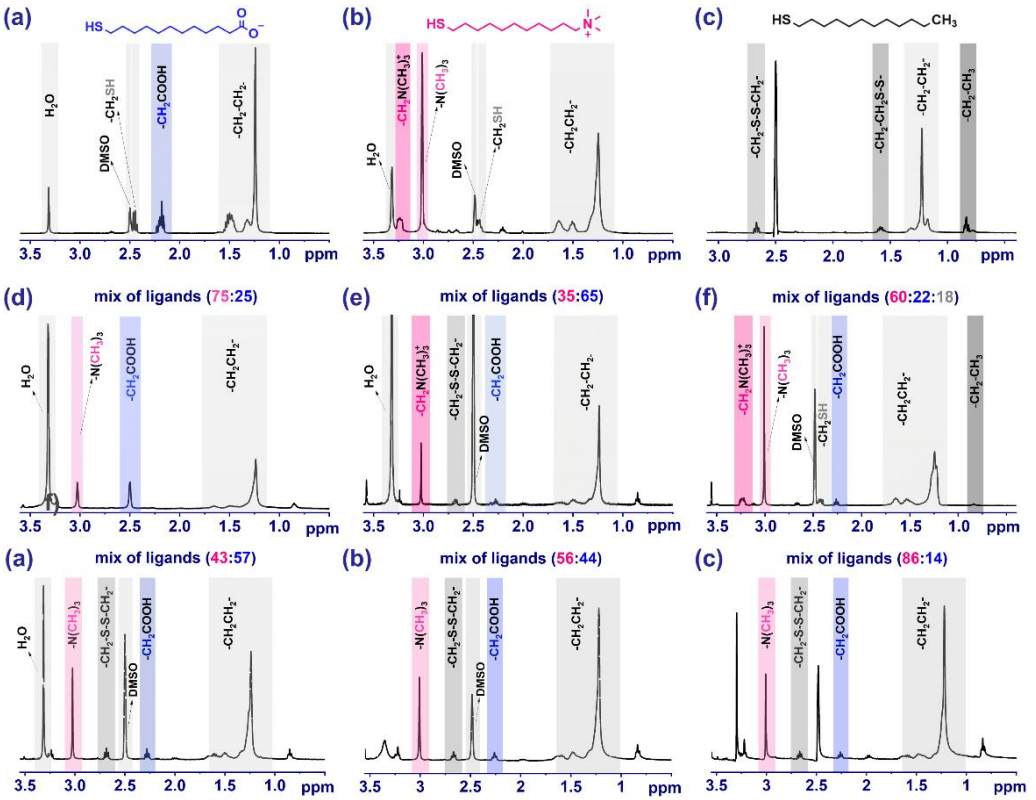

Figure 24. NMR spectra of ligands after removal of gold nanoparticles via iodine (I_2) washing. **(a)** NMR spectrum of mercaptoundecanoic acid (MUA), **(b)** NMR spectrum of (11-mercaptoundecyl)-N,N,N-trimethylammonium (TMA), **(c)** NMR spectrum of dodecanethiol (DDT), **(d)** NMR spectrum of a ligand mixture with a 75:25 ratio of TMA:MUA, **(e)** NMR spectrum of a ligand mixture with a 35:65 ratio of TMA:MUA, 60:22:18 ratio of TMA:MUA:DDT **(f)**, 43:57 ratio of TMA:MUA:DDT **(g)**, 56:44 ratio of TMA:MUA:DDT **(h)**, and **(i)** 86:14 ratio of TMA:MUA:DDT. Figure reproduced from Raza et al., 'Engineering hydrophobic and electrostatic interactions for selective inactivation of bacteriophages by mixed-ligand nanoparticles,' *Nanoscale, 2025,* DOI: 10.1039/D5NR00612K, licensed under CC BY 4.0.

Table 2: Chemical shifts of relevant H groups (s – singlet; t – triplet; q – quartet; m – multiplet).

Type of H Group	Chemical Shift (ppm)
-**CH$_2$**-N$^+$(CH$_3$)$_3$	3.29 – 3.21 (m)
-CH$_2$-N$^+$(**CH$_3$**)$_3$	3.02 (s)
-**CH$_2$**-SS-**CH$_2$**-	2.72 – 2.65 (t)
-**CH$_2$**-COOH	2.30 – 2.23 (t)
-**CH$_2$**-COO$^-$	2.20 – 2.15 (t)
CH$_2$-**CH$_2$**-CH$_2$	1.71 – 1.19 (m)
-CH$_2$-**CH$_3$**	0.88 – 0.80 (t)
-**CH$_2$**-SH	2.56 – 2.48 (q)
-CH$_2$-**SH**	2.22 – 2.17 (t)

6.2.2 Antimicrobial tests

Next, concentrations of MLNPs ranging from 10^{-7} up to 1 mg/mL were tested, and double overlay titration was carried out to determine the extent of phage inactivation of T4 bacteriophages. The dosage compensation experiment established that a concentration of 0.1 mg/mL of MLNPs was sufficient to deactivate over 90% of T4 bacteriophages (**Figure 25**). This was in line with our previous research [157].

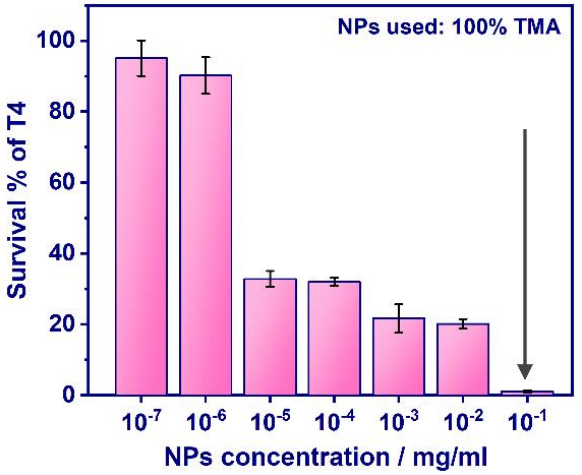

Figure 25. Dosage compensation of the survival % of T4 bacteriophages against 100% positive (only TMA, 100:0:0) nanoparticles. The virions were exposed to MLNPs concentrations, ranging from 10^{-7} mg/mL to 1 mg/mL. The starting concentration of T4 was 10^{7} PFU/mL. Figure reproduced from Raza et al., 'Engineering hydrophobic and electrostatic interactions for selective inactivation of bacteriophages by mixed-ligand nanoparticles,' *Nanoscale, 2025,* DOI: 10.1039/D5NR00612K, licensed under CC BY 4.0.

The hourly experiment determined that TMA-functionalized nanoparticles (100:0:0) inactivated over 99% of T4 bacteriophages within 5 hours at a concentration of 0.1 mg/mL while maintaining approximately 80% *E. coli* viability (**Figure 26b**). The nanoparticles were tested against T4 and *E. coli* as model organisms for bacteriophages and bacteria. The virions and bacterial cells were individually exposed to each set of nanoparticles, and any changes in their respective concentrations were recorded. It was observed that nanoparticles with a higher number of positive ligands (TMA) inactivated both phages and bacteria, whereas nanoparticles with a higher ratio of negative ligands [n] had little to no effect on either phage titer or bacterial cell concentration. The shaded area between the plots in **Figure 26c** shows the difference in survival percentages of *E. coli* and T4 bacteriophages, where MLNPs were more efficient against virions than bacterial cells, i.e., ligand ratios allowing for selectivity.

The nanoparticles were further modified by adding a hydrophobic ligand (dodecanethiol, DDT), as shown in **Figure 26d**, to obtain nanoparticles with a 60:22:18 ratio of TMA:MUA:DDT. We knew from previous work that the introduction of hydrophobic ligands [h] to all [n] NPs increased the efficacy of phage inactivation [157]. Here, we aimed to achieve phage eradication at 37 °C and at a shorter time scale, and thus, a mixture of three different ligands (TMA:MUA:DDT) was tested. Such MLNPs were tested against both *E. coli* and T4 bacteriophages to assess their impact on bacterial cell viability and phage titer. The experimental procedure followed the same protocol as described above, and the differences in concentrations were recorded. It was found after 5 hours that approximately 87% of T4 were inactivated, while 90% of all bacterial cells survived (**Figure 26e**). These findings underscore the potential of the tested nanoparticles as effective agents against bacteriophages while preserving bacterial cell viability.

Several efforts have been made to modify gold particles to facilitate their interaction with viral proteins [293,294]. In an interesting study, researchers explored the interplay of electrostatic forces between modified gold nanoparticles and *S. aureus* phages, leading to the formation of Au-phage complexes and offering promising avenues for versatile applications [295]. Other research has shown the interaction between phage capsids and gold nanoparticles by forming an amide bond between the terminal carboxylic groups on ligands and amine groups on phage capsids [296].

In our STEM images obtained subsequent to a 5-hour incubation period of T4 bacteriophages with hy-MLNPs, we observed an apparent interaction between our nanoparticles and the capsids of T4 phages (**Figure 26f**). Specifically, nanoparticles formed chain-like structures around the T4 phage capsids, likely disrupting their structural integrity and preventing successful phage infection. The phages exhibited a pattern of clustering wherein they formed chains enveloped by nanoparticles surrounding the capsid. In our previous study, TEM analysis of bacteriophages T4 interacting with modified gold nanoparticles reveals that hydrophobic ligands (OT) interact with the

bacteriophage capsid fibers, leading to structural changes and deactivation, which aligns with the chain-like agglomeration [157].

The first proposed mechanism of action for MLNPs involves disrupting electrostatic interactions at the target surface. Upon approaching the surface, the high surface charge of the MLNPs alters the local ionic environment, reducing ionic strength and shortening the Debye length, which controls the range of electrostatic forces [280]. This disruption weakens the interactions that maintain the structural integrity of virions, which agrees with the findings of Wennerström et al., who emphasized the critical role of electrostatic interactions in colloidal stability [297].

The second mechanism relates to osmotic pressure changes induced by the high charge density of the MLNPs and their counterions. This creates a localized osmotic imbalance [298], leading to water influx near the virions. Virions are particularly susceptible to such osmotic fluctuations due to the high internal pressure within their capsid, resulting from the tightly packed genetic material [299]. The increased osmotic stress may compromise capsid integrity, further inhibiting the virion’s functionality [299].

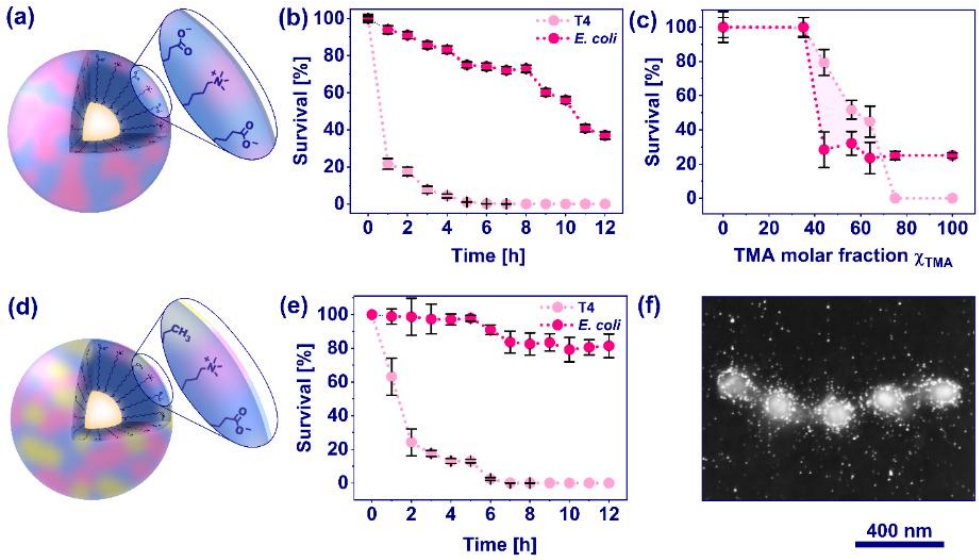

Figure 26. (a) Schematic representation of mixed ligand nanoparticles functionalized with TMA and MUA **(b)** The graph depicts an hourly experiment conducted to monitor the fluctuation in survival percentages of T4 bacteriophages over time following exposure to all-TMA nanoparticles (100:0:0). **(c)** The graph shows the survival percentage trends of T4 and *E. coli* treated with MLNPs. The shaded area between the plots shows the difference in survival percentages. The starting concentration of T4 was 10^7 PFU/mL, while that of *E. coli* was 10^4 CFU/mL. The experiment was conducted for 5 hours at 37 °C, 220 rpm. The concentration of nanoparticles was 10^{-1} mg/mL. **(d)** Schematic representation of mixed ligand nanoparticles functionalized with TMA, MUA, and DDT. **(e)** Effect of nanoparticles containing positive, negative, and hydrophobic ligands on the survivability of *E. coli* and T4. The starting concentration of *E. coli* was 10^5 CFU/mL, while that of T4 was 10^7 PFU/mL. The experiment was conducted for 5 hours at 37 °C, 220 rpm. The concentration of nanoparticles was 10^{-1} mg/mL. **(f)** STEM visualization of T4 bacteriophages in the presence of hydrophobic mixed ligand nanoparticles after 5 hours of incubation at 37 °C, 220 rpm. The bar represents 400 nm. Figure reproduced from Raza et al., 'Engineering hydrophobic and electrostatic interactions for selective inactivation of bacteriophages by mixed-ligand nanoparticles,' *Nanoscale, 2025,* DOI: 10.1039/D5NR00612K, licensed under CC BY 4.0.

In the next experiment, the mixed-ligand nanoparticles with a 60:22:18 ratio of TMA:MUA:DDT were tested against several model bacteriophages, including MS2, M13, Qβ, LR1_PA01, and vB_SauS_CS1 (**Figure 27**). The nanoparticles achieved complete inactivation (100%, 7 log reduction) of all phages within 9 hours. A comparison between the phages and their corresponding bacterial strains is shown in **Figure 27**. M13 exhibited the most rapid inactivation, with approximately 91% inactivation within just 3 hours (**Figure 27**). Following closely were LR1_PAO1 and MS2, demonstrating around 95% inactivation after 5 hours of exposure to the nanoparticles. vB_SauS_CS1 was fully inactivated after 8 hours, although it required longer incubation than the aforementioned phages. These results demonstrate the broad-spectrum efficacy of the mixed-ligand nanoparticles in inactivating a wide range of bacteriophages, suggesting that the combination of TMA, MUA, and DDT ligands is effective against various phage structures.

Despite this strong antiviral action, the nanoparticles exhibited high selectivity, as they were able to inactivate the phages without significantly harming bacterial cells, maintaining over 60% bacterial viability. This selective targeting of phages makes the nanoparticles highly suitable for applications in industries where bacteriophage contamination must be controlled without compromising the productivity of beneficial bacterial cultures [157].

The large diversity of phages makes it challenging to target a specific phage while ensuring the protection of bacterial cells. Thus, the developed method should be selective enough to protect bacteria against phages but not restricted to any specific phage. Our approach utilizes multivalent interactions between surface-functionalized Au NPs and the surface of the target. The mosaic of surface charges and hydrophobic domains at the outermost surface differs even for Gram-positive and Gram-negative bacteria, allowing for selectivity, as proved by the group of Grzybowski [279]. The surface of capsids of bacteriophages is vastly different from bacteria as it is composed of proteins (most phages are not enveloped), while peptidoglycans or lipopolysaccharides and phospholipids are present at the surface of bacteria [300].

The selectivity of mixed ligand nanoparticles (MLNPs) arises from the precise tuning of surface ligands designed to mimic the complex mosaic of functional groups present on the outer surfaces of the target entities, whether they are bacteriophages or bacteria. Previous research has demonstrated that such fine-tuning of surface chemistry can effectively differentiate Gram-negative from Gram-positive bacteria [279]. Our study extended this concept by successfully distinguishing bacteriophages from bacterial cells based on their surface characteristics.

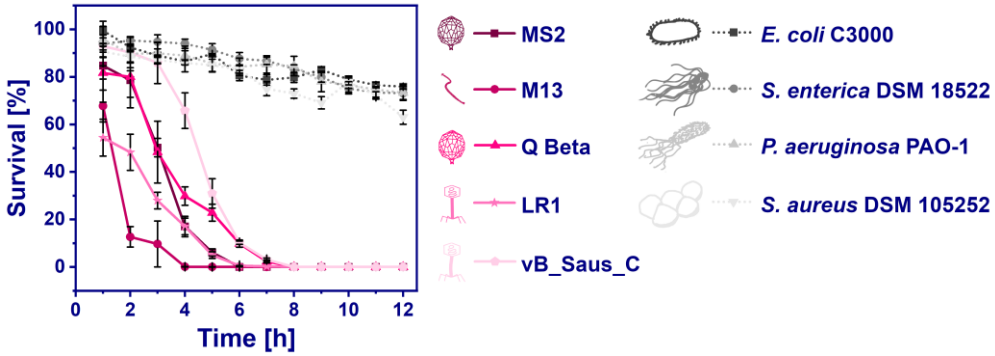

Figure 27. The graph shows investigating the impact of nanoparticles with mixed ligands (TMA, MUA, and DDT) in a ratio of 60:22:18, respectively, on diverse model phages (MS2, M13, Q Beta, LR1_PA01, and vB_SauS_CS1) for quantifying their inactivation over 12 hours. Initial phage concentration: 10^7 PFU/mL. Experiments were conducted at 37 °C, 220 rpm, with nanoparticle concentration at 0.1 mg/mL. Figure reproduced from Raza et al., 'Engineering hydrophobic and electrostatic interactions for selective inactivation of bacteriophages by mixed-ligand nanoparticles,' *Nanoscale, 2025,* DOI: 10.1039/D5NR00612K, licensed under CC BY 4.0.

6.2.3 Sterilising secondary reactants - antibiotics

In bacteria-based industries, antibiotics are often incorporated as raw materials for killing or stopping the growth of harmful bacteria. However, antibiotics cannot undergo standard sterilization processes due to their fragile nature and susceptibility to high temperatures. This limitation poses a significant contamination risk, as unsterilized antibiotic solutions

may harbor bacteriophages, potentially introducing these contaminants into bioreactors.

Given this challenge, we hypothesized that mixed ligand nanoparticles (MLNPs) could serve as a novel solution for either sterilizing antibiotic solutions or directly targeting any phages that these antibiotics might introduce. However, before considering such an application, it was essential to ensure that MLNPs do not interfere with the antibiotics' efficacy.

Initially, we conducted control experiments to independently assess the effects of T4 phages and MLNPs on *E. coli*. The results showed that T4 phages alone reduced *E. coli* CFU/mL by up to 50%. However, when MLNPs were introduced alongside the phages, they effectively protected the bacteria, as indicated by no significant drop in CFU/mL (**Figure 28**, panel '**without antibiotic**').

Next, we introduced kanamycin into the study as our *E. coli* strain is kanamycin-resistant. We repeated the control experiments with T4 phages and MLNPs, confirming that MLNPs protected the bacteria from phage attacks without compromising the antibiotic's effectiveness. The CFU/mL of cultures treated with kanamycin, with or without MLNPs, showed no significant difference (marked as ns in **Figure 28**, panel '**kanamycin**'), indicating that MLNPs did not interfere with kanamycin's activity.

Finally, we evaluated the effect of MLNPs on ampicillin by comparing samples containing only *E. coli* and ampicillin with those containing *E. coli*, ampicillin, and MLNPs. The results revealed no significant difference in CFU/mL between the two groups (marked as ns in **Figure 28**, panel '**ampicillin**'), demonstrating that MLNPs did not interfere with ampicillin's efficacy.

These findings suggest that MLNPs can potentially safeguard bacterial cultures by inactivating bacteriophages introduced through antibiotics without compromising the antibiotics' effectiveness in biotechnological processes.

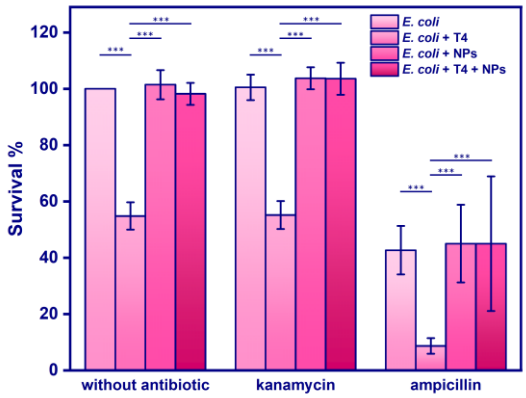

Figure 28. The survival rate of *E. coli* after interaction with nanoparticles containing positive, negative, and hydrophobic ligands, bacteriophage T4, and antibiotics – kanamycin and ampicillin.

6.2.4 Biocompatibility assay

To assess the biocompatibility of our nanoparticles with mammalian cells, an Alamar Blue assay was performed using the 3T3 NIH fibroblast cell line. Three distinct nanoparticle formulations were evaluated: gold nanoparticles without ligand functionalization, mixed-ligand nanoparticles (MLNPs) with a 56:44:0 ratio of TMA to MUA, and MLNPs incorporating a hydrophobic ligand at a 60:22:18 ratio of TMA:MUA:DDT. The nanoparticle concentration was set at 0.1 mg/mL, selected based on its effectiveness in previous phage inactivation experiments (**Figure 25**).

The 3T3 NIH cells were exposed to these nanoparticle formulations, AuNPs, MLNPs (56:44:0), and MLNPs (60:22:18), for durations of 24 and 48 hours. Cell viability was evaluated through the Alamar Blue assay, which quantifies cellular metabolic activity by measuring the reduction of resazurin to the fluorescent compound resorufin. The results, illustrated in **Figure 27f**, revealed cell viabilities exceeding 90% across all nanoparticle treatments and time points. MLNPs (56:44:0) demonstrated particularly high cell viability, indicating minimal cytotoxicity at the tested concentration.

Morphological observations further corroborated the biocompatibility of the nanoparticles. Untreated control cells (**Figure 29a**)

retained their typical elongated, spindle-like morphology, characteristic of healthy 3T3 fibroblasts. Similarly, cells exposed to gold nanoparticles without ligands (**Figure 29b**) and MLNPs with TMA and MUA ligands (56:44, **Figure 29c**) exhibited no significant deviations in morphology compared to control cells. Cells treated with MLNPs containing hydrophobic ligands (60:22:18, **Figure 29d**) showed slightly increased nanoparticle interaction but maintained their fibroblast morphology. In contrast, cells treated with Triton X-100 (1%; **Figure 29e**) displayed spherical, shrunken morphologies, indicative of cellular damage, thus validating the assay's sensitivity in detecting cytotoxic effects.

These findings demonstrate that both MLNPs and hydrophobic ligand-incorporated MLNPs exhibit high biocompatibility with 3T3 NIH cells, with cell viability consistently surpassing 90%. This minimal cytotoxicity, combined with the effective phage inactivation previously observed, highlights the potential of these nanoparticles for medical and antimicrobial applications. Their ability to selectively inactivate phages without compromising mammalian cell health aligns with previous studies, which suggest that ligand-functionalized nanoparticles—especially those with carboxyl or hydrophobic groups—enhance biocompatibility and exhibit selective targeting capabilities against microbial contaminants while preserving mammalian cell integrity.

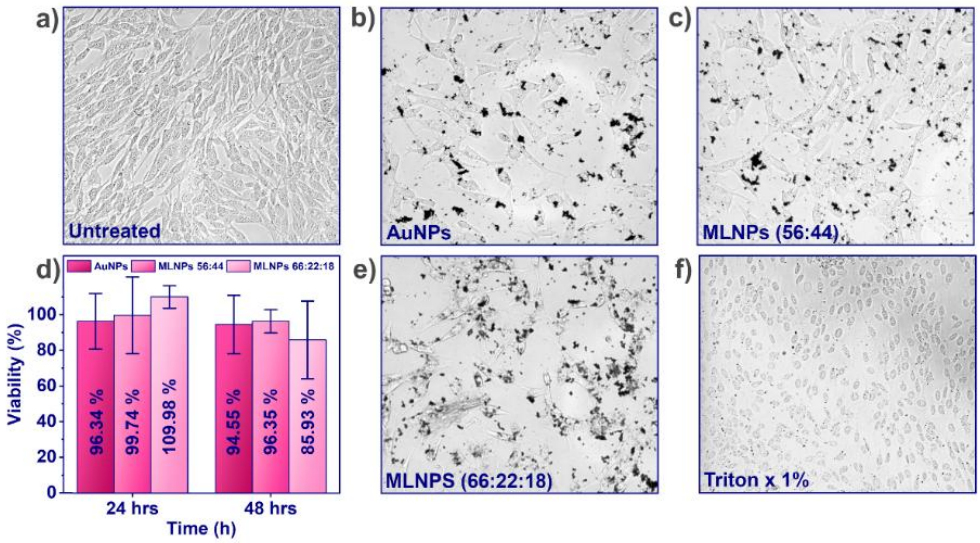

Figure 29. Optical microscopic images of 3T3 NIH fibroblast cells after 24 hours of incubation with different nanoparticle treatments: **(a)** Untreated control cells, **(b)** Cells treated with gold nanoparticles (AuNPs, 0.1 mg/mL), **(c)** Cells treated with mixed ligand nanoparticles (MLNPs, 56:44 TMA:MUA, 0.1 mg/mL), **(d)** Viability of cells treated with AuNPs, MLNPs (56:44), and MLNPs (60:22:18) after 24 and 48 hours of incubation. **(e)** Cells treated with MLNPs (60:22:18 TMA:MUA:DDT, 0.1 mg/mL), and **(f)** Cells treated with 1% Triton X. Figure reproduced from Raza et al., 'Engineering hydrophobic and electrostatic interactions for selective inactivation of bacteriophages by mixed-ligand nanoparticles,' *Nanoscale, 2025,* DOI: 10.1039/D5NR00612K, licensed under CC BY 4.0.

6.3 Polypyrrole Nanoparticles

6.3.1 Nanoparticles' synthesis and characterisation

Conducting polymer-based nanoparticles have gained much attention for biomedical applications because of their unique physicochemical properties, including electrical conductivity and biocompatibility [301–304]. These nanoparticles are used in drug delivery, wearable bioelectronics like transistors, and wound healing. Combinations of bacteriophages and polymers are also promising for targeted drug delivery, microbial decontamination, antibiotic alternatives,

bacteriophage encapsulation, and controlled phage inactivation [305–309]. Among conducting polymers, polypyrrole stands out due to its good electrical conductivity when doped, thermal stability up to 300 °C, and simple synthesis [310]. In this study, we developed a new method for phage inactivation by creating poly(vinyl alcohol) (PVA)-based polypyrrole nanoparticles cross-linked with a pyrrole derivative containing carboxyl groups. Polymerization was initiated with iron(III) chloride to enhance conductivity [311], and excess PVA chains stopped the reaction, forming small, uniform nanoparticles around 50 nm in size [312]. Adding carboxylated pyrrole improved the nanoparticles' electrostatic properties [313]. The nanoparticles were characterized using SEM, EDX, XPS, DLS, zeta potential, Raman spectroscopy, and FTIR (**Figure 30**). SEM showed smooth, spherical nanoparticles that became smaller as more carboxyl groups were added, ranging from 47.24 ± 0.13 nm to 34.55 ± 0.17 nm (**Figure 30a-e**). EDX confirmed elemental composition and successful functionalization (**Figure 30g**), while XPS revealed chemical changes linked to the carboxyl groups (**Figure 30h**). DLS measurements confirmed the size decrease and swelling in buffer solutions (**Figure 30i**). Zeta potential analysis showed increasingly negative surface charges with higher carboxyl content, improving colloidal stability **Figure 30j**. Raman and FTIR confirmed structural integrity and chemical modification, supporting the successful incorporation of carboxyl groups (**Figure 30k-l**).

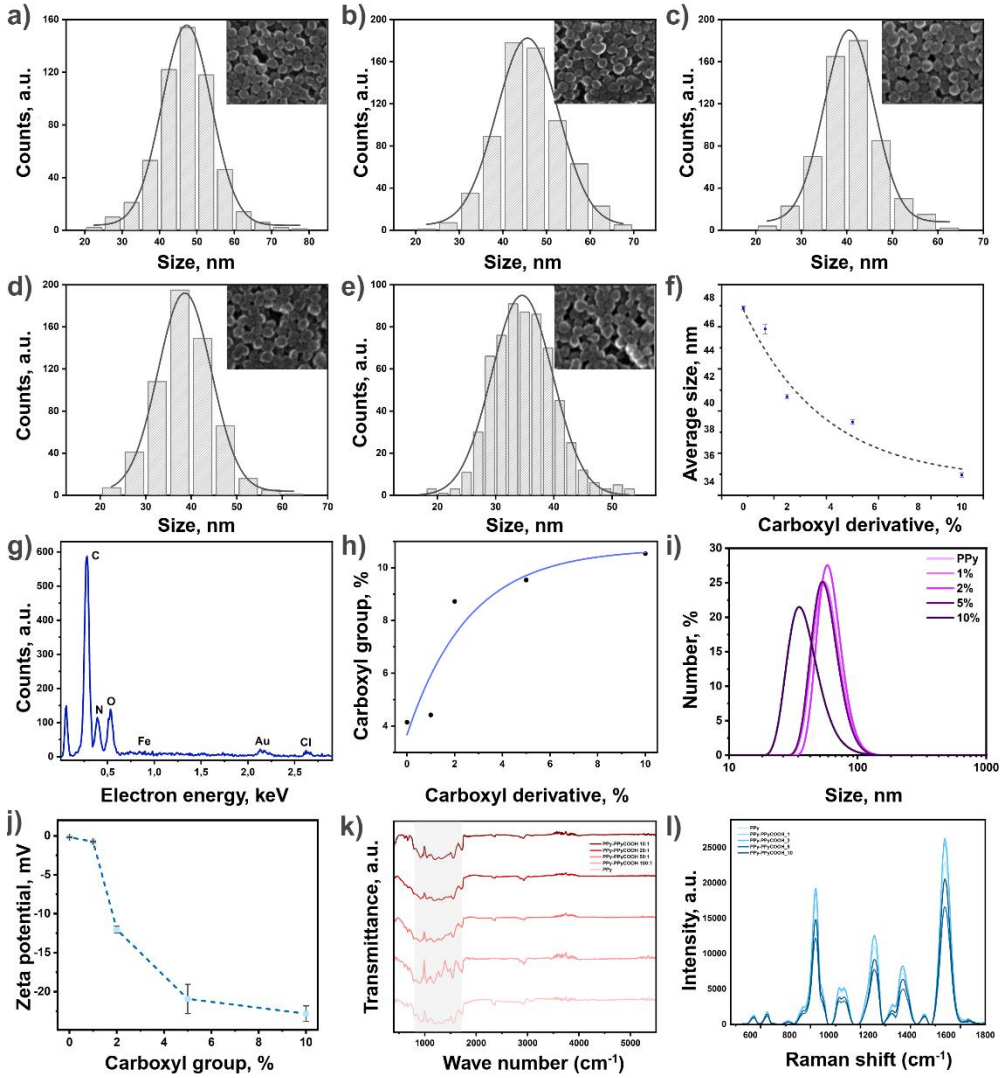

Figure 30. SEM images and statistical size distribution with bell curve fitting and of **(a)** PPy, **(b)** PPy:PPyCOOH 100:1, **(c)** 50:1, **(d)** 20:1, **(e)** 10:1 nanoparticles **(f)** Dependence of the average diameter of nanoparticles on the addition of PyCOOH during their synthesis. **(g)** EDX spectra of PPy and PPyCOOH (1–10 mol%) recorded by 5 kV electron beam at the image magnitude of 3,000 times. **(h)** Results of XPS quantitative analysis on carboxylic groups. Results of DLS analysis on PPy and PPy-PPyCOOH nanoparticles in TM buffer regarding **(i)** their percentage share by quantity **(j)** zeta potential of nanoparticles with different percentage of COOH groups, **(k)** Fourier-transform infrared spectroscopy results and **(l)** Raman spectra of the synthesized nanoparticles.

6.3.2 Antimicrobial assay

The antiviral activity of polypyrrole nanoparticles (PPy NPs) was evaluated against three model bacteriophages: T4, MS2, and vB_SauS_CS1. These phages serve as representative models for abundant phage types, eukaryotic viruses, and Gram-positive bacteria-infecting phages.

Figure 31 demonstrates the inactivation efficiency of PPy NPs at varying concentrations over 24 hours. A concentration-dependent inactivation trend was observed, with 90% inactivation for T4, 70% for MS2, and 60% for vB_SauS_CS1 at the highest concentration tested. The results showed that even without carboxyl groups, PPy nanoparticles were able to inactivate phages in a concentration-dependent way. At the highest concentration tested, the inactivation rates were 76.6 ± 1.64% for T4, 58.62 ± 1.71% for MS2, and 93.12 ± 0.98% for vB_SauS_CS1. Based on these findings, we chose 0.3 mg/mL as the working concentration for further experiments. This concentration caused about 40% or less inactivation for all tested phages, providing a low baseline. This made it possible to clearly observe any extra inactivation caused by the COOH groups in the functionalized nanoparticles.

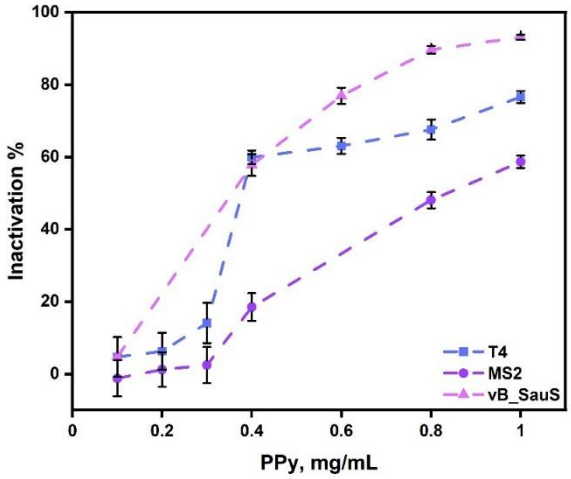

Figure 31. Inactivation percentage depending on the concentration of nanoparticles for chosen bacteriophages: T4, MS2, and vB_SauS_CS1. The starting concentrations of the bacteriophages were in the range of 10^7 PFU/mL.

Figure 32 shows how P(Py:PyCOOH) nanoparticles with different amounts of carboxyl groups (100:1, 100:2, 100:5, and 100:10) affected phage inactivation. Surprisingly, instead of seeing more inactivation with higher COOH content, the nanoparticles with the lowest amount of carboxyl groups (100:1) were the most effective. P(Py:PyCOOH) 100:1 nanoparticles completely inactivated the T4 phage (7 log reduction), and reduced MS2 and vB_SauS_CS1 by 99.98 ± 6.36 % and 99.97 ± 14.53 %, respectively. As the amount of PyCOOH increased to 5% and 10%, the inactivation rates dropped. For the 100:5 ratio, inactivation rates were 82.86 ± 11.53 % (T4), 61.22 ± 7.38 % (MS2), and 98.17 ± 19.14 % (vB_SauS_CS1). The weakest effect was seen with the 100:10 nanoparticles, which reduced T4 by 36.42 ± 17.13 %, MS2 by 24.49 ± 9.99 %, and vB_SauS_CS1 by 11.66 ± 10.31 %. These results suggest that the 100:1 nanoparticles achieved the best interaction with the phage capsids, leading to the most effective disruption of the phages' structure [314].

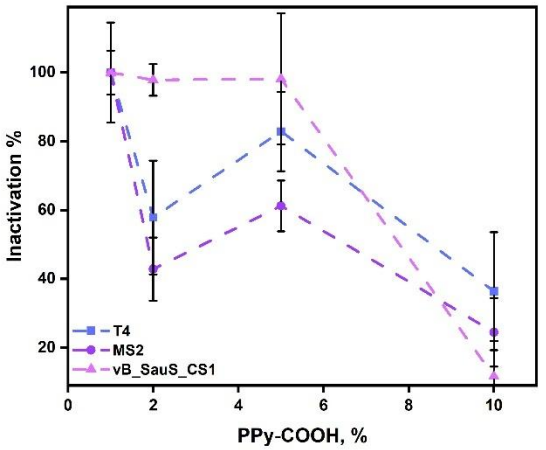

Figure 32. The effect of PPyCOOH nanoparticles (1%, 2%, 5%, and 10%) on the survivability of chosen phages – T4, MS2, and vB_SauS_CS1. The starting concentrations of the bacteriophages were in the range of 10^7 PFU/mL.

Next, the effect of P(Py:PyCOOH) 100:1 nanoparticle on both phages and their bacterial hosts was evaluated (**Figure 33**). The nanoparticles showed high selectivity by effectively inactivating the phages while having little impact on the viability of their hosts. For instance, the T4 phage titer was reduced by 100% (7 log), while 96.62 ± 2.87 % of its host, *E. coli* BL21, remained viable. Similarly, 99.98 ± 6.36 % of MS2 phages and 99.97 ± 14.53 % of vB_SauS_CS1 phages were inactivated, with their hosts, *E. coli* C3000 and *S. aureus* DSM105272, maintaining 94.87 ± 4.07 % and 96.19 ± 5.01 % viability, respectively. This strong selectivity is important for applications requiring phage control without harming beneficial bacteria [315].

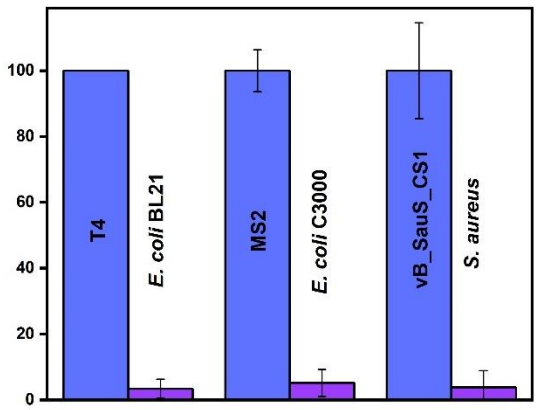

Figure 33. The effect of PPyCOOH nanoparticles (1%) on the survivability of chosen bacteria phages – T4, MS2, and vB_SauS_CS1 phages and their respective bacteria – *E. coli* BL21, *E. coli* C3000, and *S. aureus*, respectively.

Transmission electron microscopy (TEM) provided valuable insights into the interaction mechanisms between 1% PPyCOOH nanoparticles and bacteriophages (**Figure 34a-c**). The observations revealed distinct interaction patterns depending on the phage type. In the case of T4 phages (**Figure 34a**), the nanoparticles primarily adhered to the tail and fiber structures, suggesting interference with regions critical for host cell attachment. For MS2 phages (**Figure 34b**), the nanoparticles induced phage clustering, likely driven by electrostatic interactions, which limited the phages' ability to access host cells. Meanwhile, vB_SauS_CS1 phages (**Figure 34c**) appeared to be completely surrounded by nanoparticles, effectively obstructing structural regions essential for bacterial attachment.

Notably, no significant morphological damage to the phages was observed, indicating that the primary mechanisms of inactivation are electrostatic interactions and physical blocking of key functional sites rather than structural disruption. The negatively charged carboxyl (COOH) groups on the nanoparticle surface likely interact with positively charged regions on the phage capsid, disrupting essential binding sites required for host attachment and infection. This mechanism highlights the

efficiency of 1% PPyCOOH nanoparticles in neutralizing phage activity while preserving the structural integrity of the viral particles.

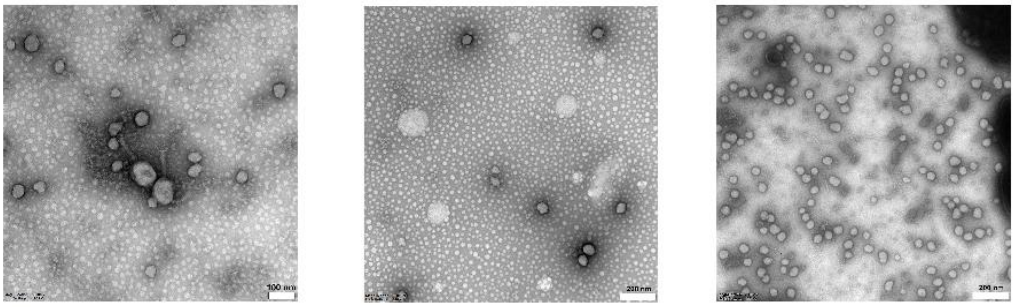

Figure 34. TEM images showing interactions between PPyCOOH 1% nanoparticles and bacteriophages: **(a)** T4 bacteriophages interacting with 1% PPyCOOH nanoparticles, **(b)** MS2 bacteriophages forming clusters away from 1% PPyCOOH nanoparticles, and **(c)** vB_SauS_CS1 bacteriophages with PPyCOOH nanoparticles surrounding the phages.

6.3.3 Biocompatibility assay

The cytotoxicity of 1% PPyCOOH nanoparticles at a concentration of 0.3 mg/mL was assessed using an Alamar Blue assay on the 3T3 NIH fibroblast cell line to ensure their safety for biomedical applications. Cell viability measurements after 24 and 48 hours of nanoparticle exposure revealed consistently high survival rates, exceeding 90% (**Figure 35d**).

Microscopic analysis of cell morphology further supported these findings, showing no significant differences between untreated control cells and those exposed to 1% PPyCOOH nanoparticles (**Figure 35a–b**). In contrast, cells treated with the cytotoxic agent Triton X-100 (1%) displayed evident signs of damage, including spherical and shrunken morphologies (**Figure 35c**).

These results confirm that 1% PPyCOOH nanoparticles demonstrate minimal cytotoxicity, even at concentrations effective for phage inactivation. The high cell viability and preserved cellular morphology underscore their potential suitability for biomedical applications where safety and biocompatibility are critical.

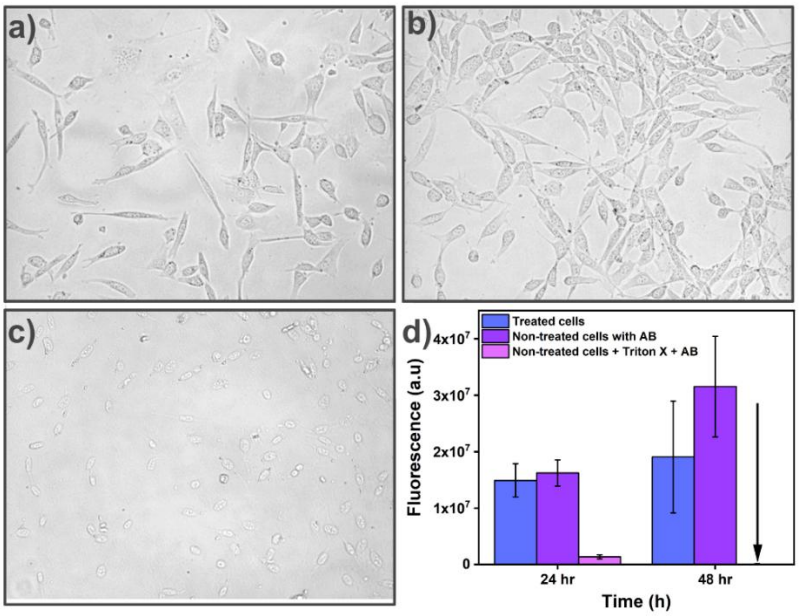

Figure 35. Morphological and cytotoxicity analysis of 3T3 NIH cells treated with PPyCOOH nanoparticles. **(a)** Untreated control cells show healthy, elongated fibroblast morphology. **(b)** Cells treated with PPyCOOH 1% at 0.3 mg/mL for 24 hours, exhibiting similar elongated morphology, indicating minimal cytotoxicity. **(c)** Cells treated with 1% Triton X-100, displaying spherical, shrunken morphology characteristic of cell death. **(d)** Quantitative analysis of cell viability using the Alamar Blue assay after 24 and 48 hours of incubation with PPyCOOH 1% nanoparticles.

6.4 Chapter Summary

Nanotechnology has significantly advanced antimicrobial strategies, with mixed-charge nanoparticles (MLNPs) emerging as a promising tool for targeted bacteriophage inactivation without harming beneficial bacteria. These nanoparticles possess both positive (cationic) and negative (anionic) ligands on their surfaces, enabling precise control over charge distribution for selective interactions with microbial surfaces.

Grzybowski et al. demonstrated that mixed-ligand gold nanoparticles (AuNPs) can differentiate between bacterial and viral surfaces based on their electrostatic and structural profiles, facilitating selective antimicrobial applications. This selective capability is

particularly valuable in environments requiring the elimination of bacteriophages without disrupting beneficial bacterial communities, such as in fermentation or probiotic industries.

Further improvements have been achieved by incorporating hydrophobic ligands, which enhance nanoparticle stability and reduce aggregation in biological environments. For example, Richter et al. showed that hydrophobic ligands like 1-octanethiol (OT) improve the phage inactivation efficiency of MLNPs while maintaining high bacterial survival rates (above 90%). Hydrophobic interactions play a crucial role in binding nanoparticles to viral capsids, disrupting their structural integrity, and preventing infection.

In this chapter, mixed-ligand nanoparticles (MLNPs) were synthesized with surface functionalization consisting of positive (cationic), negative (anionic), and sometimes hydrophobic ligands. This unique combination allows precise control over charge distribution, enabling selective interactions with bacterial and viral surfaces. In studies, MLNPs demonstrated over 90% bacterial survival rates while achieving 99% inactivation of T4 bacteriophages within 5 hours at a concentration of 0.1 mg/mL. The addition of hydrophobic ligands, such as dodecanethiol (DDT), improved nanoparticle stability and increased phage inactivation efficiency by facilitating stronger hydrophobic interactions. MLNPs' selective antimicrobial properties and stability in biological environments make them highly effective. The fine-tuning of ligand ratios ensures targeted action, optimizing MLNPs for selective phage inactivation while maintaining high bacterial viability and minimal toxicity to mammalian cells.

Polypyrrole nanoparticles (PPyNPs), functionalized with carboxyl (COOH) groups, also exhibited exceptional stability, selectivity, and efficiency in antimicrobial applications. At an optimal concentration of 0.3 mg/mL, 1% COOH-functionalized PPyNPs achieved 100 % inactivation of T4 phages, 99.98 ± 6.36 % of MS2 phages, and 99.97 ± 14.53 % of vB_SauS_CS1 phages, while maintaining over 90% bacterial viability. Additionally, mammalian cell viability remained above 90% after exposure to PPyNPs for 24–48 hours, confirming their biocompatibility.

The balance between electrostatic interactions and surface functionality makes PPyNPs highly effective for bacteriophage targeting without harming bacterial or mammalian cells.

Both MLNPs and PPyNPs demonstrate highly selective antimicrobial properties, with MLNPs achieving 99% phage inactivation and PPyNPs demonstrating up to 85% inactivation rates under optimal conditions. While MLNPs rely on a mosaic of positive, negative, and hydrophobic ligands for precise charge interactions, PPyNPs utilize carboxyl functional groups to achieve similar results through electrostatic and steric interactions. Importantly, both nanoparticles maintain over 90% bacterial survival rates and over 90% mammalian cell viability, highlighting their biocompatibility. Together, these nanomaterials provide a powerful and complementary approach to combating microbial infections, offering targeted, efficient, and safe solutions for biotechnological and medical applications.

CHAPTER 7
Summary and conclusions

The main goal of this thesis was to develop novel strategies for bacteriophage inactivation, focusing on selective targeting of phages while preserving beneficial bacterial populations. Unlike conventional antimicrobial approaches that broadly eliminate microorganisms, this thesis emphasized the need for more refined, phage-specific inactivation methods applicable across biotechnology, industrial microbiology, and medical fields.

This study explored various types of small molecules, polymers, and nanomaterials to achieve selective bacteriophage deactivation. The work transitioned from broad-spectrum antimicrobial nanomaterials toward more specialized systems demonstrating engineered selectivity, aiming to preserve microbial ecosystems where needed. Each chapter concluded a distinct project focused on designing, testing, and evaluating materials for bacteriophage control, integrating their mechanisms of action, effectiveness, and practical applications.

In Chapter 4, I investigated the use of nanotechnology in combating bacteriophage contamination, focusing on green-synthesized silver nanoparticles (TeaNPs), iron-based nanoparticles (ZVI), and copper oxide nanocoatings. While TeaNPs exhibited strong antibacterial and antifungal properties, they were not significantly effective against phages alone. However, combining TeaNPs with bacteriophages in phage–nanoparticle cocktails significantly enhanced antibacterial efficacy. ZVI nanoparticles exhibited broad-spectrum antiviral mechanisms involving adsorption, redox reactions, and ion release, while copper oxide nanocoatings demonstrated strong antiviral and antibacterial properties, providing versatile antimicrobial surfaces. Additionally, other nanomaterials, such as copper-based nanocoatings, were evaluated for their antiviral potential. While these materials demonstrated measurable inactivation of some phages, their broad-spectrum activity and limited selectivity reinforced the need for more targeted antiphage solutions, especially in applications requiring precision and minimal disruption to beneficial microbial communities.

In Chapter 5, I introduced indigo carmine (IC), a naturally occurring FDA-approved food dye, as a selective antiphage agent. IC selectively

inactivated DNA phages (e.g., T4, T7, λ, and P001) without affecting bacterial viability, while remaining ineffective against RNA phages such as MS2. Mechanistic studies indicated that IC binds preferentially to double-stranded DNA, leading to structural damage and irreversible tail sheath contraction in bacteriophages. This chapter demonstrated for the first time that selective phage inactivation using a small, food-safe molecule is feasible, representing a critical milestone toward developing safe, scalable antiphage solutions.

In Chapter 6, I further advanced the concept of engineered selectivity by designing mixed-ligand nanoparticles (MLNPs) and polypyrrole nanoparticles (PPyNPs). MLNPs were developed with precisely controlled combinations of positive, negative, and hydrophobic ligands to achieve selective phage targeting while preserving bacterial and mammalian cell viability. MLNPs achieved 99% inactivation of bacteriophages with over 90% bacterial and mammalian cell survival. In parallel, polypyrrole nanoparticles functionalized with carboxyl groups (PPy-COOH NPs) showed broad phage inactivation while maintaining bacterial viability. Both systems demonstrated the potential of rational surface engineering for achieving highly selective and biocompatible phage inactivation.

Altogether, the findings presented in this thesis contribute new knowledge to the emerging field of selective phage inactivation. By moving from natural selectivity (Chapter 5) to rationally engineered selectivity (Chapter 6), this work bridges molecular biology, physical chemistry, and materials science to develop innovative tools for safeguarding microbial processes. Furthermore, these strategies are versatile, scalable, and compatible with industrial, biotechnological, and medical applications.

Bacteriophages, biological entities existing at the intersection of chemistry and biology, challenge conventional analytical methods due to their bimodal nature: too large for small-molecule techniques and too small for direct microscopy without amplification. Their interactions with small molecules and nanomaterials must be studied indirectly, as shown throughout this thesis. The successful design of selective inactivation

strategies reflects a deep understanding of these unique challenges and offers a path forward for future research.

In summary, this thesis demonstrates that effective, selective, and safe inactivation of bacteriophages is achievable through both the discovery of natural compounds and the engineering of novel nanomaterials. Future efforts should continue integrating knowledge from diverse fields to further improve the selectivity, efficiency, and applicability of antiphage strategies across different industrial and clinical settings.

CHAPTER 8
References

[1] G.O. Canny, B.A. McCormick, Bacteria in the intestine, helpful residents or enemies from within?, Infect. Immun. 76 (2008) 3360–3373. https://doi.org/10.1128/IAI.00187-08.

[2] T. Aanniz, M. Ouadghiri, M. Melloul, J. Swings, E. Elfahime, J. Ibijbijen, M. Ismaili, M. Amar, Thermophilic bacteria in moroccan hot springs, salt marshes and desert soils, Brazilian J. Microbiol. 46 (2015) 443–453. https://doi.org/10.1590/S1517-838246220140219.

[3] S. Bijlani, E. Stephens, N.K. Singh, K. Venkateswaran, C.C.C. Wang, Advances in space microbiology, IScience. 24 (2021) 102395. https://doi.org/10.1016/j.isci.2021.102395.

[4] J.A. Gilbert, J.D. Neufeld, Life in a World without Microbes, PLoS Biol. 12 (2014) 1–3. https://doi.org/10.1371/journal.pbio.1002020.

[5] M.C. Wibowo, Z. Yang, M. Borry, A. Hübner, K.D. Huang, B.T. Tierney, S. Zimmerman, F. Barajas-Olmos, C. Contreras-Cubas, H. García-Ortiz, A. Martínez-Hernández, J.M. Luber, P. Kirstahler, T. Blohm, F.E. Smiley, R. Arnold, S.A. Ballal, S.J. Pamp, J. Russ, F. Maixner, O. Rota-Stabelli, N. Segata, K. Reinhard, L. Orozco, C. Warinner, M. Snow, S. LeBlanc, A.D. Kostic, Reconstruction of ancient microbial genomes from the human gut, Nature. 594 (2021) 234–239. https://doi.org/10.1038/s41586-021-03532-0.

[6] J.W. Wilson, M.J. Schurr, C.L. LeBlanc, R. Ramamurthy, K.L. Buchanan, C.A. Nickerson, Mechanisms of bacterial pathogenicity, Postgrad. Med. J. 78 (2002) 216–224. https://doi.org/10.1136/pmj.78.918.216.

[7] Doron. Gorbach, Bacterial Infections, Pediatrics. (2008) 839–847. https://doi.org/10.1016/B978-0-323-01199-0.50123-7.

[8] J.I. Prosser, B.J.M. Bohannan, T.P. Curtis, R.J. Ellis, M.K. Firestone, R.P. Freckleton, J.L. Green, L.E. Green, K. Killham, J.J. Lennon, A.M. Osborn, M. Solan, C.J. Van Der Gast, J.P.W. Young, The role of ecological theory in microbial ecology, Nat. Rev. Microbiol. 5 (2007) 384–392.

[9] J. Johnson, C. Curtin, J. Waite-Cusic, The Cheese Production

Facility Microbiome Exhibits Temporal and Spatial Variability, Front. Microbiol. 12 (2021) 1–13. https://doi.org/10.3389/fmicb.2021.644828.

[10] Z. Chen, J. Kang, Y. Zhang, X. Yi, X. Pang, H. Li-Byarlay, X. Gao, Differences in the bacterial profiles and physicochemical between natural and inoculated fermentation of vegetables from Shanxi Province, Ann. Microbiol. 70 (2020). https://doi.org/10.1186/s13213-020-01605-5.

[11] S. Nosheen, I. Ajmal, Y. Song, Microbes as biofertilizers, a potential approach for sustainable crop production, Sustain. 13 (2021) 1–20. https://doi.org/10.3390/su13041868.

[12] K. Govender, T. Naicker, J. Lin, S. Baijnath, A.A. Chuturgoon, N.S. Abdul, T. Docrat, H.G. Kruger, T. Govender, A novel and more efficient biosynthesis approach for human insulin production in Escherichia coli (E. coli), AMB Express. 10 (2020). https://doi.org/10.1186/s13568-020-00969-w.

[13] Economic Uses and Benefits of Microorganisms, World Microbiol. Immunol. (2022) 1–5. https://www.encyclopedia.com/science/encyclopedias-almanacs-transcripts-and-maps/economic-uses-and-benefits-microorganisms.

[14] R. Shyamkumar, I. Muthu, G. Moorthy, K. Ponmurugan, Production of L-glutamic Acid with Corynebacterium glutamicum (NCIM 2168) and Pseudomonas reptilivora (NCIM 2598): A Study on Immobilization and Reusability, 6 (2014).

[15] S. Sanchez, A.L. Demain, Review Metabolic regulation and overproduction of primary metabolites, 1 (2008) 283–319. https://doi.org/10.1111/j.1751-7915.2007.00015.x.

[16] R. Breitling, A. Ceniceros, A. Jankevics, E. Takano, Metabolomics for Secondary Metabolite Research, Metabolites. 3 (2013) 1076–1083. https://doi.org/10.3390/metabo3041076.

[17] A.S. Abdel-razek, M.E. El-naggar, A. Allam, O.M. Morsy, S.I. Othman, Microbial Natural Products in Drug Discovery, 5 (n.d.) 1–

19.

[18] P.S. Nigam, Microbial enzymes with special characteristics for biotechnological applications, Biomolecules. 3 (2013) 597–611. https://doi.org/10.3390/biom3030597.

[19] M.F. Moradali, B.H.A. Rehm, Bacterial biopolymers : from pathogenesis to advanced materials, Nat. Rev. Microbiol. 18 (2020) 195–210. https://doi.org/10.1038/s41579-019-0313-3.

[20] G.S. Burrill, The Biotechnology Industry : An Engine of Innovation, Elsevier, 2014. https://doi.org/10.1016/B978-0-12-404730-3.00003-8.

[21] N. Khan, Microbes Role in the Economic Development of a World, University of Agriculture, 2019.

[22] M. Colombo, N.P.A. Castilho, S.D. Todorov, L.A. Nero, Beneficial properties of lactic acid bacteria naturally present in dairy production, (2018) 1–12.

[23] E. Rosenberg, E.F. DeLong, F. Thompson, S. Lory, E. Stackebrandt, The prokaryotes: Applied bacteriology and biotechnology, Prokaryotes Appl. Bacteriol. Biotechnol. 9783642313 (2013) 1–393. https://doi.org/10.1007/978-3-642-31331-8.

[24] Z. Erginkaya, G. Konuray-Altun, Potential biotherapeutic properties of lactic acid bacteria in foods, Food Biosci. 46 (2022). https://doi.org/10.1016/j.fbio.2022.101544.

[25] M. Łoś, Strategies of phage contamination prevention in industry, Open J. Bacteriol. 4 (2020) 020–023. https://doi.org/10.17352/ojb.000014.

[26] C. Zhong, Industrial-Scale Production and Applications of Bacterial Cellulose, Front. Bioeng. Biotechnol. 8 (2020) 1–19. https://doi.org/10.3389/fbioe.2020.605374.

[27] P. Vaishnav, A.L. Demain, Unexpected applications of secondary metabolites, Biotechnol. Adv. 29 (2010) 223–229. https://doi.org/10.1016/j.biotechadv.2010.11.006.

[28] J. V. Pham, M.A. Yilma, A. Feliz, M.T. Majid, N. Maffetone, J.R. Walker, E. Kim, H.J. Cho, J.M. Reynolds, M.C. Song, S.R. Park, Y.J. Yoon, A review of the microbial production of bioactive natural products and biologics, Front. Microbiol. 10 (2019) 1–27. https://doi.org/10.3389/fmicb.2019.01404.

[29] B. Al-Shayeb, R. Sachdeva, L.X. Chen, F. Ward, P. Munk, A. Devoto, C.J. Castelle, M.R. Olm, K. Bouma-Gregson, Y. Amano, C. He, R. Méheust, B. Brooks, A. Thomas, A. Lavy, P. Matheus-Carnevali, C. Sun, D.S.A. Goltsman, M.A. Borton, A. Sharrar, A.L. Jaffe, T.C. Nelson, R. Kantor, R. Keren, K.R. Lane, I.F. Farag, S. Lei, K. Finstad, R. Amundson, K. Anantharaman, J. Zhou, A.J. Probst, M.E. Power, S.G. Tringe, W.J. Li, K. Wrighton, S. Harrison, M. Morowitz, D.A. Relman, J.A. Doudna, A.C. Lehours, L. Warren, J.H.D. Cate, J.M. Santini, J.F. Banfield, Clades of huge phages from across Earth's ecosystems, Nature. 578 (2020) 425–431. https://doi.org/10.1038/s41586-020-2007-4.

[30] G. Bogosian, The Bacteriophages, in: R. Calendar (Ed.), Second Edi, Oxford University Press, 2006: pp. 667–673.

[31] M.B. Marcó, S. Moineau, A. Quiberoni, Bacteriophages and dairy fermentations, Bacteriophage. 2 (2012) 149–158. https://doi.org/10.4161/bact.21868.

[32] A.G. de Melo, S. Levesque, S. Moineau, Phages as friends and enemies in food processing, Curr. Opin. Biotechnol. 49 (2018) 185–190. https://doi.org/10.1016/j.copbio.2017.09.004.

[33] E.C. Keen, A century of phage research: Bacteriophages and the shaping of modern biology, BioEssays. 37 (2015) 6–9. https://doi.org/10.1002/bies.201400152.

[34] F. Rohwer, Global phage diversity, Cell. 113 (2003) 141. https://doi.org/10.1016/S0092-8674(03)00276-9.

[35] K. Paramasivam, Y. Shen, J. Yuan, I. Waheed, C. Mao, X. Zhou, Advances in the Development of Phage-Based Probes for Detection of Bio-Species, Biosensors. 12 (2022) 1–22. https://doi.org/10.3390/bios12010030.

[36] S. Michniewski, B. Rihtman, R. Cook, M.A. Jones, W.H. Wilson, D.J. Scanlan, A. Millard, A new family of “megaphages” abundant in the marine environment, ISME Commun. 1 (2021) 12–15. https://doi.org/10.1038/s43705-021-00064-6.

[37] Y. Su, W. Zhang, Y. Liang, H. Wang, Y. Liu, K. Zheng, Z. Liu, H. Yu, L. Ren, Identification and genomic analysis of temperate Halomonas bacteriophage vB_HmeY_H4907 from the surface sediment of the Mariana Trench at a depth of 8,900 m, Bacteriophage. 11 (2023) 1–15. https://doi.org/https://doi.org/10.1128/spectrum.01912-23.

[38] M. Wurtz, Bacteriophage structure, Electron Microsc. Rev. 5 (1992) 283–309. https://doi.org/10.1016/0892-0354(92)90013-G.

[39] M.M. Poranen, S. Mäntynen, ICTV virus taxonomy profile: Cystoviridae, J. Gen. Virol. 98 (2017) 2423–2424. https://doi.org/10.1099/jgv.0.000928.

[40] N.J. Adcock, E.W. Rice, M. Sivaganesan, J.D. Brown, D.E. Stallknecht, D.E. Swayne, The use of bacteriophages of the family Cystoviridae as surrogates for H5N1 highly pathogenic avian influenza viruses in persistence and inactivation studies, J. Environ. Sci. Heal. - Part A Toxic/Hazardous Subst. Environ. Eng. 44 (2009) 1362–1366. https://doi.org/10.1080/10934520903217054.

[41] A. Lopes, P. Tavares, M.A. Petit, R. Guérois, S. Zinn-Justin, Automated classification of tailed bacteriophages according to their neck organization, BMC Genomics. 15 (2014) 1–17. https://doi.org/10.1186/1471-2164-15-1027.

[42] H.W. Ackermann, Phage classification and characterization., Methods Mol. Biol. 501 (2009) 127–140. https://doi.org/10.1007/978-1-60327-164-6_13.

[43] Z. Naureen, A. Dautaj, K. Anpilogov, G. Camilleri, K. Dhuli, B. Tanzi, P.E. Maltese, F. Cristofoli, L. De Antoni, T. Beccari, M. Dundar, M. Bertelli, Bacteriophages presence in nature and their role in the natural selection of bacterial populations, Acta Biomed.

91 (2020) 1–13. https://doi.org/10.23750/abm.v91i13-S.10819.

[44] Z. Hobbs, S.T. Abedon, Diversity of phage infection types and associated terminology: the problem with “Lytic or lysogenic,” FEMS Microbiol. Lett. 363 (2016) 1–8. https://doi.org/10.1093/femsle/fnw047.

[45] E. Aurell, E. Aurell, E. Aurell, K. Sneppen, Epigenetics as a First Exit Problem, Phys. Rev. Lett. 88 (2002) 4. https://doi.org/10.1103/PhysRevLett.88.048101.

[46] A. Fillol-Salom, J.T. Rostøl, A.D. Ojiogu, J. Chen, G. Douce, S. Humphrey, J.R. Penadés, Bacteriophages benefit from mobilizing pathogenicity islands encoding immune systems against competitors, Cell. 185 (2022) 3248-3262.e20. https://doi.org/10.1016/j.cell.2022.07.014.

[47] R. Dey, E. Dlusskaya, N.J. Ashbolt, SARS-CoV-2 surrogate (Phi6) environmental persistence within free-living amoebae, J. Water Health. 20 (2022) 83–91. https://doi.org/10.2166/WH.2021.167.

[48] A.. Coulliette, K.. Perry, E.. Fisher, E. J.R, S. R.E, J. Noble-Wang, MS2 Coliphage as a Surrogate for 2009 Pandemic Influenza A (H1N1) Virus (pH1N1) in Surface Survival Studies on N95 Filtering Facepiece Respirators A.D., J Int Soc Respir Prot. 176 (2014) 139–148.

[49] B. Bicudo, G. Medema, D. van Halem, Inactivation of Escherichia coli and somatic coliphage ΦX174 by oxidation of electrochemically produced Fe2+, J. Water Process Eng. 47 (2022) 102683. https://doi.org/10.1016/j.jwpe.2022.102683.

[50] M.T. Moghadam, N. Amirmozafari, A. Shariati, M. Hallajzadeh, S. Mirkalantari, A. Khoshbayan, F.M. Jazi, How phages overcome the challenges of drug resistant bacteria in clinical infections, Infect. Drug Resist. 13 (2020) 45–61. https://doi.org/10.2147/IDR.S234353.

[51] J.P. Pirnay, Phage Therapy in the Year 2035, Front. Microbiol. 11 (2020) 1–8. https://doi.org/10.3389/fmicb.2020.01171.

[52] A. Wright, C.H. Hawkins, E.E. Änggård, D.R. Harper, A controlled clinical trial of a therapeutic bacteriophage preparation in chronic otitis due to antibiotic-resistant Pseudomonas aeruginosa; A preliminary report of efficacy, Clin. Otolaryngol. 34 (2009) 349–357. https://doi.org/10.1111/j.1749-4486.2009.01973.x.

[53] L. Leitner, A. Ujmajuridze, N. Chanishvili, M. Goderdzishvili, I. Chkonia, S. Rigvava, A. Chkhotua, G. Changashvili, S. McCallin, M.P. Schneider, M.D. Liechti, U. Mehnert, L.M. Bachmann, W. Sybesma, T.M. Kessler, Intravesical bacteriophages for treating urinary tract infections in patients undergoing transurethral resection of the prostate: a randomised, placebo-controlled, double-blind clinical trial, Lancet Infect. Dis. 3099 (2020) 1–10. https://doi.org/10.1016/S1473-3099(20)30330-3.

[54] P. Speck, A. Smithyman, Safety and efficacy of phage therapy via the intravenous route, FEMS Microbiol. Lett. 363 (2015) 1–5. https://doi.org/10.1093/femsle/fnv242.

[55] S. Aslam, E. Lampley, D. Wooten, M. Karris, C. Benson, S. Strathdee, R.T. Schooley, Lessons learned from the first 10 consecutive cases of intravenous bacteriophage therapy to treat multidrug-resistant bacterial infections at a single center in the United States, Open Forum Infect. Dis. 7 (2020). https://doi.org/10.1093/ofid/ofaa389.

[56] R. Voelker, FDA Approves Bacteriophage Trial, Jama. 321 (2019) 638. https://doi.org/10.1001/jama.2019.0510.

[57] S. Gazeev, Applications of Phage Therapy in Veterinary Medicine Applications of Phage Therapy in Veterinary Medicine Fagterapi och dess Tillämpning inom Veterinärmedicin, (2018) 18. https://stud.epsilon.slu.se.

[58] L. Endersen, A. Coffey, The use of bacteriophages for food safety, Curr. Opin. Food Sci. 36 (2020) 1–8. https://doi.org/10.1016/j.cofs.2020.10.006.

[59] J.D. Van Belleghem, K. Dąbrowska, M. Vaneechoutte, J.J. Barr, P.L. Bollyky, Interactions between bacteriophage, bacteria, and

the mammalian immune system, Viruses. 11 (2019). https://doi.org/10.3390/v11010010.

[60] A.A. Cisek, I. Dąbrowska, K.P. Gregorczyk, Z. Wyżewski, Phage Therapy in Bacterial Infections Treatment: One Hundred Years After the Discovery of Bacteriophages, Curr. Microbiol. 74 (2017) 277–283. https://doi.org/10.1007/s00284-016-1166-x.

[61] P. Manohar, A.J. Tamhankar, S. Leptihn, N. Ramesh, Pharmacological and Immunological Aspects of Phage Therapy, Infect. Microbes Dis. 1 (2019) 34–42.

[62] B. Maciejewska, T. Olszak, Z. Drulis-Kawa, Applications of bacteriophages versus phage enzymes to combat and cure bacterial infections: an ambitious and also a realistic application?, Appl. Microbiol. Biotechnol. 102 (2018) 2563–2581. https://doi.org/10.1007/s00253-018-8811-1.

[63] G. Vukotic, M. Obradovic, K. Novovic, M. Di Luca, B. Jovcic, D. Fira, H. Neve, M. Kojic, O. McAuliffe, Characterization, Antibiofilm, and Depolymerizing Activity of Two Phages Active on Carbapenem-Resistant Acinetobacter baumannii, Front. Med. 7 (2020) 1–12. https://doi.org/10.3389/fmed.2020.00426.

[64] C. Ferriol-González, P. Domingo-Calap, Phages for Biofilm Removal, Antibiotics. 9 (2020) 1–16. https://doi.org/10.3390/antibiotics9050268.

[65] T. Morrisette, R. Kebriaei, S. Morales, M.J. Rybak, Bacteriophage-Antibiotic Combinations: A Promising Alternative for Refractory Infections?, Contagion. 5 (2020). https://www.contagionlive.com/view/bacteriophageantibiotic-combinations-a-promising-alternative-for-refractory-infections.

[66] C.G. Liu, S.I. Green, L. Min, J.R. Clark, K.C. Salazar, A.L. Terwilliger, H.B. Kaplan, B.W. Trautner, R.F. Ramig, A.W. Maresso, Phage-antibiotic synergy is driven by a unique combination of antibacterial mechanism of action and stoichiometry, MBio. 11 (2020) 1–19. https://doi.org/10.1128/mBio.01462-20.

[67] J. Paczesny, Ł. Richter, R. Hołyst, Recent progress in the detection of bacteria using bacteriophages: A review, Viruses. 12 (2020) 1–22. https://doi.org/10.3390/v12080845.

[68] S. Banuelos, H. Gulbudak, M.A. Horn, Q. Huang, A. Nandi, H. Ryu, R. Segal, Investigating the impact of combination phage and antibiotic therapy: A modeling study, BioRxiv. (2020). https://doi.org/10.1101/2020.01.08.899476.

[69] A. Górski, J. Borysowski, R. Międzybrodzki, Phage therapy: Towards a successful clinical trial, Antibiotics. 9 (2020) 1–7. https://doi.org/10.3390/antibiotics9110827.

[70] N. Niño-mart, M. Felipe, S. Orozco, G. Mart, F. Torres, F. Ruiz, Molecular Mechanisms of Bacterial Resistance to Metal and Metal Oxide Nanoparticles, Int. J. Mol. Sci. 20 (2019) 1–14.

[71] H. Peng, R.E. Borg, L.P. Dow, B.L. Pruitt, I.A. Chen, Controlled phage therapy by photothermal ablation of specific bacterial species using gold nanorods targeted by chimeric phages, Proc. Natl. Acad. Sci. U. S. A. 117 (2020) 1951–1961. https://doi.org/10.1073/pnas.1913234117.

[72] J. Paczesny, K. Bielec, Application of bacteriophages in nanotechnology, Nanomaterials. 10 (2020) 1–25. https://doi.org/10.3390/nano10101944.

[73] K.S. Sunderland, M. Yang, C. Mao, Phage-Enabled Nanomedicine: From Probes to Therapeutics in Precision Medicine, Angew. Chemie - Int. Ed. 56 (2017) 1964–1992. https://doi.org/10.1002/anie.201606181.

[74] L. Fernández, A. Rodríguez, P. García, Phage or foe: An insight into the impact of viral predation on microbial communities, ISME J. 12 (2018) 1171–1179. https://doi.org/10.1038/s41396-018-0049-5.

[75] S. Gandon, Y. Michalakis, Local adaptation, evolutionary potential and host-parasite coevolution: Interactions between migration, mutation, population size and generation time, J. Evol. Biol. 15 (2002) 451–462. https://doi.org/10.1046/j.1420-

9101.2002.00402.x.

[76] D.B. Stouffer, J. Bascompte, Compartmentalization increases food-web persistence, Proc. Natl. Acad. Sci. U. S. A. 108 (2011) 3648–3652. https://doi.org/10.1073/pnas.1014353108.

[77] N.M. Morella, A.L. Gomez, G. Wang, M.S. Leung, B. Koskella, The impact of bacteriophages on phyllosphere bacterial abundance and composition, Mol. Ecol. 27 (2018) 2025–2038. https://doi.org/10.1111/mec.14542.

[78] H. Brüssow, C. Canchaya, W.-D. Hardt, Phages and the Evolution of Bacterial Pathogens: from Genomic Rearrangements to Lysogenic Conversion, Microbiol. Mol. Biol. Rev. 68 (2004) 560–602. https://doi.org/10.1128/mmbr.68.3.560-602.2004.

[79] K. Ghosh, H.S. Kang, W. Bin Hyun, K.P. Kim, High prevalence of Bacillus subtilis-infecting bacteriophages in soybean-based fermented foods and its detrimental effects on the process and quality of Cheonggukjang, Food Microbiol. 76 (2018) 196–203. https://doi.org/10.1016/j.fm.2018.05.007.

[80] M. Łos, A. Czyz, E. Sell, A. Węgrzyn, P. Neubauer, G. Węgrzyn, Bacteriophage contamination: Is there a simple method to reduce its deleterious effects in laboratory cultures and biotechnological factories?, J. Appl. Genet. 45 (2004) 111–120.

[81] S.D. Quistad, J.A. Grasis, J.J. Barr, F.L. Rohwer, Viruses and the origin of microbiome selection and immunity, ISME J. 11 (2017) 835–840. https://doi.org/10.1038/ismej.2016.182.

[82] J.A. Zahn, M.C. Halter, Surveillance and Elimination of Bacteriophage Contamination in an Industrial Fermentation Process, Bacteriophages - Perspect. Futur. (2020) 1–18. https://doi.org/10.5772/intechopen.81151.

[83] G. Wegrzyn, M. Łoś, P. Neubauer, A simple emergency procedure to be used if biotechnological protein production is endangered by bacteriophage infection of Escherichia coli cultures: effective inhibition of bacteriophage lytic development in infected cultures by removing a carbon source, Microb. Cell Fact.

5 (2006) 1–2. https://doi.org/10.1186/1475-2859-5-S1-P81.

[84] J.E. Garneau, S. Moineau, Bacteriophages of lactic acid bacteria and their impact on milk fermentations, Microb. Cell Fact. 10 (2011) 1–10. https://doi.org/10.1186/1475-2859-10-S1-S20.

[85] S. Fister, P. Mester, A.K. Witte, J. Sommer, D. Schoder, P. Rossmanith, Part of the problem or the solution? Indiscriminate use of bacteriophages in the food industry can reduce their potential and impair growth-based detection methods, Trends Food Sci. Technol. 90 (2019) 170–174. https://doi.org/10.1016/j.tifs.2019.02.031.

[86] M.L. Capra, F. Patrignani, A. del L. Quiberoni, J.A. Reinheimer, R. Lanciotti, M.E. Guerzoni, Effect of high pressure homogenization on lactic acid bacteria phages and probiotic bacteria phages, Int. Dairy J. 19 (2009) 336–341. https://doi.org/10.1016/j.idairyj.2008.11.002.

[87] D.M. Guglielmotti, D.J. Mercanti, J.A. Reinheimer, A. Quiberoni, Review: Efficiency of physical and chemical treatments on the inactivation of dairy bacteriophages, Front. Microbiol. 2 (2012) 1–11. https://doi.org/10.3389/fmicb.2011.00282.

[88] X. Chen, Y. Liu, M. Fan, Z. Wang, W. Wu, J. Wang, Thermal and chemical inactivation of Lactobacillus virulent bacteriophage, J. Dairy Sci. (2017) 7041–7050. https://doi.org/10.3168/jds.2016-12451.

[89] S. Agún, L. Fernández, E. González-Menéndez, B. Martínez, A. Rodríguez, P. García, Study of the interactions between bacteriophage phiIPLA-RODI and four chemical disinfectants for the elimination of Staphylococcus aureus contamination, Viruses. 10 (2018). https://doi.org/10.3390/v10030103.

[90] S. Hayes, J. Murphy, J. Mahony, G.A. Lugli, M. Ventura, J.P. Noben, C.M.A.P. Franz, H. Neve, A. Nauta, D. Van Sinderen, Biocidal inactivation of Lactococcus lactis bacteriophages: Efficacy and targets of commonly used sanitizers, Front. Microbiol. 8 (2017). https://doi.org/10.3389/fmicb.2017.00107.

[91] S.P. MB Marcó, VB Suárez, A Quiberoni, Inactivation of Dairy Bacteriophages by Thermal and Chemical Treatments, Viruses. 11 (2019) 1–28. https://doi.org/http://dx.doi.org/10.3390/v11050480.

[92] K.G. Freeman, M.A. Behrens, K.A. Streletzky, U. Olsson, A. Evilevitch, Portal Stability Controls Dynamics of DNA Ejection from Phage, J. Phys. Chem. B. 120 (2016) 6421–6429. https://doi.org/10.1021/acs.jpcb.6b04172.

[93] D.W. Bauer, A. Evilevitch, Influence of Internal DNA Pressure on Stability and Infectivity of Phage λ, J. Mol. Biol. 427 (2015) 3189–3200. https://doi.org/10.1016/j.jmb.2015.07.023.

[94] A. Brié, I. Bertrand, M. Meo, N. Boudaud, C. Gantzer, The Effect of Heat on the Physicochemical Properties of Bacteriophage MS2, Food Environ. Virol. 8 (2016) 251–261. https://doi.org/10.1007/s12560-016-9248-2.

[95] Z. Atamer, J. Dietrich, M. Müller-Merbach, H. Neve, K.J. Heller, J. Hinrichs, Screening for and characterization of Lactococcus lactis bacteriophages with high thermal resistance, Int. Dairy J. 19 (2009) 228–235. https://doi.org/10.1016/j.idairyj.2008.10.012.

[96] T. Bolumar, V. Orlien, A. Sikes, K. Aganovic, K.H. Bak, C. Guyon, A.S. Stübler, M. de Lamballerie, C. Hertel, D.A. Brüggemann, High-pressure processing of meat: Molecular impacts and industrial applications, Compr. Rev. Food Sci. Food Saf. 20 (2021) 332–368. https://doi.org/10.1111/1541-4337.12670.

[97] M. Smiddy, A.L. Kelly, M.F. Patterson, C. Hill, High pressure-induced inactivation of Qβ coliphage and c2 phage in oysters and in culture media, Int. J. Food Microbiol. 106 (2006) 105–110. https://doi.org/10.1016/j.ijfoodmicro.2005.05.015.

[98] Y. Ye, P.H. Chang, J. Hartert, K.R. Wigginton, Reactivity of Enveloped Virus Genome, Proteins, and Lipids with Free Chlorine and UV254, Environ. Sci. Technol. 52 (2018) 7698–7708. https://doi.org/10.1021/acs.est.8b00824.

[99] L.I.G. D. Becker, J.T.Redpath, Radiation Inactivation of T7

Phage, 73 (1978) 51–74.

[100] S. Lee, M. Nakamura, S. Ohgaki, Inactivation of phage Qβ by 254nm UV light and titanium dioxide photocatalyst, J. Environ. Sci. Heal. - Part A Toxic/Hazardous Subst. Environ. Eng. 33 (1998) 1643–1655. https://doi.org/10.1080/10934529809376809.

[101] D.B. Misstear, L.W. Gill, The inactivation of phages MS2, Φx174 and PR772 using UV and solar photocatalysis, J. Photochem. Photobiol. B Biol. 107 (2012) 1–8. https://doi.org/10.1016/j.jphotobiol.2011.10.012.

[102] M.S. Rahaman, C.D. Vecitis, M. Elimelech, Electrochemical carbon-nanotube filter performance toward virus removal and inactivation in the presence of natural organic matter, Environ. Sci. Technol. 46 (2012) 1556–1564. https://doi.org/10.1021/es203607d.

[103] R. Zandi, D. Reguera, Mechanical properties of viral capsids, Phys. Rev. E - Stat. Nonlinear, Soft Matter Phys. 72 (2005) 1–12. https://doi.org/10.1103/PhysRevE.72.021917.

[104] V. Zárybnický, P. Horáček, Influence of ionic strength on the stability of phage t2r to osmotic shock, Folia Microbiol. (Praha). 13 (1968) 391–400. https://doi.org/10.1007/BF02869189.

[105] P.M. S.P. Leibo, Effect of osmotic shock and low salt concentration on survival and density of bacteriophages T4B and T4B01, (1966) 747–772.

[106] K. Richards, D.J. Malik, Bacteriophage encapsulation in ph-responsive core-shell capsules as an animal feed additive, Viruses. 13 (2021). https://doi.org/10.3390/v13061131.

[107] M. Varbanov, I. Bertrand, S. Philippot, C. Retourney, M. Gardette, C. Hartard, H. Jeulin, R.E. Duval, J.F. Loret, E. Schvoerer, C. Gantzer, Somatic coliphages are conservative indicators of SARS-CoV-2 inactivation during heat and alkaline pH treatments, Sci. Total Environ. 797 (2021) 149112. https://doi.org/10.1016/j.scitotenv.2021.149112.

[108] R. Cheng, Y. Zhang, T. Zhang, F. Hou, X. Cao, L. Shi, P. Jiang,

The inactivation of bacteriophages MS2 and PhiX174 by nanoscale zero-valent iron : Resistance difference and mechanisms, Front. Environ. Sci. Eng. 16 (2022).

[109] F.L. Nobrega, A.R. Costa, J.F. Santos, M.F. Siliakus, J.W.M. Van Lent, S.W.M. Kengen, J. Azeredo, L.D. Kluskens, Genetically manipulated phages with improved pH resistance for oral administration in veterinary medicine, Sci. Rep. 6 (2016) 1–12. https://doi.org/10.1038/srep39235.

[110] E.K. C. Shalitin, D. Danon, Inactivation of Escherichia coli Bacteriophage T2 by Poly-L-lysine. I Nature of the Inactivation Process, Arch. Biochem. Biophys. 99 (1962) 494–507.

[111] E.K. ProperC. Shalitin, Inactivation of Escherichia coli Bacteriophage T2 by Poly-L-lysine. II Properties of the Irreversibly Inactivated Phage, Arch. Biochem. Biophys. 99 (1962) 508–516.

[112] S. Shima, Y. Fukuhara, H. Sakai, Inactivation of bacteriophages by e-poly-l-lysine produced by streptomyces, Agric. Biol. Chem. 46 (1982) 1917–1919. https://doi.org/10.1080/00021369.1982.10865352.

[113] M.S. J. Haimovich, Inactivation of Poly-DL-Alanyl Bacteriophage T4 with Antisera Specific toward Poly-DL-Dalanine, J. Immunol. 97 (1966) 338–343.

[114] S.S. Shima, Y. Fukuhara, H. Sakai, Inactivation of Bacteriophages by £-Poly-L-lysine Produced, Agric. Biol. Chem. 46 (1982) 1917–1919.

[115] R.H. Bianculli, J.D. Mase, M.D. Schulz, Antiviral Polymers: Past Approaches and Future Possibilities, Macromolecules. 53 (2020) 9158–9186. https://doi.org/10.1021/acs.macromol.0c01273.

[116] H. Otsuka, Y. Nagasaki, K. Kataoka, PEGylated nanoparticles for biological and pharmaceutical applications, Adv. Drug Deliv. Rev. 55 (2003) 403–419. https://doi.org/10.1016/S0169-409X(02)00226-0.

[117] S. Xiaowei, S. Zivanovic, D.H. D'Souza, Effect of chitosan on the infectivity of murine norovirus, feline calicivirus, and

bacteriophage MS2, J. Food Prot. 72 (2009) 2623–2628. https://doi.org/10.4315/0362-028x-72.12.2623.

[118] N. Jarach, H. Dodiuk, S. Kenig, Polymers in the medical antiviral front-line, Polymers (Basel). 12 (2020). https://doi.org/10.3390/POLYM12081727.

[119] Z.M. Kochkina, S.N. Chirkov, Effect of chitosan oligomer on phage particles and reproduction of phage 1-97A in Bacillus thuringiensis culture, Mikrobiologiia. 70 (2001) 820–824.

[120] S.N. Chirkov, The antiviral activity of chitosan (review), Appl. Biochem. Microbiol. 38 (2002) 1–8. https://doi.org/10.1023/A:1013206517442.

[121] K. Hodyra-Stefaniak, P. Miernikiewicz, J. Drapała, M. Drab, E. Jonczyk-Matysiak, D. Lecion, Z. Kazmierczak, W. Beta, J. Majewska, M. Harhala, B. Bubak, A. Kłopot, A. Górski, K. Dabrowska, Mammalian Host-Versus-Phage immune response determines phage fate in vivo, Sci. Rep. 5 (2015) 1–13. https://doi.org/10.1038/srep14802.

[122] A. Górski, R. Miedzybrodzki, J. Borysowski, Phage therapy: A practical approach, 2019. https://doi.org/10.1007/978-3-030-26736-0.

[123] K. Gembara, K. Dąbrowska, Phage-specific antibodies, Curr. Opin. Biotechnol. 68 (2021) 186–192. https://doi.org/10.1016/j.copbio.2020.11.011.

[124] M.M. D.W. Bradley, R.A. Hess, F. Tao, L. Sciaba-Lentz, A.T. Remaley, J.A. Laugharn, Pressure Cycling Technology: A Novel Approach To Virus Inactivation in Plasma, Transfusion. 40 (2000) 193–200. https://doi.org/https://doi.org/10.1046/j.1537-2995.2000.40020193.x.

[125] C.S. Yang, G. Chen, Q. Wu, Recent scientific studies of a traditional Chinese medicine, tea, on prevention of chronic diseases, J. Tradit. Complement. Med. 4 (2014) 17–23. https://doi.org/10.4103/2225-4110.124326.

[126] R.S. De Siqueira, C.E.R. Dodd, C.E.D. Rees, Evaluation of the

natural virucidal activity of teas for use in the phage amplification assay, 111 (2006) 259–262. https://doi.org/10.1016/j.ijfoodmicro.2006.04.047.

[127] W. Qureshi, F. Saeed, M. Ajaz, S.A. Rasool, In vitro antimicrobial, antibiofilm and antiphage activity of thyme (Thymus vulgaris), Pakistan J. Bot. 54 (2022) 1121–1128. https://doi.org/10.30848/pjb2022-3(43).

[128] M. Ordon, P. Nawrotek, X. Stachurska, A. Schmidt, M. Mizielińska, Mixtures of Scutellaria baicalensis and Glycyrrhiza L. Extracts as antibacterial and antiviral agents in active coatings, Coatings. 11 (2021) 1–21. https://doi.org/10.3390/coatings11121438.

[129] M. Ordon, M. Zdanowicz, P. Nawrotek, X. Stachurska, M. Mizielińska, Polyethylene films containing plant extracts in the polymer matrix as antibacterial and antiviral materials, Int. J. Mol. Sci. 22 (2021) 1–17. https://doi.org/10.3390/ijms222413438.

[130] D.H. D'Souza, Phytocompounds for the control of human enteric viruses, Curr. Opin. Virol. 4 (2014) 44–49. https://doi.org/10.1016/j.coviro.2013.12.006.

[131] M. Oh, S.Y. Bae, J.H. Lee, K.J. Cho, K.H. Kim, M.S. Chung, Antiviral effects of black raspberry (Rubus coreanus) juice on foodborne viral surrogates, Foodborne Pathog. Dis. 9 (2012) 915–921. https://doi.org/10.1089/fpd.2012.1174.

[132] A. Hardy, L. Kever, J. Frunzke, Antiphage small molecules produced by bacteria – beyond protein-mediated defenses, Trends Microbiol. (2022) 1–15. https://doi.org/10.1016/j.tim.2022.08.001.

[133] S. Kronheim, M. Daniel-Ivad, Z. Duan, S. Hwang, A.I. Wong, I. Mantel, J.R. Nodwell, K.L. Maxwell, A chemical defence against phage infection, Nature. 564 (2018) 283–286. https://doi.org/10.1038/s41586-018-0767-x.

[134] A. Phumyen, S. Jantasorn, A. Jumnainsong, C. Leelayuwat, Doxorubicin-conjugated bacteriophages carrying anti-MHC class I

chain-related A for targeted cancer therapy in vitro, Onco. Targets. Ther. 7 (2014) 2183–2195. https://doi.org/10.2147/OTT.S69315.

[135] S.D. Branston, E.C. Stanley, J.M. Ward, E. Keshavarz-Moore, Determination of the survival of bacteriophage M13 from chemical and physical challenges to assist in its sustainable bioprocessing, Biotechnol. Bioprocess Eng. 18 (2013) 560–566. https://doi.org/10.1007/s12257-012-0776-9.

[136] M.L. Capra, A. Quiberoni, J.A. Reinheimer, Thermal and chemical resistance of Lactobacillus casei and Lactobacillus paracasei bacteriophages, (2004) 499–504. https://doi.org/10.1111/j.1472-765X.2004.01525.x.

[137] D.E. Halfhide, B.W. Gannon, C.M. Hayes, J.M. Roe, Wide variation in effectiveness of laboratory disinfectants against bacteriophages, Lett. Appl. Microbiol. 47 (2008) 608–612. https://doi.org/10.1111/j.1472-765X.2008.02474.x.

[138] R.J. Bull, D.A. Reckhow, X. Li, A.R. Humpage, C. Joll, S.E. Hrudey, Potential carcinogenic hazards of non-regulated disinfection by-products : Haloquinones , halo-cyclopentene and cyclohexene derivatives , N -halamines , halonitriles , and heterocyclic amines, Toxicology. 286 (2011) 1–19. https://doi.org/10.1016/j.tox.2011.05.004.

[139] Y.N. Chang, F.I. Wei, High-temperature chlorine corrosion of metals and alloys - A review, J. Mater. Sci. 26 (1991) 3693–3698. https://doi.org/10.1007/BF01184958.

[140] L.T. Dien, N.V. Linh, T.T. Mai, S. Senapin, S. St-Hilaire, C. Rodkhum, H.T. Dong, Impacts of oxygen and ozone nanobubbles on bacteriophage in aquaculture system, Aquaculture. 551 (2022) 737894. https://doi.org/10.1016/j.aquaculture.2022.737894.

[141] V.I. Syngouna, C. V. Chrysikopoulos, Inactivation of MS2 bacteriophage by titanium dioxide nanoparticles in the presence of quartz sand with and without ambient light, J. Colloid Interface Sci. 497 (2017) 117–125.

https://doi.org/10.1016/j.jcis.2017.02.059.

[142] R. Miedzybrodzki, K. Switala-Jelen, W. Fortuna, B. Weber-Dabrowska, A. Przerwa, M. Lusiak-Szelachowska, K. Dabrowska, A. Kurzepa, J. Boratynski, D. Syper, G. Pozniak, C. Lugowski, A. Gorski, Bacteriophage preparation inhibition of reactive oxygen species generation by endotoxin-stimulated polymorphonuclear leukocytes, Virus Res. 131 (2008) 233–242. https://doi.org/10.1016/j.virusres.2007.09.013.

[143] S.K. Sharma, P. Goloubinoff, P. Christen, Heavy metal ions are potent inhibitors of protein folding, Biochem. Biophys. Res. Commun. 372 (2008) 341–345. https://doi.org/10.1016/j.bbrc.2008.05.052.

[144] L. Yang, K. Arora, W.A. Beard, S.H. Wilson, T. Schlick, Critical role of magnesium ions in DNA polymerase β's closing and active site assembly, J. Am. Chem. Soc. 126 (2004) 8441–8453. https://doi.org/10.1021/ja049412o.

[145] M.H. ADAMS, The stability of bacterial viruses in solutions of salts., J. Gen. Physiol. 32 (1949) 579–594. https://doi.org/10.1085/jgp.32.5.579.

[146] J.A.R. V.B. Suares, M.L. Capra, M. Rivera, Inactivation of calcium-dependent LAB phages by phosphates salts.pdf, J. Food Prot. 70 (2007) 1518–1522.

[147] J. Mahony, D. van Sinderen, Novel strategies to prevent or exploit phages in fermentations, insights from phage-host interactions, Curr. Opin. Biotechnol. 32 (2015) 8–13. https://doi.org/10.1016/j.copbio.2014.09.006.

[148] T.T. Kuo, T.Y. Chow, Y.T. Lin, C.M. Yang, H.W. Li, Specific dissociation of phage Xp12 by sodium citrate., J. Gen. Virol. 10 (1971) 199–202. https://doi.org/10.1099/0022-1317-10-2-199.

[149] S.E. A.P. Krueger, Reversible Inactivation of bacteriophage by KCN, Proc. Soc. Exp. Biol. Med. 31 (1933) 483–485. https://doi.org/https://doi.org/10.3181/00379727-31-7180P.

[150] Z. Liu, Y. Fei, H. Shi, L. Mo, J. Qi, Prediction of high-risk areas of

soil heavy metal pollution with multiple factors on a large scale in industrial agglomeration areas, Sci. Total Environ. 808 (2022). https://doi.org/10.1016/j.scitotenv.2021.151874.

[151] M. Jaishankar, T. Tseten, N. Anbalagan, B.B. Mathew, K.N. Beeregowda, Toxicity, mechanism and health effects of some heavy metals, Interdiscip. Toxicol. 7 (2014) 60–72. https://doi.org/10.2478/intox-2014-0009.

[152] S. Chandra, T. Hu, From Prevention to Therapy : A Roadmap of Nanotechnologies to Stay Ahead of Future Pandemics, (2022). https://doi.org/10.1021/acsnano.2c04148.

[153] K. Gokulan, A.Z. Bekele, K.L. Drake, S. Khare, Responses of intestinal virome to silver nanoparticles: Safety assessment by classical virology, whole-genome sequencing and bioinformatics approaches, Int. J. Nanomedicine. 13 (2018) 2857–2867. https://doi.org/10.2147/IJN.S161379.

[154] Q.L. Shimabuku, T. Ueda-Nakamura, R. Bergamasco, M.R. Fagundes-Klen, Chick-Watson kinetics of virus inactivation with granular activated carbon modified with silver nanoparticles and/or copper oxide, Process Saf. Environ. Prot. 117 (2018) 33–42. https://doi.org/10.1016/j.psep.2018.04.005.

[155] E.B. Gilcrease, R. Williams, R. Goel, Evaluating the effect of silver nanoparticles on bacteriophage lytic infection cycle-a mechanistic understanding, Water Res. 181 (2020) 115900. https://doi.org/10.1016/j.watres.2020.115900.

[156] M. Cho, E.L. Cates, J.-H.H. Kim, Inactivation and surface interactions of MS-2 bacteriophage in a TiO2 photoelectrocatalytic reactor, Water Res. 45 (2011) 2104–2110. https://doi.org/10.1016/j.watres.2010.12.017.

[157] Ł. Richter, K. Paszkowska, U. Cendrowska, F. Olgiati, P.J. Silva, M. Gasbarri, Z.P. Guven, J. Paczesny, F. Stellacci, Broad-spectrum nanoparticles against bacteriophage infections, Nanoscale. 13 (2021) 18684–18694. https://doi.org/10.1039/d1nr04936d.

[158] S. Bharti, S. Mukherji, S. Mukherji, Antiviral application of colloidal and immobilized silver nanoparticles, Nanotechnology. 32 (2021). https://doi.org/10.1088/1361-6528/abe489.

[159] G. Rosati, A. Cunego, F. Fracchetti, A. Del Casale, M. Scaramuzza, A. De Toni, S. Torriani, A. Paccagnella, Inkjet printed interdigitated biosensor for easy and rapid detection of bacteriophage contamination: A preliminary study for milk processing control applications, Chemosensors. 7 (2019). https://doi.org/10.3390/chemosensors7010008.

[160] S.J. Park, Y.S. Ko, H. Jung, C. Lee, K. Woo, G.P. Ko, Disinfection of waterborne viruses using silver nanoparticle-decorated silica hybrid composites in water environments, Sci. Total Environ. 625 (2018) 477–485. https://doi.org/10.1016/j.scitotenv.2017.12.318.

[161] Y.H. Joe, D.H. Park, J. Hwang, Evaluation of Ag nanoparticle coated air filter against aerosolized virus: Anti-viral efficiency with dust loading, J. Hazard. Mater. 301 547–553 Contents. 301 (2016) 547–553.

[162] Y. Haeng, K. Woo, J. Hwang, Fabrication of an anti-viral air filter with SiO2–Ag nanoparticles and performance evaluation in a continuous airflow condition, J. Hazard. Mater. 280 356–363 Contents. 280 (2014) 356–363. www.elsevier.com/locate/jhazmat%0AFabrication.

[163] Michael Vincent Liga, Virus Inactivation by Silver Doped Titanium Dioxide Nanoparticles for Drinking Water Treatment, 2009.

[164] Q.L. Shimabuku, F.S. Arakawa, M. Fernandes Silva, P. Ferri Coldebella, T. Ueda-Nakamura, M.R. Fagundes-Klen, R. Bergamasco, Water treatment with exceptional virus inactivation using activated carbon modified with silver (Ag) and copper oxide (CuO) nanoparticles, Environ. Technol. (United Kingdom). 38 (2017) 2058–2069. https://doi.org/10.1080/09593330.2016.1245361.

[165] C. Shi, J. Wei, Y. Jin, K.E. Kniel, P.C. Chiu, Removal of viruses and bacteriophages from drinking water using zero-valent iron,

Sep. Purif. Technol. 84 (2012) 72–78. https://doi.org/10.1016/j.seppur.2011.06.036.

[166] R. Cademartiri, H. Anany, I. Gross, R. Bhayani, M. Griffiths, M.A. Brook, Immobilization of bacteriophages on modified silica particles, Biomaterials. 31 (2010) 1904–1910. https://doi.org/10.1016/j.biomaterials.2009.11.029.

[167] S. Bone, A. Alum, J. Markovski, K. Hristovski, E. Bar-Zeev, Y. Kaufman, M. Abbaszadegan, F. Perreault, Physisorption and chemisorption of T4 bacteriophages on amino functionalized silica particles, J. Colloid Interface Sci. 532 (2018) 68–76. https://doi.org/10.1016/j.jcis.2018.07.107.

[168] R. Li, L. Cui, M. Chen, Y. Huang, Nanomaterials for Airborne Virus Inactivation: A Short Review, Aerosol Sci. Eng. 5 (2021) 1–11. https://doi.org/10.1007/s41810-020-00080-4.

[169] J. Kim, H. Lee, J.Y. Lee, K.H. Park, W. Kim, J.H. Lee, H.J. Kang, S.W. Hong, H.J. Park, S. Lee, J.H. Lee, H.D. Park, J.Y. Kim, Y.W. Jeong, J. Lee, Photosensitized Production of Singlet Oxygen via C60 Fullerene Covalently Attached to Functionalized Silica-coated Stainless-Steel Mesh: Remote Bacterial and Viral Inactivation, Appl. Catal. B Environ. 270 (2020) 118862. https://doi.org/10.1016/j.apcatb.2020.118862.

[170] M. Cho, J. Lee, Y. MacKeyev, L.J. Wilson, P.J.J. Alvarez, J.B. Hughes, J.H. Kim, Visible light sensitized inactivation of MS-2 bacteriophage by a cationic amine-functionalized C60 derivative, Environ. Sci. Technol. 44 (2010) 6685–6691. https://doi.org/10.1021/es1014967.

[171] J.F. Budarz, A.R. Badireddy, S. Chellam, M.R. Wiesner, Bacteriophage inactivation by UV-A illuminated fullerenes: Role of nanoparticle-virus association, Environ. Sci. Technol. 46 (2012) 5963–5970.

[172] Y. Ni, R. Wang, W. Zhang, S. Shi, W. Zhu, M. Liu, C. Yang, X. Xie, J. Wang, Graphitic carbon nitride (g-C3N4)-based nanostructured materials for photodynamic inactivation:

Synthesis, efficacy and mechanism, Chem. Eng. J. 404 (2021) 126528. https://doi.org/10.1016/j.cej.2020.126528.

[173] N.H. Barbhuiya, S.P. Singh, A. Makovitzki, P. Narkhede, Z. Oren, Y. Adar, E. Lupu, L. Cherry, A. Monash, C.J. Arnusch, Virus inactivation in water using laser-induced graphene filters, Materials (Basel). 14 (2021) 1–11. https://doi.org/10.3390/ma14123179.

[174] X. Hu, L. Mu, J. Wen, Q. Zhou, Covalently synthesized graphene oxide-aptamer nanosheets for efficient visible-light photocatalysis of nucleic acids and proteins of viruses, Carbon N. Y. 50 (2012) 2772–2781. https://doi.org/10.1016/j.carbon.2012.02.038.

[175] K.L. Dreher, Health and environmental impact of nanotechnology: Toxicological assessment of manufactured nanoparticles, Toxicol. Sci. 77 (2004) 3–5. https://doi.org/10.1093/toxsci/kfh041.

[176] G. Bystrzejewska-Piotrowska, J. Golimowski, P.L. Urban, Nanoparticles: Their potential toxicity, waste and environmental management, Waste Manag. 29 (2009) 2587–2595. https://doi.org/10.1016/j.wasman.2009.04.001.

[177] M. Salas-Orozco, N. Niño-Martínez, G.A. Martínez-Castañón, F.T. Méndez, M.E.C. Jasso, F. Ruiz, Mechanisms of resistance to silver nanoparticles in endodontic bacteria: A literature review, J. Nanomater. 2019 (2019). https://doi.org/10.1155/2019/7630316.

[178] S. Raza, K. Matuła, S. Karoń, J. Paczesny, Resistance and adaptation of bacteria to non-antibiotic antibac- terial agents : physical stressors , nanoparticles , and bacterio- phages, (2021) 1–26.

[179] M. Nakhjavani, V. Nikkhah, M.M. Sarafraz, S. Shoja, M. Sarafraz, Green synthesis of silver nanoparticles using green tea leaves: Experimental study on the morphological, rheological and antibacterial behaviour, Heat Mass Transf. Und Stoffuebertragung. 53 (2017) 3201–3209. https://doi.org/10.1007/s00231-017-2065-9.

[180] N.R. Jana, X. Peng, Single-Phase and Gram-Scale Routes

toward Nearly Monodisperse Au and Other Noble Metal Nanocrystals, J. Am. Chem. Soc. 125 (2003) 14280–14281. https://doi.org/10.1021/ja038219b.

[181] G.C. Delgado-Ramos, Nano-conceptions: a sociological insight of nanotechnology conceptions, J. Philos. Sci. Law. 6 (2006) 25–57.

[182] K. et al Pushparaj, Nano- from nature to nurture: A comprehensive review on facets, trends, perspectives and sustainability of nanotechnology in the food sector, Energy. 240 (2022) 1–15. https://doi.org/10.1016/j.energy.2021.122732.

[183] S.H. Nile, V. Baskar, D. Selvaraj, A. Nile, J. Xiao, G. Kai, Nanotechnologies in Food Science: Applications, Recent Trends, and Future Perspectives, Springer Singapore, 2020. https://doi.org/10.1007/s40820-020-0383-9.

[184] S.M. Moghimi, A.C. Hunter, J.C. Murray, Nanomedicine: current status and future prospects, FASEB J. 19 (2005) 311–330. https://doi.org/10.1096/fj.04-2747rev.

[185] J.P. Rolland, B.W. Maynor, L.E. Euliss, A.E. Exner, G.M. Denison, J.M. DeSimone, Direct fabrication and harvesting of monodisperse, shape-specific nanobiomaterials, J. Am. Chem. Soc. 127 (2005) 10096–10100. https://doi.org/10.1021/ja051977c.

[186] A.K. Tiwari, A. Mishra, G. Pandey, M.K. Gupta, P.C. Pandey, Nanotechnology: A Potential Weapon to Fight against COVID-19, Part. Part. Syst. Charact. 39 (2022) 1–26. https://doi.org/10.1002/ppsc.202100159.

[187] K. Kalantar-Zadeh, S.A. Ward, K. Kalantar-Zadeh, E.M. El-Omar, Considering the Effects of Microbiome and Diet on SARS-CoV-2 Infection: Nanotechnology Roles, ACS Nano. 14 (2020) 5179–5182. https://doi.org/10.1021/acsnano.0c03402.

[188] W.H. De Jong, J.B. Paul, Drug delivery and nanoparticles : Applications and hazards, Int. J. Nanomedicine. 3 (2008) 133–149.

[189] A. Kakkar, G. Traverso, O.C. Farokhzad, R. Weissleder, R. Langer, Evolution of macromolecular complexity in drug delivery

systems, Nat. Rev. Chem. 1 (2017) 0063. https://doi.org/10.1038/s41570-017-0063.

[190] K. Ishihara, W. Chen, Y. Liu, Y. Tsukamoto, Y. Inoue, Cytocompatible and multifunctional polymeric nanoparticles for transportation of bioactive molecules into and within cells., Sci. Technol. Adv. Mater. 17 (2016) 300–312. https://doi.org/10.1080/14686996.2016.1190257.

[191] Q. Miao, C. Xie, X. Zhen, Y. Lyu, H. Duan, X. Liu, J. V Jokerst, K. Pu, Molecular afterglow imaging with bright, biodegradable polymer nanoparticles, Nat. Biotechnol. 35 (2017) 1102. https://doi.org/10.1038/nbt.3987.

[192] K. Pu, N. Chattopadhyay, J. Rao, Recent advances of semiconducting polymer nanoparticles in in vivo molecular imaging, J. Control. Release. 240 (2016) 312–322. https://doi.org/10.1016/J.JCONREL.2016.01.004.

[193] B.A. Kairdolf, X. Qian, S. Nie, Bioconjugated Nanoparticles for Biosensing, in Vivo Imaging, and Medical Diagnostics, Anal. Chem. 89 (2017) 1015–1031. https://doi.org/10.1021/acs.analchem.6b04873.

[194] S. Van Rijt, P. Habibovic, Enhancing regenerative approaches with nanoparticles, J. R. Soc. Interface. 14 (2017) 1–10. https://doi.org/10.1098/rsif.2017.0093.

[195] S.J. Lam, E.H.H. Wong, C. Boyer, G.G. Qiao, Antimicrobial polymeric nanoparticles, Prog. Polym. Sci. 76 (2018) 40–64. https://doi.org/10.1016/j.progpolymsci.2017.07.007.

[196] S.W.& M.C. Jiang H., Li Y., Cosnier S., Yang M., Exploring phage engineering to advance nanobiotechnology, Mater. Today Nano. 19 (2022) 1–56. https://doi.org/https://doi.org/10.1016/j.mtnano.2022.100229.

[197] S. Raza, J. Paczesny, Nanotechnology for bacteriophages, bacteriophages for nanotechnology, Nanoscience. (2023) 243–271. https://doi.org/10.1039/9781839169427-00243.

[198] I.X. Yin, J. Zhang, I.S. Zhao, M.L. Mei, Q. Li, C.H. Chu, The

antibacterial mechanism of silver nanoparticles and its application in dentistry, Int. J. Nanomedicine. 15 (2020) 2555–2562. https://doi.org/10.2147/IJN.S246764.

[199] T. Bruna, F. Maldonado-Bravo, P. Jara, N. Caro, Silver nanoparticles and their antibacterial applications, Int. J. Mol. Sci. 22 (2021) 1–21. https://doi.org/10.3390/ijms22137202.

[200] A. Elsayed, A. Safwat, A.S. Abdelsattar, K. Essam, S. Makky, A. El-shibiny, A. Elsayed, A. Safwat, A.S. Abdelsattar, K. Essam, The antibacterial and biofilm inhibition activity of encapsulated silver nanoparticles in emulsions and its synergistic effect with E . coli bacteriophage, Inorg. Nano-Metal Chem. 0 (2022) 1–11. https://doi.org/10.1080/24701556.2022.2081191.

[201] W. Yan, P. Banerjee, M. Xu, S. Mukhopadhyay, M. Ip, N.B. Carrigy, D. Lechuga-Ballesteros, K.K.W. To, S.S.Y. Leung, Formulation strategies for bacteriophages to target intracellular bacterial pathogens, Adv. Drug Deliv. Rev. 176 (2021) 113864. https://doi.org/10.1016/j.addr.2021.113864.

[202] B. De Gusseme, L. Sintubin, T. Hennebel, N. Boon, W. Verstraete, L. Baert, M. Uyttendaele, Inactivation of viruses in water by biogenic silver innovative and environmentally friendly disinfection technique, 2010 4th Int. Conf. Bioinforma. Biomed. Eng. ICBBE 2010. (2010) 1–5. https://doi.org/10.1109/ICBBE.2010.5515631.

[203] S. Cao, X. Wu, J. Zhao, X. Jia, Clinical Study of the Treatment of Klebsiella pneumoniae with Comprehensive Nursing Intervention Combined with New Nano Silver , J. Nanosci. Nanotechnol. 20 (2020) 6063–6069. https://doi.org/10.1166/jnn.2020.18600.

[204] X. Zhang, H. Yu, P. Sun, M. Huang, B. Li, Antiviral Effects and Mechanisms of Active Ingredients in Tea, Molecules. 29 (2024) 1–18. https://doi.org/10.3390/molecules29215218.

[205] K.R. Helsley, T.M. Brown, K. Furlong, K.E. Williamson, Applications and limitations of tea extract as a virucidal agent to assess the role of phage predation in soils, Biol. Fertil. Soils. 50

(2013) 263–274. https://doi.org/10.1007/s00374-013-0855-x.

[206] K. Naumenko, S. Zahorodnia, C. V. Pop, N. Rizun, Antiviral activity of silver nanoparticles against the influenza A virus, J. Virus Erad. 9 (2023). https://doi.org/10.1016/j.jve.2023.100330.

[207] K.M. Bark, J.E. Yeom, J.I. Yang, I.J. Yang, C.H. Park, H.R. Park, Spectroscopic studies on the oxidation of catechin in aqueous solution, Bull. Korean Chem. Soc. 32 (2011) 3443–3447. https://doi.org/10.5012/bkcs.2011.32.9.3443.

[208] L.S. Dorobantu, C. Fallone, A.J. Noble, J. Veinot, G. Ma, G.G. Goss, R.E. Burrell, Toxicity of silver nanoparticles against bacteria, yeast, and algae, J. Nanoparticle Res. 17 (2015) 1–13. https://doi.org/10.1007/s11051-015-2984-7.

[209] S.R. Lockhart, Candida auris and multidrug resistance: Defining the new normal, Fungal Genet. Biol. 131 (2019). https://doi.org/10.1016/j.fgb.2019.103243.

[210] A. Chakrabarti, S. Singh, Multidrug-resistant Candida auris: an epidemiological review, Expert Rev. Anti. Infect. Ther. 18 (2020) 551–562. https://doi.org/10.1080/14787210.2020.1750368.

[211] I.E. Mba, E.I. Nweze, Mechanism of Candida pathogenesis: revisiting the vital drivers, Eur. J. Clin. Microbiol. Infect. Dis. 39 (2020) 1797–1819. https://doi.org/10.1007/s10096-020-03912-w.

[212] L.P. Wang, Y., Bandara, H. M. H. N., Mikkelsen, D., and Samaranayake, Effects of tea extracts on the colonization behaviour of Candida species: attachment inhibition and biofilm enhancement, J. Med. Microbiol. 66 (2017). https://doi.org/https://doi.org/10.1099/jmm.0.000555.

[213] E.W.C. Chan, E.Y. Soh, P.P. Tie, Y.P. Law, Antioxidant and antibacterial properties of green, black, and herbal teas of Camellia sinensis, Pharmacognosy Res. 3 (2011) 266–272. https://doi.org/10.4103/0974-8490.89748.

[214] M. Szymczak, J.A. Pankowski, A. Kwiatek, B. Grygorcewicz, J. Karczewska-Golec, K. Sadowska, P. Golec, An effective antibiofilm strategy based on bacteriophages armed with silver

nanoparticles, Sci. Rep. 14 (2024) 1–15. https://doi.org/10.1038/s41598-024-59866-y.

[215] M. Pardo-Freire, P. Domingo-Calap, Phages and Nanotechnology: New Insights against Multidrug-Resistant Bacteria, BioDesign Res. 5 (2023) 1–13. https://doi.org/10.34133/bdr.0004.

[216] S. Raza, M. Wdowiak, M. Grotek, W. Adamkiewicz, K. Nikiforow, P. Mente, J. Paczesny, Enhancing the antimicrobial activity of silver nanoparticles against ESKAPE bacteria and emerging fungal pathogens by using tea extracts, Nanoscale Adv. 5 (2023) 5786–5798. https://doi.org/10.1039/d3na00220a.

[217] C. Bonnain, M. Breitbart, K.N. Buck, The Ferrojan horse hypothesis: Iron-virus interactions in the ocean, Front. Mar. Sci. 3 (2016) 1–11. https://doi.org/10.3389/fmars.2016.00082.

[218] D. Muratore, J.S. Weitz, Infect while the iron is scarce: nutrient-explicit phage-bacteria games, Theor. Ecol. 14 (2021) 467–487. https://doi.org/10.1007/s12080-021-00508-8.

[219] K. Kim, J. Narayanan, A. Sen, S. Chellam, Virus Removal and Inactivation Mechanisms during Iron Electrocoagulation: Capsid and Genome Damages and Electro-Fenton Reactions, Environ. Sci. Technol. (2021). https://doi.org/10.1021/acs.est.0c04438.

[220] J. Heffron, B. McDermid, B.K. Mayer, Bacteriophage inactivation as a function of ferrous iron oxidation, Environ. Sci. Water Res. Technol. 5 (2019) 1309–1317. https://doi.org/10.1039/c9ew00190e.

[221] J.I. Nieto-Juarez, T. Kohn, Virus removal and inactivation by iron (hydr)oxide-mediated Fenton-like processes under sunlight and in the dark, Photochem. Photobiol. Sci. 12 (2013) 1596–1605. https://doi.org/10.1039/c3pp25314g.

[222] L. Gutierrez, X. Li, J. Wang, G. Nangmenyi, J. Economy, T.B. Kuhlenschmidt, M.S. Kuhlenschmidt, T.H. Nguyen, Adsorption of rotavirus and bacteriophage MS2 using glass fiber coated with hematite nanoparticles, Water Res. 43 (2009) 5198–5208.

https://doi.org/10.1016/j.watres.2009.08.031.

[223] I. Bradley, A. Straub, P. Maraccini, S. Markazi, T.H. Nguyen, Iron oxide amended biosand filters for virus removal, Water Res. 45 (2011) 4501–4510. https://doi.org/10.1016/j.watres.2011.05.045.

[224] M.M. Fidalgo De Cortalezzi, M. V. Gallardo, F. Yrazu, G.J. Gentile, O. Opezzo, R. Pizarro, H.R. Poma, V.B. Rajal, Virus removal by iron oxide ceramic membranes, J. Environ. Chem. Eng. 2 (2014) 1831–1840. https://doi.org/10.1016/j.jece.2014.08.006.

[225] Y. You, J. Han, P.C. Chiu, Y. Jin, Removal and inactivation of waterborne viruses using zerovalent iron, Environ. Sci. Technol. 39 (2005) 9263–9269. https://doi.org/10.1021/es050829j.

[226] M. Briggiler Marcó, A. del L. Quiberoni, A.C. Negro, J.A. Reinheimer, O.M. Alfano, Evaluation of the photocatalytic inactivation efficiency of dairy bacteriophages, Chem. Eng. J. 172 (2011) 987–993. https://doi.org/10.1016/j.cej.2011.07.012.

[227] J.I. Nieto-Juarez, K. Pierzchla, A. Sienkiewicz, T. Kohn, Inactivation of MS2 coliphage in Fenton and Fenton-like systems: Role of transition metals, hydrogen peroxide and sunlight, Environ. Sci. Technol. 44 (2010) 3351–3356. https://doi.org/10.1021/es903739f.

[228] J.Y. Kim, C. Lee, D.L. Sedlak, J. Yoon, K.L. Nelson, Inactivation of MS2 coliphage by Fenton's reagent, Water Res. 44 (2010) 2647–2653. https://doi.org/10.1016/j.watres.2010.01.025.

[229] L. Hu, M.A. Page, T. Sigstam, T. Kohn, B.J. Mariñas, T.J. Strathmann, Inactivation of bacteriophage MS2 with potassium ferrate(VI), Environ. Sci. Technol. 46 (2012) 12079–12087. https://doi.org/10.1021/es3031962.

[230] R. Cheng, G. Li, L. Shi, X. Xue, M. Kang, X. Zheng, The mechanism for bacteriophage f2 removal by nanoscale zero-valent iron, Water Res. 105 (2016) 429–435. https://doi.org/10.1016/j.watres.2016.09.025.

[231] R. Cheng, G. Li, C. Cheng, P. Liu, L. Shi, Z. Ma, X. Zheng,

Removal of bacteriophage f2 in water by nanoscale zero-valent iron and parameters optimization using response surface methodology, Chem. Eng. J. 252 (2014) 150–158. https://doi.org/10.1016/j.cej.2014.05.003.

[232] A.E.H. Shearer, K.E. Kniel, Enhanced removal of norovirus surrogates, murine norovirus and tulane virus, from aqueous systems by zero-valent iron, J. Food Prot. 81 (2018) 1432–1438. https://doi.org/10.4315/0362-028X.JFP-18-054.

[233] X. Guo, Z. Yang, H. Liu, X. Lv, Q. Tu, Q. Ren, X. Xia, C. Jing, Common oxidants activate the reactivity of zero-valent iron (ZVI) and hence remarkably enhance nitrate reduction from water, Sep. Purif. Technol. 146 (2015) 227–234. https://doi.org/10.1016/j.seppur.2015.03.059.

[234] R. Mokete, O. Eljamal, Y. Sugihara, Exploration of the reactivity of nanoscale zero-valent iron (NZVI) associated nanoparticles in diverse experimental conditions, Chem. Eng. Process. - Process Intensif. 150 (2020) 107879. https://doi.org/10.1016/j.cep.2020.107879.

[235] Z. Foltynowicz, A. Bardenshtein, S. Sängerlaub, H. Antvorskov, W. Kozak, Nanoscale, zero valent iron particles for application as oxygen scavenger in food packaging, Food Packag. Shelf Life. 11 (2017) 74–83. https://doi.org/10.1016/j.fpsl.2017.01.003.

[236] K.K. Z. Foltynowicz, W. Kozak, J. Stoińska, M. Urbańska, K. Muc, A. Forysiak, Nanoiron-based oxygen scavengers, Patent EPO EP2658666A1, 2018.

[237] H. Peng, C.I. Pearce, W. Huang, Z. Zhu, A.T. N'Diaye, K.M. Rosso, J. Liu, Reversible Fe(II) uptake/release by magnetite nanoparticles, Environ. Sci. Nano. 5 (2018) 1545–1555. https://doi.org/10.1039/c8en00328a.

[238] J.D. Hem, W.H. Cropper, Survey of Ferrous-Ferric Chemical Equilibria and Redox Potentials, Chem. Iron Nat. Water. (1962) 268.

[239] A. Armanious, M. Aeppli, R. Jacak, D. Refardt, T. Sigstam, T.

Kohn, M. Sander, Viruses at Solid-Water Interfaces: A Systematic Assessment of Interactions Driving Adsorption, Environ. Sci. Technol. 50 (2016) 732–743. https://doi.org/10.1021/acs.est.5b04644.

[240] A. Totsuka, K. Ohtaki, The Effects of Amino Acids and Metals on the Infectivity of Poliovirus Ribonucleic Acid, Jpn. J. Microbiol. 18 (1974) 107–112.

[241] J. Sagripanti, M.M. Lightfoote, Cupric and Ferric Ions Inactivate HIV, AIDS Res. Hum. Retroviruses. 12 (1996) 333–336.

[242] G. Borkow, J. Gabbay, Putting copper into action: copper-impregnated products with potent biocidal activities, FASEB J. 1 (2004) 1–19. https://doi.org/10.1096/fj.04-2029fje.

[243] S. Jose, W. Quality, W. Science, Inactivation of coliphage MS2 and poliovirus by copper, silver, and chlorine, Can. J. Microbiol. 38 (1992) 430–435.

[244] J. Sagripanti, L.B. Routson, C.D. Lytle, Virus Inactivation by Copper or Iron Ions Alone and in the Presence of Peroxide, Appl. Environ. Microbiol. 59 (1993) 4374–4376.

[245] I. Salah, I.P. Parkin, E. Allan, Copper as an antimicrobial agent : recent advances, RSC Adv. 11 (2021) 18179–18186. https://doi.org/10.1039/d1ra02149d.

[246] Z. Yan, H. Liu, Z. Hao, M. Yu, X. Chen, J. Chen, Electrodeposition of (hydro)oxides for an oxygen evolution electrode, Chem. Sci. 11 (2020) 10614–10625. https://doi.org/10.1039/d0sc01532f.

[247] M. Stumpp, D. Damtew, D. Stock, K. Hess, D. Schröder, D. Schlettwein, Controlled Electrodeposition of Zinc Oxide on Conductive Meshes and Foams Enabling Its Use as Secondary Anode, J. Electrochem. Soc. 165 (2018) D461–D466. https://doi.org/10.1149/2.0941810jes.

[248] E.M. Abebe, M. Ujihara, Simultaneous Electrodeposition of Ternary Metal Oxide Nanocomposites for High-Efficiency Supercapacitor Applications, ACS Omega. (2022).

https://doi.org/10.1021/acsomega.2c00826.

[249] Z. Zhang, W. Hu, Y. Deng, C. Zhong, H. Wang, Y. Wu, L. Liu, The effect of complexing agents on the oriented growth of electrodeposited microcrystalline cuprous oxide film, Mater. Res. Bull. 47 (2012) 2561–2565. https://doi.org/10.1016/j.materresbull.2012.04.146.

[250] Q.T. Du, J.S. Tan, Q.T. Wang, C.Y. Li, X.H. Liu, R.S. Cai, Y.H. Ding, Y.Q. Wang, Electrochemical deposition and formation mechanism of single-crystalline Cu 2O octahedra on aluminum, J. Anal. Methods Chem. 1 (2012) 2–9. https://doi.org/10.1155/2012/406162.

[251] A. Kusior, J. Mazurkow, P. Jelen, M. Bik, S. Raza, M. Wdowiak, K. Nikiforov, J. Paczesny, Copper Oxide Electrochemical Deposition to Create Antiviral and Antibacterial Nanocoatings, Langmuir. 40 (2024) 14838–14846. https://doi.org/10.1021/acs.langmuir.4c00642.

[252] A. Kusior, Voltammetric Detection of Glucose—The Electrochemical Behavior of the Copper Oxide Materials with Well-Defined Facets, Sensors. 22 (2022). https://doi.org/10.3390/s22134783.

[253] K. Matuła, Ł. Richter, W. Adamkiewicz, B. Åkerstrom, J. Paczesny, R. Hołyst, Influence of nanomechanical stress induced by ZnO nanoparticles of different shapes on the viability of cells †, Soft Matter. 12 (2016) 4162–4169. https://doi.org/10.1039/c6sm00336b.

[254] P.H. Beswick, G.H. Hall, A.J. Hook, K. Little, Copper toxicity: evidence for the conversion of cupric to cuprous copper in vivo under anaerobic conditions, Chem. Interact. 14 (1976) 347–356.

[255] C. Dupont, G. Grass, C. Rensing, Copper toxicity and the origin of bacterial resistance — new insights and applications w, Metallomics. 3 (2011) 1109–1118. https://doi.org/10.1039/c1mt00107h.

[256] Z. Chegini, A. Khoshbayan, M. Taati Moghadam, I. Farahani, P.

Jazireian, A. Shariati, Bacteriophage therapy against Pseudomonas aeruginosa biofilms: A review, Ann. Clin. Microbiol. Antimicrob. 19 (2020) 1–17. https://doi.org/10.1186/s12941-020-00389-5.

[257] E. Jończyk, M. Kłak, R. Międzybrodzki, A. Górski, The influence of external factors on bacteriophages-review, Folia Microbiol. (Praha). 56 (2011) 191–200. https://doi.org/10.1007/s12223-011-0039-8.

[258] M. Wdowiak, J. Paczesny, S. Raza, Enhancing the Stability of Bacteriophages Using Physical, Chemical, and Nano-Based Approaches: A Review, Pharmaceutics. 14 (2022). https://doi.org/10.3390/pharmaceutics14091936.

[259] B. Ma, Y.S. Linden, P.M. Gundy, C.P. Gerba, M.D. Sobsey, K.G. Linden, Inactivation of coronaviruses and phage Phi6 from irradiation across UVC wavelengths, Environ. Sci. Technol. Lett. 8 (2021) 425–430. https://doi.org/10.1021/acs.estlett.1c00178.

[260] Z. Atamer, S. Meike, H. Neve, K.J. Heller, J. Hinrichs, Review: Elimination of bacteriophages in whey and whey products, Front. Microbiol. 4 (2013) 1–9. https://doi.org/10.3389/fmicb.2013.00191.

[261] T. Morin, H. Martin, C. Soumet, R. Fresnel, S. Lamaudière, A.L. Le Sauvage, K. Deleurme, P. Maris, Comparison of the virucidal efficacy of peracetic acid, potassium monopersulphate and sodium hypochlorite on bacteriophages P001 and MS2, J. Appl. Microbiol. 119 (2015) 655–665. https://doi.org/10.1111/jam.12870.

[262] P.I. Hora, S.G. Pati, P.J. McNamara, W.A. Arnold, Increased Use of Quaternary Ammonium Compounds during the SARS-CoV-2 Pandemic and Beyond: Consideration of Environmental Implications, Environ. Sci. Technol. Lett. 7 (2020) 622–631. https://doi.org/10.1021/acs.estlett.0c00437.

[263] Ł. Richter, C.A. Stevens, P.J. Silva, L.R. Julià, C. Malinverni, L. Wei, M. Łoś, F. Stellacci, Peptide-Grafted Nontoxic Cyclodextrins

and Nanoparticles against Bacteriophage Infections, ACS Nano. 16 (2022) 18990–19001. https://doi.org/10.1021/acsnano.2c07896.

[264] P. Tu, R. Tian, Y. Lu, Y. Zhang, H. Zhu, L. Ling, H. Li, D. Chen, Beneficial effect of Indigo Naturalis on acute lung injury induced by influenza A virus, Chinese Med. (United Kingdom). 15 (2020) 1–18. https://doi.org/10.1186/s13020-020-00415-w.

[265] Y. Qi-yue, Z. Ting, H. Ya-nan, H. Sheng-jie, D. Xuan, H. Li, X. Chun-guang, From natural dye to herbal medicine: a systematic review of chemical constituents, pharmacological effects and clinical applications of indigo naturalis, Chinese Med. (United Kingdom). 15 (2020) 1–13. https://doi.org/10.1186/s13020-020-00406-x.

[266] C.Y. Huang, J.Y. Chang, G.L. Riskowski, W.K. Chan, J.T. Lai, A.C. Chang, Antimicrobial activity of indigowoad (Isatis indigotica fort) and plains wild indigo (Baptisia bracteata) roots, Res. J. Med. Plant. 10 (2016) 237–245. https://doi.org/10.3923/rjmp.2016.237.245.

[267] S.J. Chang, Y.C. Chang, K.Z. Lu, Y.Y. Tsou, C.W. Lin, Antiviral activity of Isatis indigotica extract and its derived indirubin against Japanese encephalitis virus, Evidence-Based Complement. Altern. Med. 2012 (2012). https://doi.org/10.1155/2012/925830.

[268] Z. Yang, Y. Wang, Z. Zheng, S. Zhao, J. Zhao, Q. Lin, C. Li, Q. Zhu, N. Zhong, Antiviral activity of Isatis indigotica root-derived clemastanin B against human and avian influenza A and B viruses in vitro, Int. J. Mol. Med. 31 (2013) 867–873. https://doi.org/10.3892/ijmm.2013.1274.

[269] M.C. Chan, R.W. Chan, C.K. Mok, N.K. Mak, R.N. Wong, Indirubin-3’-oxime as an antiviral and immunomodulatory agent in treatment of severe human influenza virus infection, Hong Kong Med. J. = Xianggang Yi Xue Za Zhi. 24 (2018) 45–47.

[270] A.D. Fuzimoto, C. Isidoro, The antiviral and coronavirus-host protein pathways inhibiting properties of herbs and natural

compounds - Additional weapons in the fight against the COVID-19 pandemic?, J. Tradit. Complement. Med. 10 (2020) 405–419. https://doi.org/10.1016/j.jtcme.2020.05.003.

[271] P.G. Leiman, F. Arisaka, M.J. Van Raaij, V.A. Kostyuchenko, A.A. Aksyuk, S. Kanamaru, M.G. Rossmann, Morphogenesis of the T4 tail and tail fibers, Virol. J. 7 (2010) 1–28. https://doi.org/10.1186/1743-422X-7-355.

[272] H. Prinz, Hill coefficients, dose-response curves and allosteric mechanisms, J. Chem. Biol. 3 (2010) 37–44. https://doi.org/10.1007/s12154-009-0029-3.

[273] M. Janczuk, Ł. Richter, G. Hoser, J. Kawiak, M. Łoś, J. Niedziółka-Jönsson, J. Paczesny, R. Hołyst, Bacteriophage-Based Bioconjugates as a Flow Cytometry Probe for Fast Bacteria Detection, Bioconjug. Chem. 28 (2017) 419–425. https://doi.org/10.1021/acs.bioconjchem.6b00596.

[274] A. Zinellu, V. Pasciu, S. Sotgia, B. Scanu, F. Berlinguer, G. Leoni, S. Succu, I. Cossu, E.S. Passino, S. Naitana, L. Deiana, C. Carru, Capillary electrophoresis with laser-induced fluorescence detection for ATP quantification in spermatozoa and oocytes, Anal. Bioanal. Chem. 398 (2010) 2109–2116. https://doi.org/10.1007/s00216-010-4186-6.

[275] A. Karpińska, M. Pilz, J. Buczkowska, P.J. Żuk, K. Kucharska, G. Magiera, K. Kwapiszewska, R. Hołyst, Quantitative analysis of biochemical processes in living cells at a single-molecule level: A case of olaparib-PARP1 (DNA repair protein) interactions, Analyst. 146 (2021) 7131–7143. https://doi.org/10.1039/d1an01769a.

[276] A.J. Kettle, B.M. Clark, C.C. Winterbourn, Superoxide converts indigo carmine to isatin sulfonic acid: Implications for the hypothesis that neutrophils produce ozone, J. Biol. Chem. 279 (2004) 18521–18525. https://doi.org/10.1074/jbc.M400334200.

[277] H.X. Li, B. Xu, L. Tang, J.H. Zhang, Z.G. Mao, Reductive decolorization of indigo carmine dye with Bacillus sp. MZS10, Int.

Biodeterior. Biodegrad. 103 (2015) 30–37. https://doi.org/10.1016/j.ibiod.2015.04.007.

[278] C. Hao, Z. Xiao, D. Xu, C. Zhang, J. Qiu, K. Liu, Saturated resin ectopic regeneration by non-thermal dielectric barrier discharge plasma, Catalysts. 7 (2017). https://doi.org/10.3390/catal7120362.

[279] P.P. Pillai, B. Kowalczyk, K. Kandere-Grzybowska, M. Borkowska, B.A. Grzybowski, Engineering Gram Selectivity of Mixed-Charge Gold Nanoparticles by Tuning the Balance of Surface Charges, Angew. Chemie - Int. Ed. 55 (2016) 8610–8614. https://doi.org/10.1002/anie.201602965.

[280] P.P. Pillai, B. Kowalczyk, B.A. Grzybowski, Self-assembly of like-charged nanoparticles into microscopic crystals, Nanoscale. 8 (2016) 157–161. https://doi.org/10.1039/c5nr06983a.

[281] D. Wang, R.J. Nap, I. Lagzi, B. Kowalczyk, S. Han, B.A. Grzybowski, I. Szleifer, How and why nanoparticle's curvature regulates the apparent pKa of the coating ligands, J. Am. Chem. Soc. 133 (2011) 2192–2197. https://doi.org/10.1021/ja108154a.

[282] D. Wang, B. Kowalczyk, I. Lagzi, B.A. Grzybowski, Bistability and hysteresis during aggregation of charged nanoparticles, J. Phys. Chem. Lett. 1 (2010) 1459–1462. https://doi.org/10.1021/jz100406w.

[283] M. Siek, K. Kandere-Grzybowska, B.A. Grzybowski, Mixed-Charge, pH-Responsive Nanoparticles for Selective Interactions with Cells, Organelles, and Bacteria, Accounts Mater. Res. 1 (2020) 188–200. https://doi.org/10.1021/accountsmr.0c00041.

[284] J.D. Clogston, A.K. Patri, Zeta Potential Measurement Jeffrey, Methods Mol. Biol. 697 (2011) 63–70. https://doi.org/10.1007/978-1-60327-198-1_6.

[285] H.J. Jang, S.H.R. Shin, H.Y. Lee, Surface property modification of well-dispersed amphiphilic gold nanoparticles as individuals, J. Nanoparticle Res. 20 (2018). https://doi.org/10.1007/s11051-018-4349-5.

[286] S.M. Ansar, S. Chakraborty, C.L. Kitchens, pH-responsive mercaptoundecanoic acid functionalized gold nanoparticles and applications in catalysis, Nanomaterials. 8 (2018) 1–12. https://doi.org/10.3390/nano8050339.

[287] R. Pamies, J.G.H. Cifre, V.F. Espín, M. Collado-González, F.G.D. Baños, J.G. De La Torre, Aggregation behaviour of gold nanoparticles in saline aqueous media, J. Nanoparticle Res. 16 (2014). https://doi.org/10.1007/s11051-014-2376-4.

[288] S. Engel, E.C. Fritz, B.J. Ravoo, New trends in the functionalization of metallic gold: From organosulfur ligands to N-heterocyclic carbenes, Chem. Soc. Rev. 46 (2017) 2057–2075. https://doi.org/10.1039/c7cs00023e.

[289] H. Häkkinen, The gold-sulfur interface at the nanoscale, Nat. Chem. 4 (2012) 443–455. https://doi.org/10.1038/nchem.1352.

[290] D.L.B. Robert M. Silverstein, Francis X. Webster, David J. Kiemle, Spectrometric Identification of Organic Compounds, 8th ed., Wiley, 2014. https://www.wiley.com/en-ae/Spectrometric+Identification+of+Organic+Compounds%2C+8th+Edition-p-9780470616376.

[291] K.B. Dillon, M.R. Harrison, F.J.C. Rossotti, A hydrogen NMR study of some carboxylic acids and their anions, J. Magn. Reson. 39 (1980) 499–508. https://doi.org/10.1016/0022-2364(80)90036-0.

[292] M.S. Gruzdev, L.E. Shmukler, N.O. Kudryakova, A.M. Kolker, L.P. Safonova, Synthesis and properties of triethanolamine-based salts with mineral and organic acids as protic ionic liquids, J. Mol. Liq. 249 (2018) 825–830. https://doi.org/10.1016/j.molliq.2017.11.127.

[293] M.S. Draz, H. Shafiee, Applications of gold nanoparticles in virus detection, Theranostics. 8 (2018) 1985–2017. https://doi.org/10.7150/thno.23856.

[294] I. Papp, C. Sieben, K. Ludwig, M. Roskamp, C. Böttcher, S. Schlecht, A. Herrmann, R. Haag, Inhibition of influenza virus

infection by multivalent sialic-acid- functionalized gold nanoparticles, Small. 6 (2010) 2900–2906. https://doi.org/10.1002/smll.201001349.

[295] N. Tawil, E. Sacher, D. Rioux, R. Mandeville, M. Meunier, Surface chemistry of bacteriophage and laser ablated nanoparticle complexes for pathogen detection, J. Phys. Chem. C. 119 (2015) 14375–14382. https://doi.org/10.1021/acs.jpcc.5b02169.

[296] N. Tawil, E. Sacher, E. Boulais, R. Mandeville, M. Meunier, X-ray photoelectron spectroscopic and transmission electron microscopic characterizations of bacteriophage-nanoparticle complexes for pathogen detection, J. Phys. Chem. C. 117 (2013) 20656–20665. https://doi.org/10.1021/jp406148h.

[297] H. Wennerström, E.V. Estrada, J. Danielsson, M. Oliveberg, Colloidal stability of the living cell, Proc. Natl. Acad. Sci. U. S. A. 117 (2020) 10113–10121. https://doi.org/10.1073/pnas.1914599117.

[298] M. Deserno, H.H. von Grünberg, Osmotic pressure of charged colloidal suspensions: A unified approach to linearized Poisson-Boltzmann theory, Phys. Rev. E. Stat. Nonlin. Soft Matter Phys. 66 (2002) 11401. https://doi.org/10.1103/PhysRevE.66.011401.

[299] W.M. Gelbart, C.M. Knobler, The physics of phages, Phys. Today. 61 (2008) 42–47. https://doi.org/10.1063/1.2835152.

[300] M.O. Mohsen, G. Augusto, M.F. Bachmann, The 3Ds in virus-like particle based-vaccines: “Design, Delivery and Dynamics,” Immunol. Rev. 296 (2020) 155–168. https://doi.org/10.1111/imr.12863.

[301] K.M. El-Say, H.S. El-Sawy, Polymeric nanoparticles: Promising platform for drug delivery, Int. J. Pharm. 528 (2017) 675–691. https://doi.org/10.1016/j.ijpharm.2017.06.052.

[302] J.H. Moon, E. Mendez, Y. Kim, A. Kaur, Conjugated polymer nanoparticles for small interfering RNA delivery, Chem. Commun. 47 (2011) 8370–8372. https://doi.org/10.1039/c1cc10991j.

[303] M.K. Satapathy, B. Nyambat, C.W. Chiang, C.H. Chen, P.C.

Wong, P.H. Ho, P.R. Jheng, T. Burnouf, C.L. Tseng, E.Y. Chuang, A gelatin hydrogel-containing nano-organic PEI–Ppy with a photothermal responsive effect for tissue engineering applications, Molecules. 23 (2018). https://doi.org/10.3390/molecules23061256.

[304] Z. Zha, Z. Deng, Y. Li, C. Li, J. Wang, S. Wang, E. Qu, Z. Dai, Biocompatible polypyrrole nanoparticles as a novel organic photoacoustic contrast agent for deep tissue imaging, Nanoscale. 5 (2013) 4462–4467. https://doi.org/10.1039/c3nr00627a.

[305] C. Kimmelshue, A.S. Goggi, R. Cademartiri, The use of biological seed coatings based on bacteriophages and polymers against Clavibacter michiganensis subsp. nebraskensis in maize seeds, Sci. Rep. 9 (2019) 1–11. https://doi.org/10.1038/s41598-019-54068-3.

[306] B. Roy, C. Philippe, M.J. Loessner, J. Goulet, S. Moineau, Production of bacteriophages by listeria cells entrapped in organic polymers, Viruses. 10 (2018). https://doi.org/10.3390/v10060324.

[307] D.J. Malik, I.J. Sokolov, G.K. Vinner, F. Mancuso, S. Cinquerrui, G.T. Vladisavljevic, M.R.J. Clokie, N.J. Garton, A.G.F. Stapley, A. Kirpichnikova, Formulation, stabilisation and encapsulation of bacteriophage for phage therapy, Adv. Colloid Interface Sci. 249 (2017) 100–133. https://doi.org/10.1016/j.cis.2017.05.014.

[308] E. V. Musin, A.L. Kim, A. V. Dubrovskii, E.B. Kudryashova, E. V. Ariskina, S.A. Tikhonenko, The influence of polyanions and polycations on bacteriophage activity, Polymers (Basel). 13 (2021) 2–7. https://doi.org/10.3390/polym13060914.

[309] D.D. Ateh, H.A. Navsaria, P. Vadgama, Polypyrrole-based conducting polymers and interactions with biological tissues, J. R. Soc. Interface. 3 (2006) 741–752. https://doi.org/10.1098/rsif.2006.0141.

[310] H.K. Chitte, G.N. Shinde, N. V. Bhat, V.E. Walunj, Synthesis of Polypyrrole Using Ferric Chloride (FeCl₃) as Oxidant Together with Some Dopants for Use in Gas Sensors,

J. Sens. Technol. 01 (2011) 47–56. https://doi.org/10.4236/jst.2011.12007.

[311] M. Cabuk, M. Oztas, F. Gode, H.I. Unal, M. Yavuz, Effects of zeta-potential on enhanced removal of hexavalent chromium by polypyrrole-graft-chitosan biodegradable copolymer, Colloids Surfaces A Physicochem. Eng. Asp. 676 (2023) 132104. https://doi.org/10.1016/j.colsurfa.2023.132104.

[312] H.A. Pearson, G.S. Sahukhal, M.O. Elasri, M.W. Urban, Phage-bacterium war on polymeric surfaces: Can surface-anchored bacteriophages eliminate microbial infections?, Biomacromolecules. 14 (2013) 1257–1261. https://doi.org/10.1021/bm400290u.

[313] S. Nyembe, G. Ndlovu, P. Shumbula, R. Harris, N. Moloto, L. Sikhwivhilu, Laser Assisted Catalytic Growth of Silicon Nanowires Using Gold and Nickel Catalysts, J. Nanosci. Nanotechnol. 21 (2021) 5260–5265. https://doi.org/10.1166/jnn.2021.19448.

[314] C.D. Vecitis, Antiviral-nanoparticle interactions and reactions, Environ. Sci. Nano. 8 (2021) 11–19. https://doi.org/10.1039/d0en00980f.

[315] S. Raza, M. Wdowiak, J. Paczesny, An Overview of Diverse Strategies To Inactivate Enterobacteriaceae - Targeting Bacteriophages, EcoSal Plus. (2023) 1–22.